THE HYDROCARBON POTENTIAL AND SEDIMENTARY ENVIRONMENT OF THE MIOCENE SILICEOUS FORMATION IN TSUGARU AND AKITA BASINS, NORTHERN JAPAN, BASED ON THE SEDIMENTOLOGICAL AND GEOCHEMICAL ANALYSES

MARTIZZI PAOLO

The hydrocarbon potential and sedimentary environment of the Miocene siliceous formation in Tsugaru and Akita basins, northern Japan, based on the sedimentological and geochemical analyses

PhD Candidate:

Martizzi Paolo

Student ID No. 6517106

PhD Supervisors:

Professor Arato Hiroyuki, Professor Chiyonobu Shun

Department of Geosciences, Geotechnology, and Materials Engineering for Resources

Graduate School of International Resource Sciences

Akita University

ABSTRACT

The area extending from Hokkaido to the northwestern side of Honshu island in Japan is where most of the Japanese oil and gas fields occur. Several present and past studies focused on the Middle-Late Miocene siliceous sedimentary formations of Akita and Aomori Prefectures, which are considered the most prospective horizons for hydrocarbons generation. These formations occur in several locations of Akita and Aomori Prefectures and provide an excellent geological record of the Miocene paleoenvironmental evolution in the Japan Sea. However, in many areas of the Akita and Aomori Prefectures, petroleum potential and paleoenvironmental studies have not yet been performed, and minimal subsurface data are available.

This study introduces new data about the hydrocarbon potential and the paleoenvironment of the Japan Sea in the Middle-Late Miocene through the sedimentological and geochemical analysis of the Miocene sedimentary succession of Tsugaru Basin (southwestern Aomori Prefecture) and the Middle-Late Miocene Onnagawa and Iwaya Formations (central Akita Prefecture).

Rock-Eval pyrolysis analysis performed on the core and outcrop samples of the studied formations indicates that the Odoji Formation in Aomori and the Onnagawa and Iwaya Formations in Akita are characterized by a fair/good organic richness. However, these formations are immature for the generation and expulsion of hydrocarbons.

According to several wells data in the Akita Prefecture, the Onnagawa Formation and its equivalents are mature for oil in various locations of the region. The main factors that determined the maturation of potential source rocks were the burial depth and the geothermal gradient anomalies determined by the intrusion of igneous bodies in the Onnagawa Formation. On the other hand, according to the wells data in the Aomori Prefecture, the increase of burial depth did not influence the thermal maturity significantly. At the current state, mature horizons for the oil generation are still not located.

Paleoenvironmental reconstruction of depositional conditions of the Miocene formations of Akita and Aomori Prefectures was inferred from the lithofacies and geochemical composition of sediments. Major oxides revealed that the composition of Middle-Late Miocene formations is dominated by SiO_2 and variable percentages of detrital oxides such as Al_2O_3 and K_2O. The detrital oxides content is low in the lower and central parts of the Onnagawa and Odoji Formations, while it tends to increase at the top of these formations and in the Late Miocene formations (ex. Akaishi Formation). Major oxides interpretation indicates that the detrital fraction originated from a felsic source, located in a continental area. This result suggests that the detrital fraction derived from the erosion of continental

rocks in the Asian continent or the land areas on the east margin of the northwestern Honshu basin. These interpretations suggest that the detrital fraction was related to the variation of the monsoon activity in the Asian continent during the Middle-Late Miocene and the variation of riverine supply from northeastern Honshu. The generally positive correlation between the TOC and the detrital oxides suggests that the dilution of organic matter by detritus contributed to the preservation of TOC.

The high concentration of the biogenic SiO_2 in the formations from both Akita and Aomori regions indicates high primary productivity in the surface waters of the Japan Sea. The intense productivity delivered considerable amounts of phytoplankton organic matter in the water column. The TOC shows a slightly negative correlation with the biogenic SiO_2, possibly indicating that the intense production of biogenic SiO_2 generated a biogenic dilution process that impacted the TOC content.

The lithofacies and framboidal pyrite size variations indicated that paleo-oxygenation of bottom waters varied throughout the Akita and Aomori regions. The massive samples with large-size framboidal pyrite of all the formations were probably deposited in oxic/dysoxic bottom waters. On the other hand, the laminated samples with small-size framboidal pyrite of the Onnagawa Formation were deposited in anoxic bottom waters. However, no consistent difference in the TOC of massive and laminated facies, suggests that the paleo-redox conditions had a low influence in the TOC preservation in the studied formations. The only evident case of oxic degradation is represented by the Akaishi Formation in which the TOC is markedly low.

Combining the data of this and previous studies, it was possible to hypothesize the paleoenvironmental setting of Akita and Aomori regions in the Middle-Late Miocene. Both regions were characterized by a detrital input from the Asian monsoon and the riverine supply, and by the widespread activity of phytoplankton on the sea surface. An intense process of upwelling stimulated by the cold surface water and the wind energy brought nutrient elements in the sea surface, favoring the surface water bio-productivity. The different paleo-oxygenation conditions in the bottom water were determined by the mixing between north Pacific OMZ and the Japan Sea waters. The OMZ waters probably did not reach the Tsugaru Basin and the Gotanzawa areas, suggesting that the paleo-depth of these basins was shallow. On the other hand, the intermittent inflow of the OMZ waters in the Ajigasawa and Sugisawa areas determined the deposition of both massive and laminated sediments. The inflow of the OMZ was regulated by the variations of the sea-level.

ACKNOWLEDGEMENTS

I express my sincere gratitude to people who have helped me to finish this dissertation. Firstly, I owe my gratitude to my supervisors, Professor Hiroyuki Arato and Professor Shun Chiyonobu, who patiently provided materials, supervision and direction with the project, and constantly stimulated my interest throughout my research.

I am very grateful to all the students from my laboratory, with whom I have discussed about our research, and helped me when I first arrived in Akita.

I am very grateful also to all the friends from Akita University, that supported me whenever I need.

I thank all my friends in Italy that, no matter the distance, listened me and supported me in all the moments.

I would like to thank all the Professors, Researchers, and Staff from Akita University that constantly help international students during their life in university. A special thank goes to my Japanese language professors, Sato Sensei, Ichishima Sensei and Hamada Sensei that taught me Japanese with passion and patience.

Lastly, I deeply dedicate this thesis to my Family and to my girlfriend Rina who always give me love, strength, and motivation.

This work was supported by the Ministry of Education, Culture, Sports, Science and Technology (MEXT) Doctorate Scholarship, obtained through the precious support of Akita University

TABLE OF CONTENTS

CHAPTER 1

Introduction

1.1 Aims and Methodologies

The area extending from Hokkaido to the northwestern side of Honshu island in Japan is where most of the Japanese oil and gas fields occur. In this area, Middle-Late Miocene sedimentary deposits composed by cherts, siliceous shales, diatomites, and hard mudstones, are considered the most productive horizons for hydrocarbons generation and have been studied by various geological investigations (Aoyagi and Omokawa, 1992; Ujiié, 1995; Kimura et al., 2004). Additionally, the Middle-Late Miocene formations deposition is strongly associated with the paleoenvironmental evolution of the Japan Sea. For this reason, the detailed description and analysis of these deposits give useful information to understand the paleoenvironmental conditions at the time of their deposition. The combination of data relative to the hydrocarbon potential and the paleoenvironmental conditions is the base for the development of current exploration projects and the prediction of the location for future exploration projects.

One of the main ways to evaluate the hydrocarbons generation potential of sedimentary successions is to assess the dispersed organic matter (OM) content and its thermal maturity. In this work, OM content (expressed as Total Organic Carbon or TOC) and the type and its thermal maturity were determined through the Rock-Eval pyrolysis method.

Paleoenvironmental conditions of sedimentary formations at the time of deposition were inferred from the visual description of cores and outcrop samples and the geochemical characterization of organic and inorganic fractions of sediments. Visual description of core and outcrop samples was focused on the identification of sedimentary structures such as laminations and bioturbations, that are extremely useful to hypothesize the degree of oxygenation of bottom water at the time of deposition (Savrda et al., 1984; Savrda and Bottjer, 1986; Tada et al., 1986). On the other hand, the geochemical composition of organic and inorganic fractions was determined through the CHNS and the X-Ray Fluorescence (XRF) analyses. Nitrogen and Sulfur content, from CHNS, are proxies for the surface water paleo-productivity and paleo-oxygenation in the bottom water. Major elements percentages from XRF define the composition of the detrital fractions in sediments and their provenance.

This thesis presents results and interpretations from the analysis of Miocene siliceous formations in three different research areas. In detail:

1) 29 samples from the Miocene succession of the Tsugaru Basin, from a 600 m-long portion of core drilled in Dake Hot Spring, near the Iwaki volcano in southwestern Aomori Prefecture (Chapter 3);
2) 18 samples from the Middle Miocene Onnagawa Formation, collected in the Sugisawa area, in the Akita Prefecture (Chapter 4);
3) 21 samples from the Middle Miocene Iwaya Formation, collected in the Gotanzawa area (Kamikoani village), in the Akita Prefecture (Chapter 4).

The age/lithological correlations between the formations in the two research areas allowed us to compare the organic richness, the thermal maturity, and the paleoenvironmental conditions. Additionally, the relationship between paleoenvironmental proxies and organic richness allowed us to understand the factors that possibly influenced the accumulation and preservation of organic matter in sediments.

1.2 Evolution of this study

The first months of the first year were spent reviewing the literature about the evolution of the Japan Sea and the geological setting in the study areas. Careful bibliographic research was dedicated to the geochemical methods and their applications to hydrocarbon potential and paleoenvironmental studies. At the same time, the preparation of samples for laboratory analysis started. The laboratory activity consisted of preparing powdered samples for the Pyrolysis Rock-Eval, CHNS, and XRF analyses. Samples from the Tsugaru Basin and Sugisawa and Gotanzawa areas were collected and analyzed with the Pyrolysis Rock-Eval method during the second semester of the first year. A preliminary interpretation of these results was performed to evaluate and compare the hydrocarbons potential and the thermal maturity in the two areas. The end of the first year was dedicated to describing the sedimentary lithofacies of core and outcrop samples. At the same time, to measure the variation of geophysical parameters throughout the different formations, Tsugaru Basin cores were analyzed through an MSCL core logger.

The second-year was dedicated to the analysis of the samples through the CHNS analyzer and XRF. The results were correlated with the lithofacies and organic content (TOC) variations. The optical observation of framboidal pyrite was performed to clarify the significance and distribution of sulfur in the studied formations.

The end of the second year and the third year were dedicated to the finalization of this study. The paleoenvironmental data in the three research areas were used to build a possible model of the evolution of the Sea of Japan.

During the development of this study, results were presented at two poster sessions and one oral session in national and international conferences: 1) IAS International Sedimentological Congress,

August 2018, Quebéc City, Canada; 2) Annual Meeting of the Sedimentary Society of Japan, April 2019, Osaka, Japan; 3) IAS Rome 2019, September 2019, Rome, Italy.

1.3 Outline of the thesis

Chapter 1 presents a general introduction of the main aims, the used methodologies, and the evolution of this research.

Chapter 2 introduces the theoretical aspects and analytical procedures of the applied methodologies.

Chapters 3 and 4 focus on the lithological and geochemical characterization of the sedimentary succession of the Tsugaru basin (southwestern Aomori Prefecture), of the Onnagawa Formation in Sugisawa area, and of the Iwaya Formation in Gotanzawa area (central Akita Prefecture). The two chapters will include results and discussions about the hydrocarbon potential of these formations, and about the paleoenvironmental conditions interpreted through geochemical proxies. For the Tsugaru basin succession, attention was given to the measurement of geophysical properties of the cored successions and the reconstruction of the thermal evolution of the Tsugaru basin, realizing a 1D thermal modeling.

Chapter 5 will present a discussion based on the comparison and correlation between the results in the two research areas and previous models. The final goal is to present a paleoenvironmental model of the Japan Sea during the Middle-Late Miocene.

Chapter 6 will contain the general conclusions of this work on the base of the main results obtained.

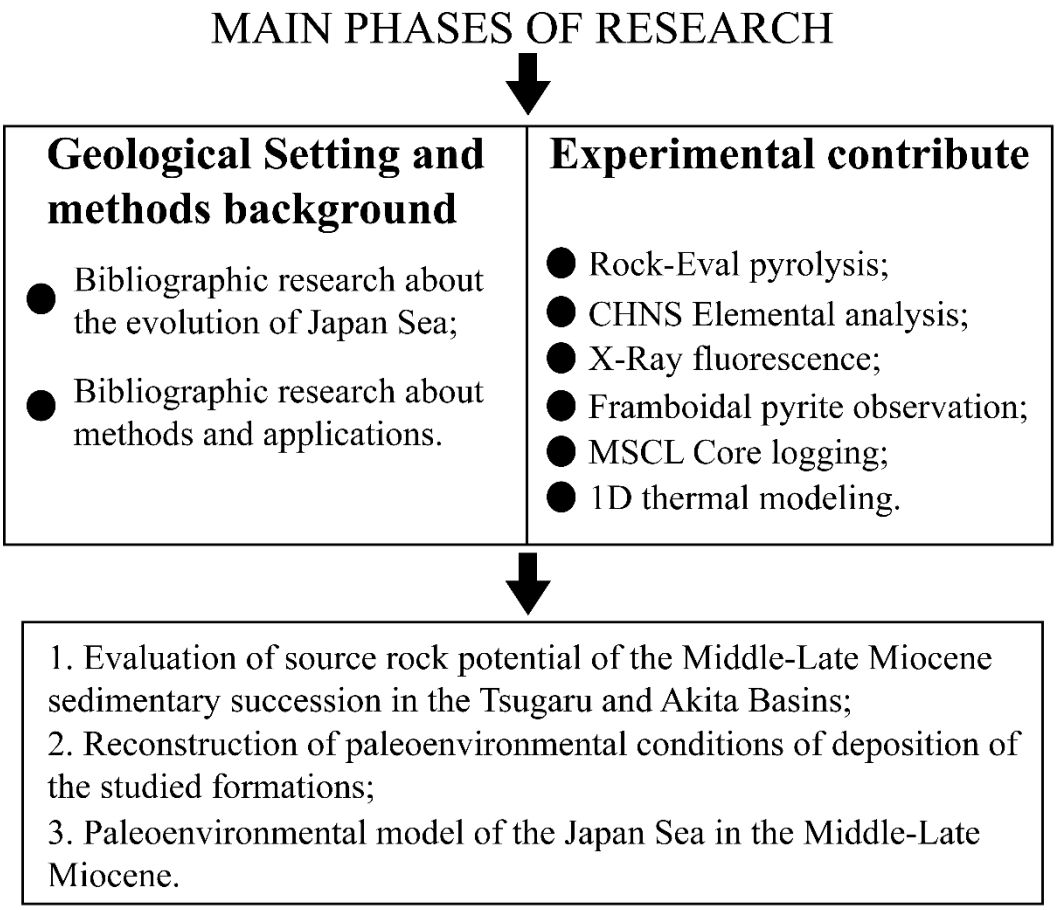

Figure 1.1. Diagram showing the study evolution

CHAPTER 2

Methodologies

In this chapter, each method's technical background (instruments and processes) and applications in this study will be explained.

.

2.1 Organic Geochemistry

2.1.1 Rock-Eval pyrolysis

The Pyrolysis Rock-Eval is a method developed by the French Institute of Petroleum (IFP). It is currently used by several scientists and oil & gas industry professionals to estimate the petroleum potential of sedimentary rocks by heating 50 to 70 mg of sample in an open pyrolysis system under non-isothermal conditions (Espitalié et al., 1977; Behar et al., 2001). The released hydrocarbons are monitored by a flame ionization detector (FID), forming two peaks called *S1* and *S2*, which represent the thermo-vaporized free hydrocarbons and the pyrolysis products respectively from the cracking of organic matter. The method is completed by combustion (oxidation) of the residual rock recovered after pyrolysis up to 850°C, under artificial air. During pyrolysis and combustion, released CO and

CO_2 are monitored through an infra-red cell. This complementary data acquisition enables determination of the organic and mineral carbon content of samples, labeled Total Organic Carbon (TOC) and Minimum Carbon (MinC), respectively. The most recent facility of Rock-Eval denominated Rock-Eval 6 (Figure 2.1) is characterized by:

1. Micro-ovens heating up to 800°C for pyrolysis and 850°C for oxidation with probes in contact with the sample;

2. Infra-red cells for a continuous on-line recording of CO2 and CO production during pyrolysis and oxidation;

3. An automatic sequenced sampler with a capacity of 48 samples.

4. Three different temperature programs denominated *Basic, Pure Organic Matters, and Reservoir*. These methods are applied respectively to Bulk Rock samples, Coals, and Reservoir samples (Lafargue et al., 1998; Behar et al., 2001).

In this study, the *Basic Method* for bulk rock samples was used (Figure 2.2). The pyrolysis stage of the Rock-Eval Basic cycle starts at an initial temperature of 300°C, which is kept for 3 minutes to release free hydrocarbons in the samples (*S1*, mg HC/g Rock). Thermal cracking of the potential hydrocarbon generating kerogen (*S2*, mg HC/g rock), and the oxygen-containing pyrolysable kerogen (*S3*, mg CO2/g rock) were released after automatic heating of 25°C/min until the maximum temperature of 650°C. The oxidation stage is performed between 300 and 850°C with a heating rate of 20°C/min to measure the residual inert organic carbon (*S4*, mg CO, and CO2/g rock and RC wt%) and a portion of the mineral carbon (MinC, wt%) (Behar et al., 2001; Kondla et al., 2017).

.

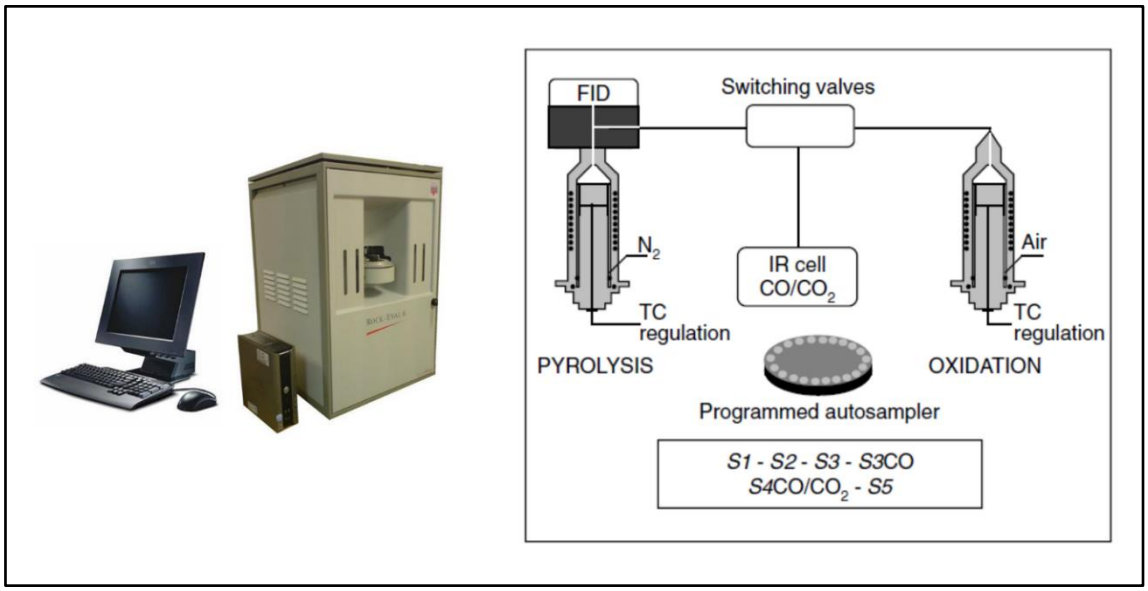

Figure 2.1. Rock-Eval 6 machine representation. On the left, the external appearance of the machine is shown. On the right, a simplified scheme of the machine structure is shown (from vinci-technologies.com).

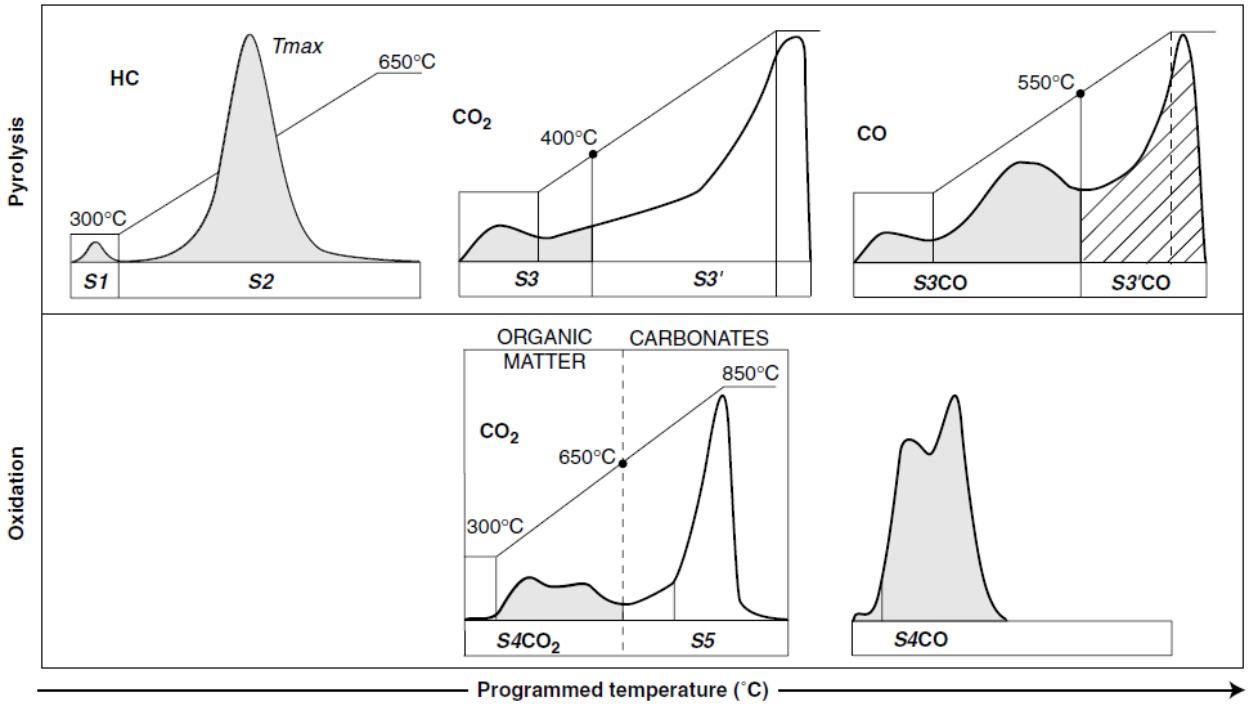

Figure 2.2. Schematic representation of the Rock-Eval Basic cycle used in this study (from Behar et al.,2001)

Some parameters acquired from Pyrolysis Rock-Eval are useful for assessing the features of sedimentary rocks, such as organic matter type and content, the thermal maturity, and the hydrocarbon potential:

TOC = weight percent (wt%) of organic carbon present in a certain amount of rock. According to the classification of Tissot and Welte (1984) and Peters (1986), the TOC value defines the organic richness of sedimentary rocks. Generally, rocks with a TOC lower than 0.5 wt% are poor source rocks. Rocks with a TOC comprised between 0.5 and 1.0 wt% are fair source rocks. Lastly, rocks with a TOC in the range of 1.0–2.0 wt% or more are considered good source rocks.

HI, and **OI** = Hydrogen Index (100*S2/TOC) and Oxygen Index (100*S3/TOC) are commonly used to distinguish the kerogen type associated with the organic matter. Determination of kerogen type is useful to understand the origin of organic matter, and whether a rock is prone to oil or gas generation or not. We can distinguish four different types of kerogen (Figure 2.3).

T_{max} = the maximum temperature is the temperature at which S2 reaches its maximum (Figure 2.4). This temperature depends on the maturity of the kerogen; the value of 435°C represents the limit between the immature and the oil-mature stages, while 455°C is the limit between the oil-mature and the gas-mature stages (Tissot and Welte, 1984). The T_{max} can be correlated to other indicators of thermal maturity, such as the Vitrinite Reflectance.

Kerogen Type (according to IFP)	*Principal biomass*	*Environment (general)*	*Original Hydrogen Index*	*Sulphur incorporation*	*Hydrocarbons generated and expelled (1)*
Type I	algae, bacteria	tectonic non-marine basin	**> 700**	low	**oils**
Type II	marine algae, bacteria	marine	**400-700**	moderate	**oils**
Type II S (sulphur rich)	marine algae, bacteria	marine, carbonatic environment	**400-700**	high	**oils**
Type III "H"	spores, pollens, cuticles, resin, lignin, bacteria	fluvial-lacustrine, coastal plains	**300-600**	low	**waxy oils**
Type III	lignin	coastal plains, deltaic, turbiditic	**50-250**	low	**gas** and **light oils** (**gas** traces when HI < 100)
Type IV	lignin	coastal plains, deltaic	**< 50**	low	none

(1) Also depending by kerogen maturity level.

Figure 2.3. Main kerogen types, origin and pyrolysis indexes (from Scotti, 2003)

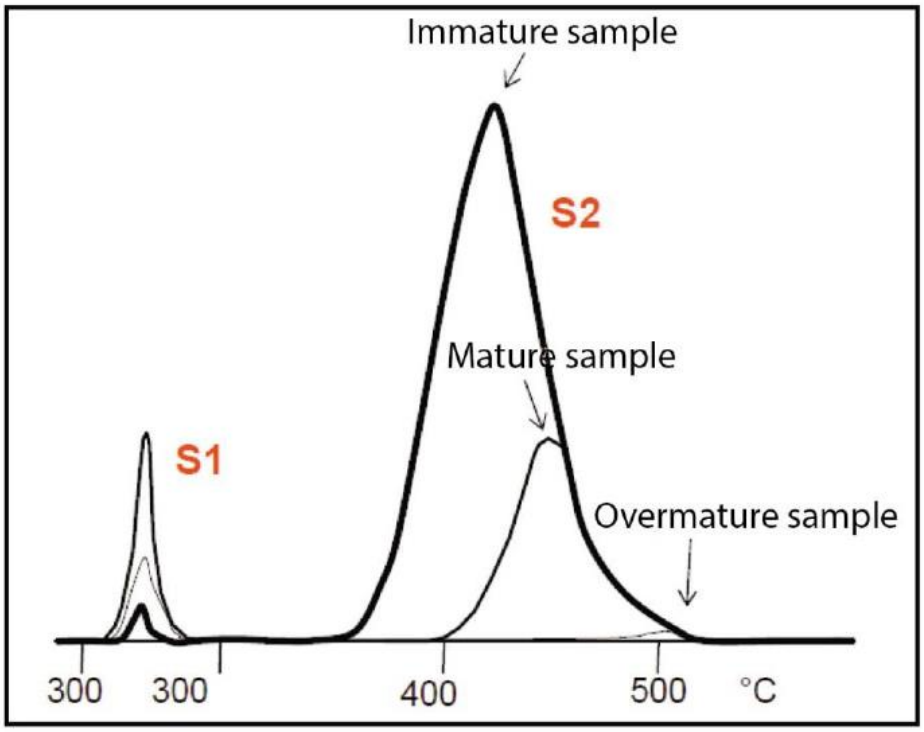

Figure 2.4. S1 and S2 peaks from pyrolysis. The image shows the change of S2 peak with the increase of the T_{max} and the thermal maturity.

2.1.2 CHNS Elemental Analysis

The CHNS Elemental Analysis is a method to quantify the content of C, H, N, and S chemical elements by a combustion process. In the combustion process (furnace at around 1000°C), carbon is converted to carbon dioxide, hydrogen to water, nitrogen to nitrogen gas or oxides of nitrogen, and sulfur to sulfur dioxide. The combustion products are swept out of the combustion chamber by an inert carrier gas such as helium and passed over a heated (about 600°C), high-purity copper. The copper is located at the base of the combustion chamber or in a separate furnace. The copper removes the residual oxygen and converts the nitrogen oxides to nitrogen gas. Lastly, absorbent traps filter the gases to leave carbon dioxide, water, nitrogen, and sulfur dioxide. Detection of the gases is carried out by Gas Chromatography separation or by infra-red and thermal conductivity cells (Thompson, 2008). In this study, the combustion analysis was performed using a CHNS628 analyzer producted by LECO (www.leco.com) (Figure 2.5). This instrument features custom software operated through an external PC, which controls the system operation and data management. Results are displayed in weight percent within 4-5 minutes.

Figure 2.5. LECO CHNS628 elemental analyzer used in this study (www.leco.com)

Weight percentages of C, N, and S elements are commonly combined and used as proxies for paleoenvironmental conditions in both marine and terrestrial environments. In this study, we are going to mention and apply the following parameters:

Total Carbon (TC) Estimate of TC contains information about both the Total Organic Carbon (TOC) from the organic matter fraction and the Total Inorganic Carbon (TIC) contained in carbonate minerals such as Calcite or Dolomite. Additionally, since the estimation of TOC and TIC (expressed as MinC) from the Pyrolysis Rock-Eval in some cases is affected by instrumental errors, the measurement of TC can be used to confirm these data.

Total Nitrogen (TN) Nitrogen, together with Phosphorus and Silica, are the essential nutrient elements for planktons, and their availability controls paleoproductivity in marine environments (Tyrrell, 1999; Tribovillard et al., 2006; Zeng et al., 2015). For this reason, Nitrogen content can be used as a proxy for surface water productivity.

Carbon to Nitrogen Ratio (C/N) The C/N ratio is used to distinguish between algal and land plant-plant origins of sedimentary organic matter (Prahl et al., 1980; Premuzic et al., 1982; Ishiwatari and Uzaki, 1987; Jasper and Gagosian, 1990; Prahl et al., 1994; Silliman et al. 1996, Meyers, 1997). According to Meyers (1997), algae have C/N ratios between 4 and 10, while land plants have C/N ratios of 20 and higher. The different types of organic matter are related to the type of depositional environment. However, the carbon and nitrogen values in marine environments can be affected by several processes, such as the degradation and decomposition of the organic matter and the mixing of different types of organic matter. These processes may lead to C/N ratios higher or lower than the theoretical value. Other authors (Keil et al., 1994; Prahl et al., 1994) report that the grain size of sediments may alter the C/N ratios. According to the authors, the high content of clay minerals in finer sediments can cause the adsorption of ammonia, resulting in the uptake of inorganic nitrogen and depression of the C/N ratio value.

Carbon to Sulfur Ratio (C/S) The Carbon to Sulfur Ratio (C/S) is a proxy created by Berner & Raiswell (1983) to assess the paleo-oxygenation conditions in the water column, in different environments. The Carbon-Sulfur relationship is determined by three processes: the organic matter decomposition, the sulfate reduction, and the pyrite formation. The occurrence and intensity of these processes are different in oxygenated (oxic) and not-oxygenated (anoxic-euxinic) environments. This difference results in sediments poor in sulfur, and high C/S ratio in the case of oxic environments, and sediments rich in sulfur, and lower C/S ratio in the case of anoxic-euxinic environments (Leventhal, 1983b; Berner & Raiswell, 1984; Berner, 1985). Berner & Raiswell (1983) state that oxic conditions can be defined by a C/S ratio of ~2.8. However, the ratio value depends not only on the

amount of Sulfur and Carbon delivered in the environment but also on the reactivity between Sulfur, Carbon, and Iron minerals to form pyrite.

2.2 Inorganic Geochemistry

2.2.1 X-Ray fluorescence

X-ray fluorescence (XRF) is one of the most well-established methods of routine estimation of geochemical compositions of rocks, sediments, and material earth samples (Oyedotun, 2018, and references attached therein). XRF is based on the wavelength-dispersive principle, which states that when excited by high-energy radiation, individual atoms emit a relative abundance of X-ray photons of energy or wavelength feature that can be estimated (Weltje & Tjallingii, 2008). A characteristic emission characterizes each chemical element; this emission is converted into the concentration of that element in the solid sample.

X-Ray fluorescence analysis was performed with a ZXS Primus II machine produced by Rigaku Corporation (Figure 2.6), in order to quantify the percentages of the ten major elements (Si, Ti, Al, Fe, Mg, Ca, Na, K, Mn, and P), after preparing 5-6 grams of sample powder.

Analysis of major elements in sedimentary rocks is applied to estimate the composition and provenance of the detrital fraction. Many older and present studies were successful in defining the provenance and the tectonic setting of detrital fraction in sediments through the combination of Ti, Al, Fe, Mg, Ca, Na, and K elements (Roser & Korsch, 1988; Hayashi et al., 1997). Additionally, studies from Nesbitt & Young (1982) and Fedo et al. (1995) defined two indexes denominated Chemical Index of Alteration (CIA) and Plagioclase Index of Alteration (PIA). These indexes are commonly used to assess the amount of chemical weathering at the source of sediments.

Figure 2.6. Rigaku ZXS Primus II machine used in this study for Major Elements analysis (www.rigaku.com)

2.2.2 Framboidal pyrite analysis

Framboids are one of the most common textures of pyrite found in sedimentary rocks. The presence of iron, sulfur, and organic matter in many marine environments favors the formation of framboidal pyrite. Additionally, marine sedimentary rocks are characterized by variable porosity, which offers space for the nucleation and growth of framboids (Sawlowicz, 2000). Traditionally, Raiswell & Berner (1985) and Wilkin et al. (1996) distinguished between two different types of framboidal pyrite: *syngenetic* pyrite, formed directly in the water column, and *early diagenetic* pyrite, formed in the pore space inside sediments (Figure 2.7). Syngenetic pyrites form at the oxic-anoxic interface under anoxic-euxinic conditions and then drop to the sediment surface when buoyancy cannot keep them suspended. The growth of syngenetic pyrite is restricted after burial; therefore, the original framboid's size is preserved. Thus, the diameter of syngenetic framboids tends to be always smaller than 5 μm (Wilkin et al., 1996; Liu et al., 2019). On the other hand, when oxic-dysoxic conditions characterize the water column, the oxic-anoxic interface falls at the water-sediment interface, and the diagenetic framboidal pyrite will grow inside the pores of the sediment. Therefore, the geometry and size of early diagenetic framboidal pyrite will be larger than 5 μm and will depend on the pore size of the sediments (Liu et al., 2019).

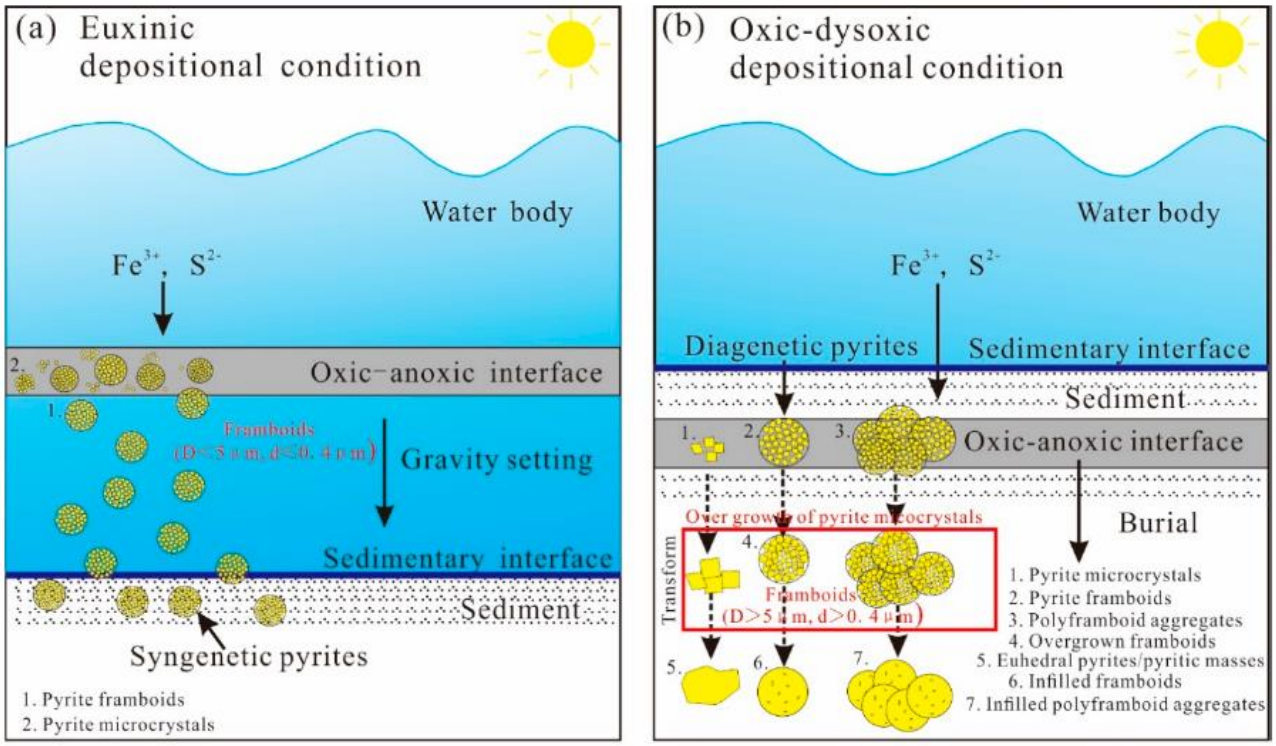

Figure 2.7. a) Mechanism of formation of the syngenetic pyrites under euxinic depositional conditions; b) Mechanisms of formation of the early diagenetic pyrites under oxic-dysoxic depositional conditions (From Liu et al., 2019).

Framboidal pyrite analysis can be easily performed through the observation of polished slides of rocks or thin sections, using standard reflected-light microscopy or scanning electron microscopy (SEM). In this study, observation of framboidal pyrite was made under reflected light, measuring the diameter of at least 100 framboids in each sample, following the method of Wilkin et al. (1996). Subsequently, framboidal pyrite mean diameter was correlated to the standard deviation of the data. Several authors (Raiswell, 1982; Wilkin et al., 1996, 1997; Wignall and Newton, 1998; Wilkin and Arthur, 2001; Wang et al., 2012; Wei et al., 2016) correlating the mean diameter of framboids to the standard deviation of size distributions, were able to detect the paleo-oxygenation conditions in the bottom water, confirming the solidity of this method (Figure 2.8). Therefore, this method was applied in this study as a paleoenvironmental geochemical proxy.

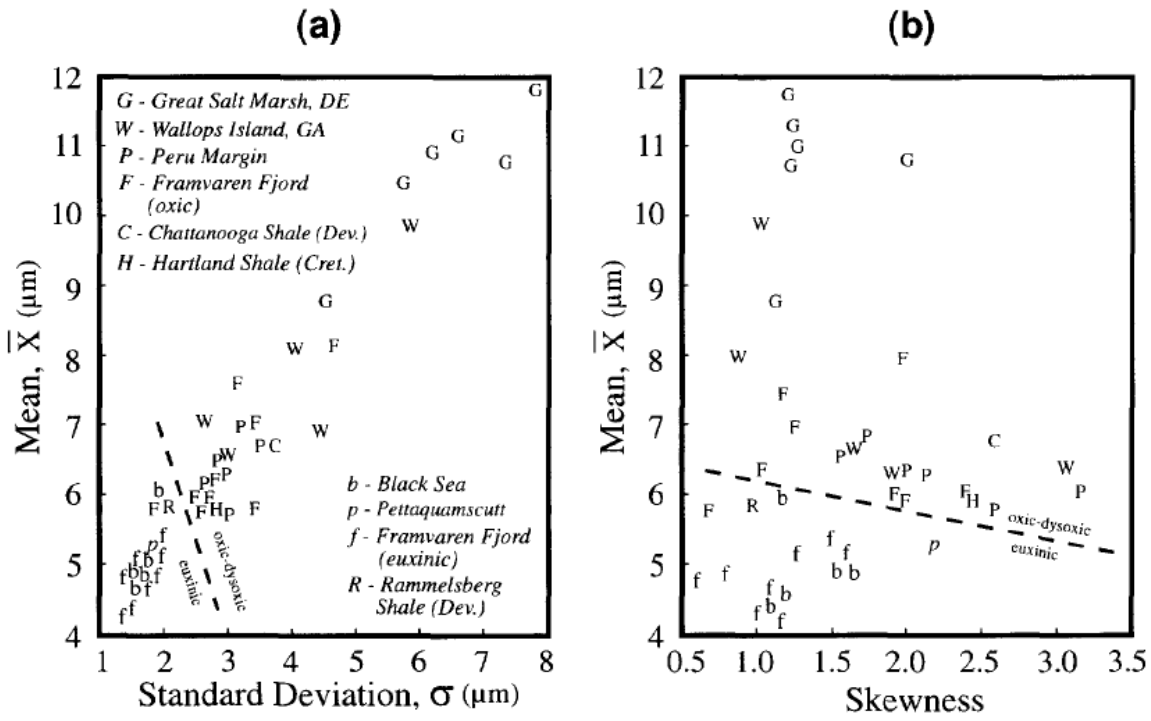

Figure 2.8. Plots for defining the paleo-oxygenation conditions in the bottom water using framboidal pyrite analysis (from Wilkin et al.,1996). a) Mean versus standard deviation of the framboid size distribution; b) Mean versus skewness of the framboid size distribution.

2.3 MSCL Core Logging

The Multi-Sensor Core Logger (MSCL) used in this study is a core measurement system produced by Geotek Limited. This system can be easily installed in buildings or field locations and can measure simultaneously and continuously multiple parameters from whole or split core samples (Figure 2.9).

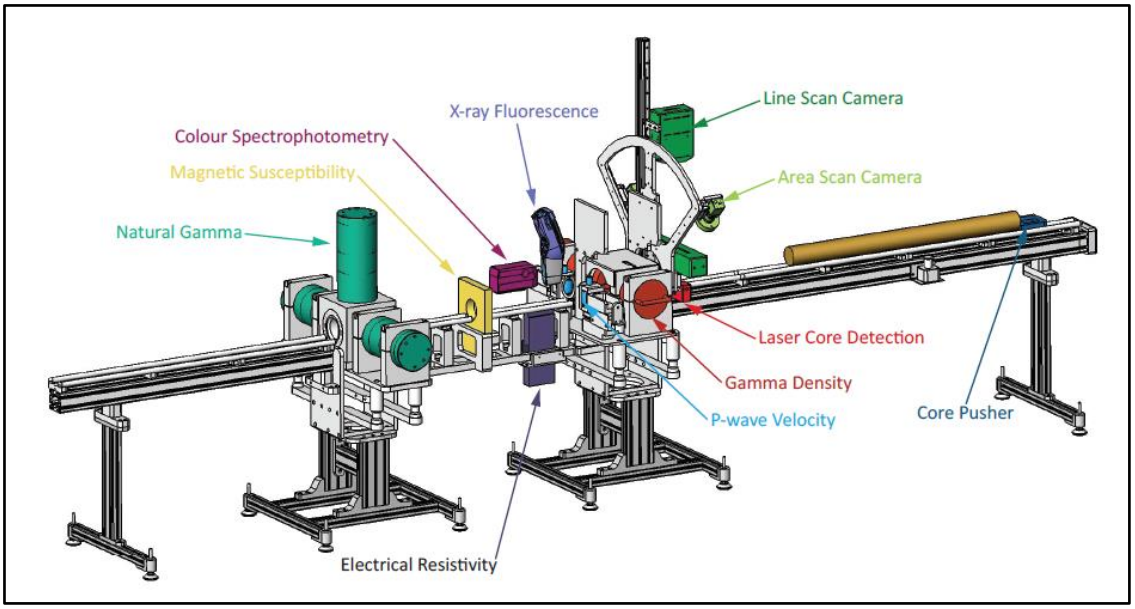

Figure 2.9. MSCL schematic layout in whole core horizontal logging mode (www.geotek.co.uk)

The MSCL machine installed in Akita University can measure the P-waves velocity, the electrical resistivity, the magnetic susceptibility, and the gamma ray of any type of lithology. In this study, we focused on P-wave velocity, magnetic susceptibility, and gamma ray.

2.3.1 P-waves velocity

P-waves (primary waves) are longitudinal or compressional waves, which means that the material they propagate through is alternately compressed and dilated in the direction of propagation. P-waves velocity depends on the density, and from the incompressibility and rigidity of the material. Therefore, P-wave velocity variations can define different lithologies. For example, Sandstones and Shales have a comparable range of velocity (2000–4000 m/s) but, carbonates and igneous rocks are characterized by a higher range of velocity (2000–6000 m/s for carbonates; 5000–6000 m/s for igneous rocks) (Telford & Sheriff, 1984). When converted to *interval transit time*, P-wave velocities can be used to estimate the bulk density and porosity of rocks (Asquith & Krygowski, 2004).

In this machine, the MSCL's P-wave transmitter produces a short P-wave pulse that propagates through the core and is detected by a receiver. The travel time of the pulse is measured and converted to velocity (m/s) from the operating software.

2.3.2 Magnetic susceptibility

Magnetic susceptibility is the degree of magnetization of a material in response to an applied magnetic field. When the magnetic susceptibility is positive, a material can be paramagnetic, ferromagnetic, ferrimagnetic, or antiferromagnetic. Alternatively, when the magnetic susceptibility is negative, the material is diamagnetic. All rocks are composed of minerals that have a different magnetic susceptibility. The magnetic susceptibility tends to increase in igneous rocks and volcano-clastic rocks. These rocks are typically rich in minerals with high Fe content. Therefore, magnetic susceptibility is a reliable property for distinguishing sedimentary and igneous portions throughout a core. Measurement of magnetic susceptibility is performed by MSCL through a loop sensor that generates a magnetic source. The operating software will record the susceptibility and convert it in χ adimensional units of magnetic susceptibility.

2.3.3 Gamma ray

Gamma ray measurement is used to quantify the natural radioactivity of rocks. Natural radioactivity in rocks is related to the presence of minerals that fix Potassium (K), Uranium (U) and Thorium (Th), and emit consistent gamma radiation. Because clay minerals fix high amounts of potassium, uranium, and thorium, the gamma Ray value can be used to discriminate between horizons

with low or high content in clay minerals. Additionally, clay minerals tend to be more abundant in finer lithologies; therefore, the gamma Ray is useful to distinguish shale formations, characterized by higher gamma ray response, from sandstones (Asquith & Krygowski, 2004). Lastly, other minerals, such as micas and feldspars, as well as organic matter, tend to fix considerable amounts of potassium and uranium, respectively; they also frequently contribute to the measured gamma ray value.

2.4 Thermal modeling

Basin and Petroleum System Modeling allows geoscientists to examine the dynamics of sedimentary basins to determine if past conditions were suitable for hydrocarbon generation and their migration to potential reservoirs.

Basin modeling allows to assess:

1) The burial history of the basin (back-stripping)
2) The thermal history of the basin
3) The maturity history of the source rocks.

In this work, basin modeling was performed using the *PetroMod-1D* software of Schlumberger. This software allows the reconstruction of the burial and thermal evolution of sedimentary sequences through various steps:

1) Input Data Setup: in this phase, the user inserts data about the top and bottom depths of single formations, type of lithology, deposited and/or eroded thickness, interval of deposition, and TOC. When the user selects the type of lithology, the software associates directly the data of porosity, permeability, and thermal conductivity contained in the library;
2) Boundary Conditions Setup: in this phase, the user selects the global mean surface temperature in the geological interval of interest, the heat flow variation (in mW/m^2), and the paleowater depth model;
3) Run of the simulation: the final product of the simulation will be the 1D burial model. The model can be modified by adding temperature information, to assess the thermal evolution and the maturation of possible source rocks. By default, Petro Mod is using the *EasyRo%* kinetic model of Sweeney and Burnham (1990). This model converts the data of temperature to Vitrinite Reflectance.

CHAPTER 3

Sedimentary and geochemical characterization of Neogene formations in the Tsugaru Basin, Japan by means of DTH27-1 well sediment analysis

3.1 Introduction

The area extending from Hokkaido to the northwestern side of Honshu island is where most of Japan's oil and gas fields are located. In the Aomori region, Middle-Late Miocene siliceous sedimentary rocks are considered the most productive horizons for hydrocarbons generation and have been studied by various geological investigations (Tada et al., 1986; Jingu and Ujiié, 1990; Aoyagi and Omokawa, 1992; Ujiié, 1995). These studies integrated sedimentological data with geochemical data to assess the hydrocarbon potential of these formations and to understand the factors that determined the accumulation and preservation of organic matter in sediments; these assessments have also focused on the Japan Sea's evolution. However, in some areas of the Aomori region, these studies have not yet been performed, and minimal subsurface data is available.

This chapter reports results from the analyses of the Miocene sedimentary succession in the southwestern Aomori region. The Pyrolysis Rock-Eval analysis was performed on samples from the entire Miocene sequence cored by the DTH27-1 well, to define the hydrocarbons potential and the thermal maturity in this area. These results have also been applied to calibrate the 1-D burial/thermal model of the Tsugaru Basin. Secondly, geophysical and sedimentological data have been correlated to define the lithological variations throughout the core. Lastly, through the interpretation of organic and inorganic geochemical proxies, a paleoenvironmental reconstruction of the Tsugaru Basin during the Middle-Late Miocene has been performed. Moreover, the factors that controlled the accumulation and the preservation of the organic matter were evaluated.

3.2 Geological Setting

The Tsugaru Basin is a Neogene sedimentary back-arc basin located at the northwestern side of Honshu island in Japan (Jingu and Ujiié, 1990; Ujiié, 1995) (Figure 3.1). A simplified geological map and a stratigraphic column of the outcropping formations in the southern sectors of the Tsugaru Basin are shown in Figures 3.2 and 3.3. The basin comprises a Neogene to Quaternary succession composed of non-marine, deep-marine, and volcanic deposits (Jingu and Ujiié, 1990; Ujiié, 1995). This succession is geologically correlated to other successions distributed in various basins of northern Japan, and these successions all provide a record of the evolution of the Japan Sea from approximately 23 Ma to present (Iijima et al., 1988).

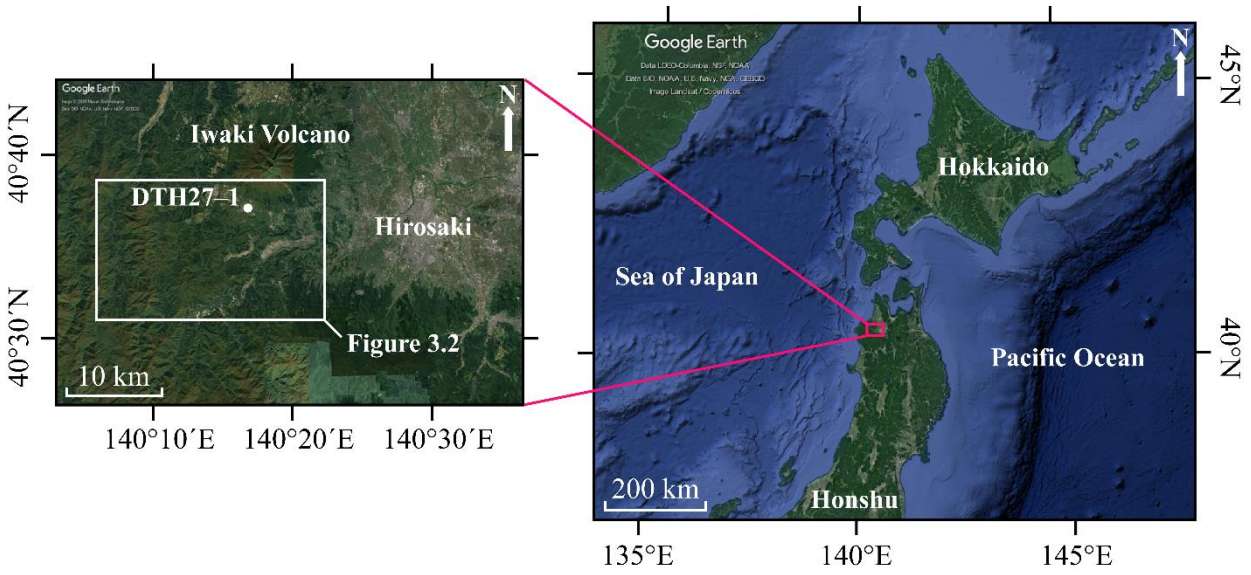

Figure 3.1. Satellite images of Japan. The pink square indicates the Tsugaru Basin area in which the DTH27-1 well used in this study is located. From Google Earth Pro (left image: Image © 2020 Maxar Technologies, Data SIO, NOOA, U.S: Navy, NGA, GEBCO; right image: Image Landsat/Copernicus, Data LDEO-Columbia, NSF, NOOA, SIO, U.S. Navy, NGA, GEBCO)

The overall thickness of the Neogene part of the succession is variable throughout the area, ranging from about 500 m in the southwestern sectors of the basin to approximately 3000 m in the center of the basin, as reported from the MITI Nishi-Tsugaru Oki borehole off the west coast of the Tsugaru Peninsula (Iwasa, 1962; Kato, 1992; Ujiié, 1995).

The base of the Tsugaru Basin succession in the southern sectors is represented by the deposition of pyroclastic rocks mixed with continental deposits (Odose Formation), and by andesitic tuffs and tuff breccias that are occasionally interfingered by marine deposits (Tanosawa Formation) (Ujiié, 1995). These units are respectively correlated with the Monzen Formation and with the Daijima Formation as well as the lower part of the Nishikurosawa Formation outcropping at the Oga Peninsula in the Akita region (Iijima et al., 1988). The deposition of the Odose and Tanosawa Formations, based on biostratigraphic data, occurred between 20 and 15 Ma (Iijima et al.,1988; Nemoto and Wakabayashi, 1995; Hanagata and Miwa, 2002).

Substrate units are followed by the siliceous mudstones of the Odoji Formation that were deposited between 15 Ma and 9 Ma (Nemoto and Wakabayashi, 1995). This and other correlated formations were deposited in the same period during an extremely rapid phase of subsidence that caused the deepening of the sea (Iijima et al., 1988; Tada, 1991, 1994). Some authors (Ingle et al., 1990; Tada, 1991, 1994) suggested that these deposits reflected a high primary bio-productivity in surface waters. At the same time, bottom waters were characterized by oxygen-deficient conditions (Matsuzaki et al., 2018, and references therein).

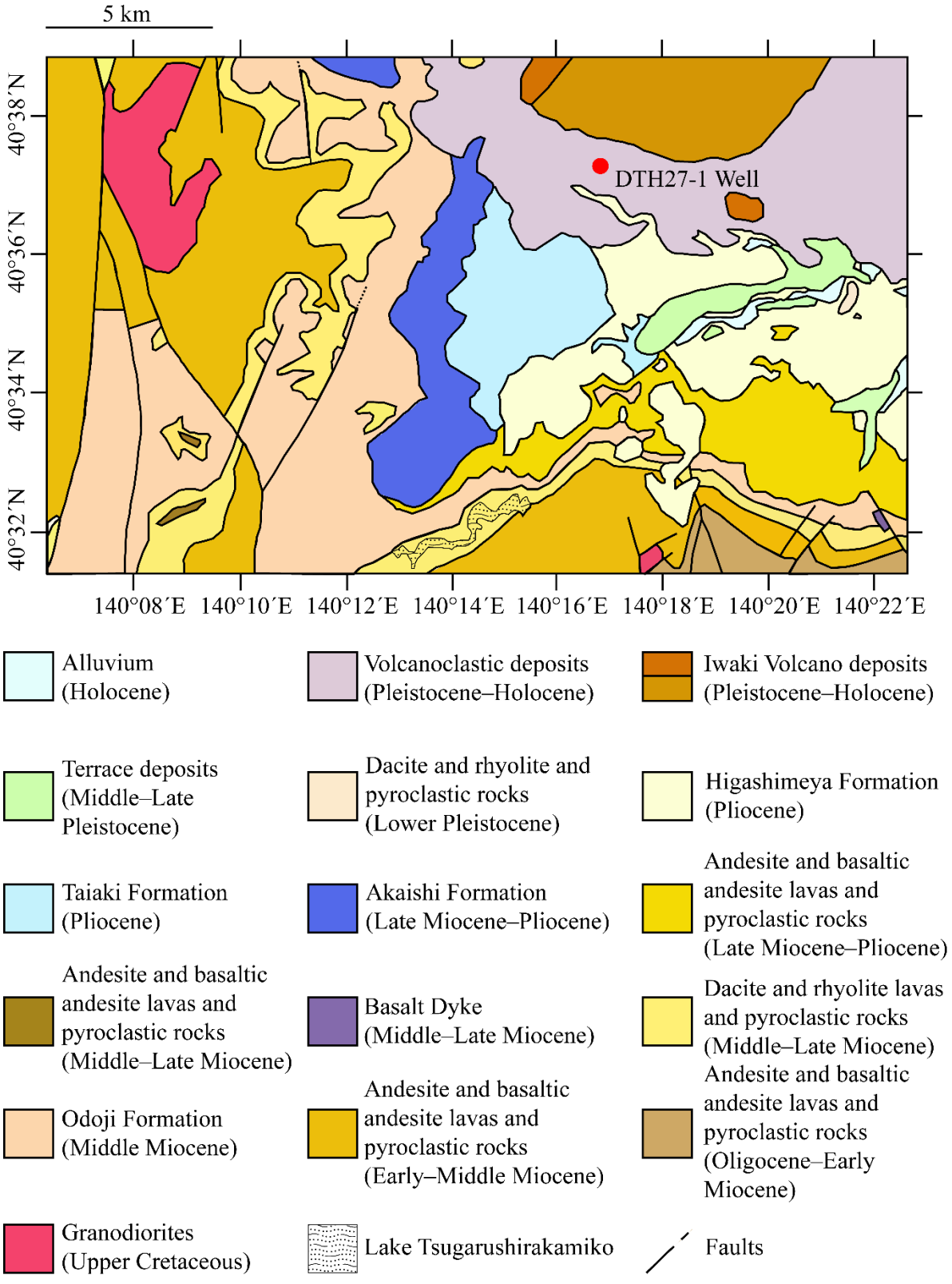

Figure 3.2. Geological map of the study area with the outcropping formations, main tectonic elements, and topographic model. The red point indicates the location of the DTH27-1 well. From Geological Survey of Japan Web Page (https://gbank.gsj.jp/geonavi/geonavi.php#12,40.62056,140.26143).

Tada (1994) suggested that oxygen-poor water was the result of the inflow of Oxygen Minimum Zone (OMZ) water from the North Pacific through a 500–1000 m deep sill. The Middle-Late Miocene subsiding phase was followed by a regressive phase associated with tectonic uplift. The compressional phase started at 7 Ma (Jolivet and Tamaki, 1992; Sato, 1994) and caused the progressive shoaling of the sill that connected the Japan Sea with the North Pacific (Tada, 1994; Matsuzaki et al., 2018). Some authors (Ingle et al., 1990 and references therein) have posited that these processes may have isolated portions of the Japan Sea, creating several shallow water basins. Additionally, the shoaling of the sill channel limited the inflow of OMZ water from the North Pacific, causing oxic conditions in the bottom water. The diatomaceous sediments mixed with acidic volcanic tuffs of the Akaishi and Taiaki Formations, deposited between 7 Ma and 3 Ma (Hanagata & Miwa, 2002), record this period. The Taiaki Formation is separated by an unconformity from the youngest units of the basin succession. This unconformity marks the beginning of an erosional process and a transition to terrestrial volcano-clastic sedimentation. This transition resulted in the deposition of tuffaceous siltstones and sandstones in the Pliocene (Higashimeya Formation) and acidic volcanic and volcano-clastic deposits associated with the activity of the Iwaki volcano in the Pleistocene–Holocene (Jingu & Ujiiè, 1990).

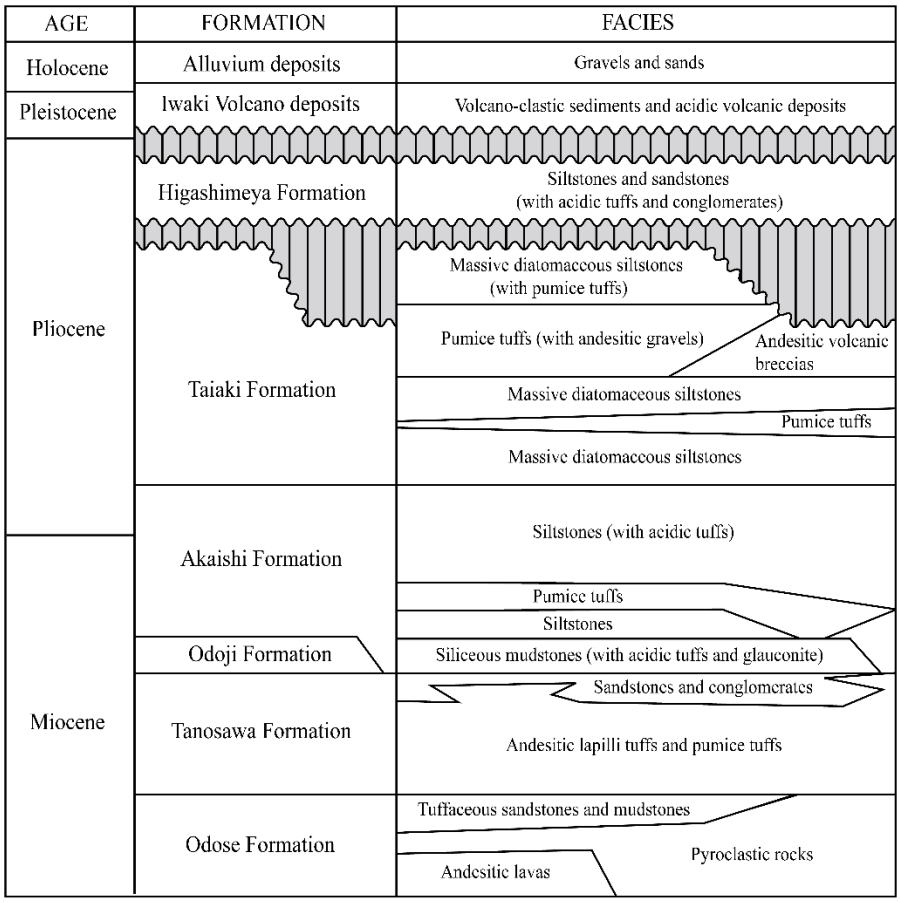

Figure 3.3. Schematic columnar section of the Tsugaru Basin succession (modified from Jingu and Ujiiè, 1990). Grey areas indicate a stratigraphic hiatus.

3.3 Materials

Samples analyzed in this work derive from a 1.5 kilometers-long well (DTH27-1) drilled and collected from August 2014 to February 2015 at Dake Hot Spring, near the Iwaki volcano in western Aomori Prefecture (Figures 3.1 and 3.2). The well covers the geological record of the Tsugaru basin from the Miocene through the Pliocene into the Quaternary. In descending order, the well intercepted 300 m of Quaternary volcanoclastic sediments, lava, and tuff breccias (Iwaki Volcano Sequence), 210 m of Pliocene tuffaceous siltstones (Higashimeya Formation), 90 m of Pliocene diatomaceous siltstones and 35 m of acidic pumice-tuffs (Taiaki Formation), 441 m of Pliocene to Late Miocene diatomaceous siltstones (Akaishi Formation), approximately 21 m of Middle Miocene siliceous mudstones (Odoji Formation), 370 m of Middle Miocene andesitic lapilli tuffs with intercalations of tuffaceous siltstones, siliceous mudstones, sandstones and conglomerates in the lowest part (Tanosawa Formation), and approximately 30 m of Early to Middle Miocene conglomerates alternated with tuffaceous sandstones and mudstones as well as small coaly horizons (Odose Formation).

In this study, the portion of the core between 900 m and 1500 m was analyzed (Figure 3.4). Specifically, the lithological descriptions, analysis of the geophysical parameters, and definition of hydrocarbons potential and thermal maturity were extended throughout all the core. On the other hand, the paleoenvironment interpretation by geochemical proxies was limited to the portion of the core between 900 m and 1100 m (Akaishi and Odoji Formations) to have a direct correlation with the formations of the same age in the Akita region.

3.4 Results

3.4.1 Lithofacies description

The analyzed interval of the DTH27-1 well was subdivided into different lithofacies based on lithology, grainsize, and geophysical properties.

3.4.1.1 Akaishi and Odoji Formations

The Akaishi Formation, which ranges from 900 m to 1076.m, was subdivided into two main lithofacies, named A and B (Figure 3.5). Lithofacies A characterizes the Akaishi Formation from 900 m to 1000 m, and it consists of light olive-gray massive diatomaceous siltstones (Figure 3.6a). Moderate to high bioturbation occurs throughout the unit, in the form of several horizontal millimeter-scale burrows. This unit is locally interlayered by light olive-gray massive levels of tuffaceous siltstones (Figure 3.6b); from 981 m to 1000 m, the unit is interlayered by yellowish-gray clast-supported tuff breccias. Tuffaceous siltstone levels are characterized by the occurrence of decimetric sub-levels composed of poorly sorted lapilli-sized fragments dispersed in a siltitic matrix (Figure

3.6b). On the other hand, the tuff breccias are characterized by centimetric to decimetric clasts of mixed volcanic and sedimentary origin.

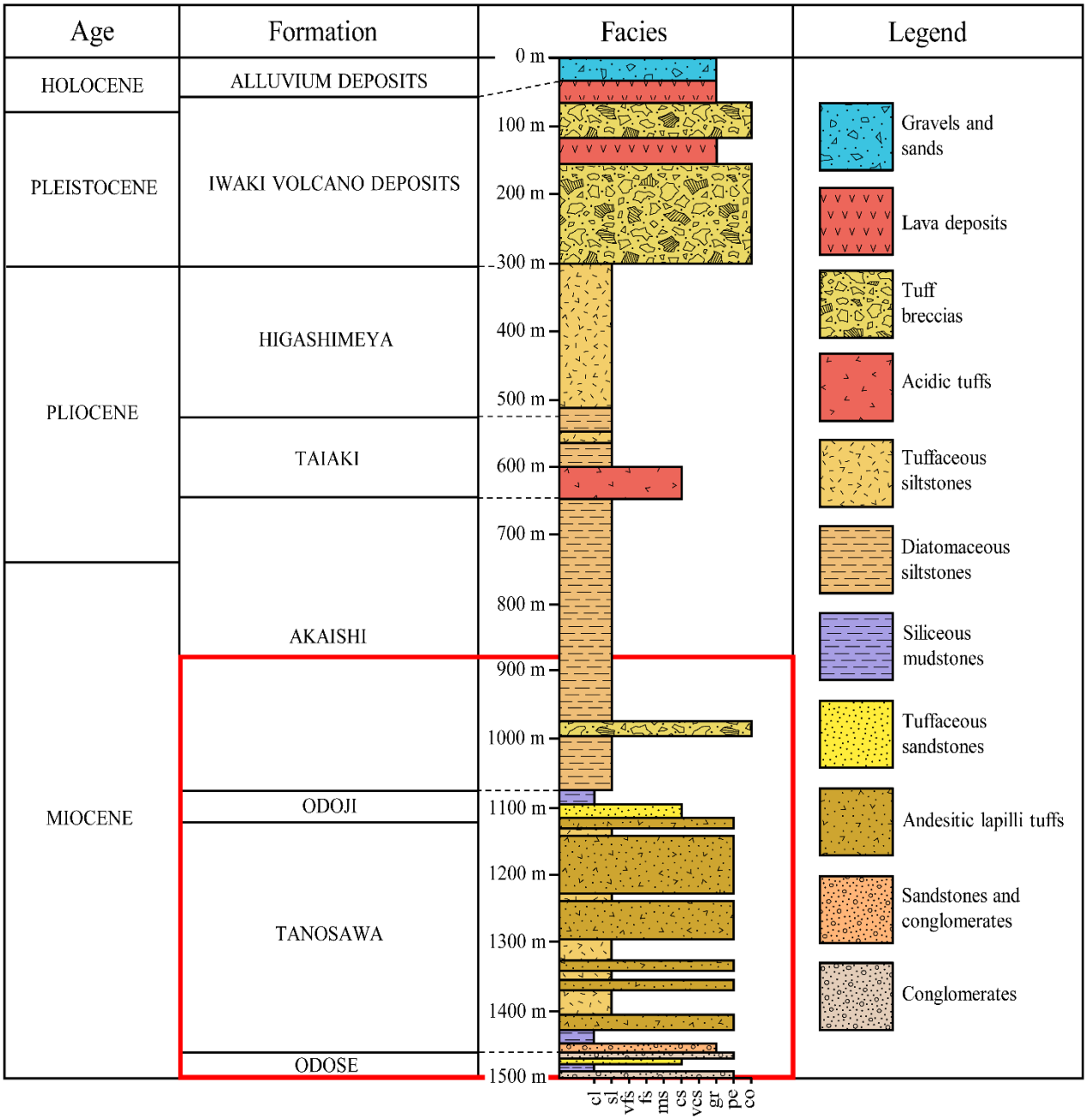

Figure 3.4. Stratigraphic column of the DTH27-1 well. The outlined red area is the portion of the core that will be described and analyzed in this study.

Geophysical parameters are variable in the different lithologies. The P-wave velocity ranges from 1500 m/s to 3500 m/s in the diatomaceous siltstones portion and increases to 3500 m/s to 6000 m/s in the tuffaceous siltstones and breccias (Figure 3.5). Magnetic susceptibility is exceedingly low in most of the siltstones, with values of about 20 (x 10^{-5}SI), but it tends to increase to values of 100–200 (x 10^{-5}SI) between 960 m and 980 m. On the other hand, magnetic susceptibility is much higher in the tuffaceous siltstones and breccias, with values in the range of 80 to 2000 (x 10^{-5}SI) (Figure 3.5).

Lastly, the gamma ray response in API degrees from 50 to 90 in the siltstones, and from 35 to 70 in the tuffaceous siltstones and breccias (Figure 3.5).

Lithofacies B ranges from 1000 m to 1076 m, and it represents the lower part of the Akaishi Formation. It is composed exclusively by light olive-gray massive diatomaceous siltstones (Figures 3.5 and 3.6c). Also, this lithofacies is characterized by moderate bioturbation in the form of burrows.

The Odoji Formation, which ranges from 1076 m to 1097.4 m, presents a single lithofacies (lithofacies C) (Figure 3.5). It consists of massive to very weakly laminated siliceous mudstones (Figures 3.7 and 3.8). Throughout the entire section, siliceous mudstones are characterized by sparse bioturbations and by an alternation of lighter and darker levels. The darker levels are generally dark gray to olive-gray, while the lighter levels color varies from light olive to yellowish-gray (Figure 3.7). The thickness of dark and light bands varies from a few centimeters to several decimeters, and the frequency of darker bands is slightly higher than the frequency of lighter bands (Figure 3.7). The P-wave velocity of this lithofacies ranges between 2700 m/s and 4000 m/s, and the magnetic susceptibility is almost 0 (x 10^{-5}SI), while gamma ray response is the highest in all the analyzed core, with values between 90 and 270 API degrees (Figure 3.5).

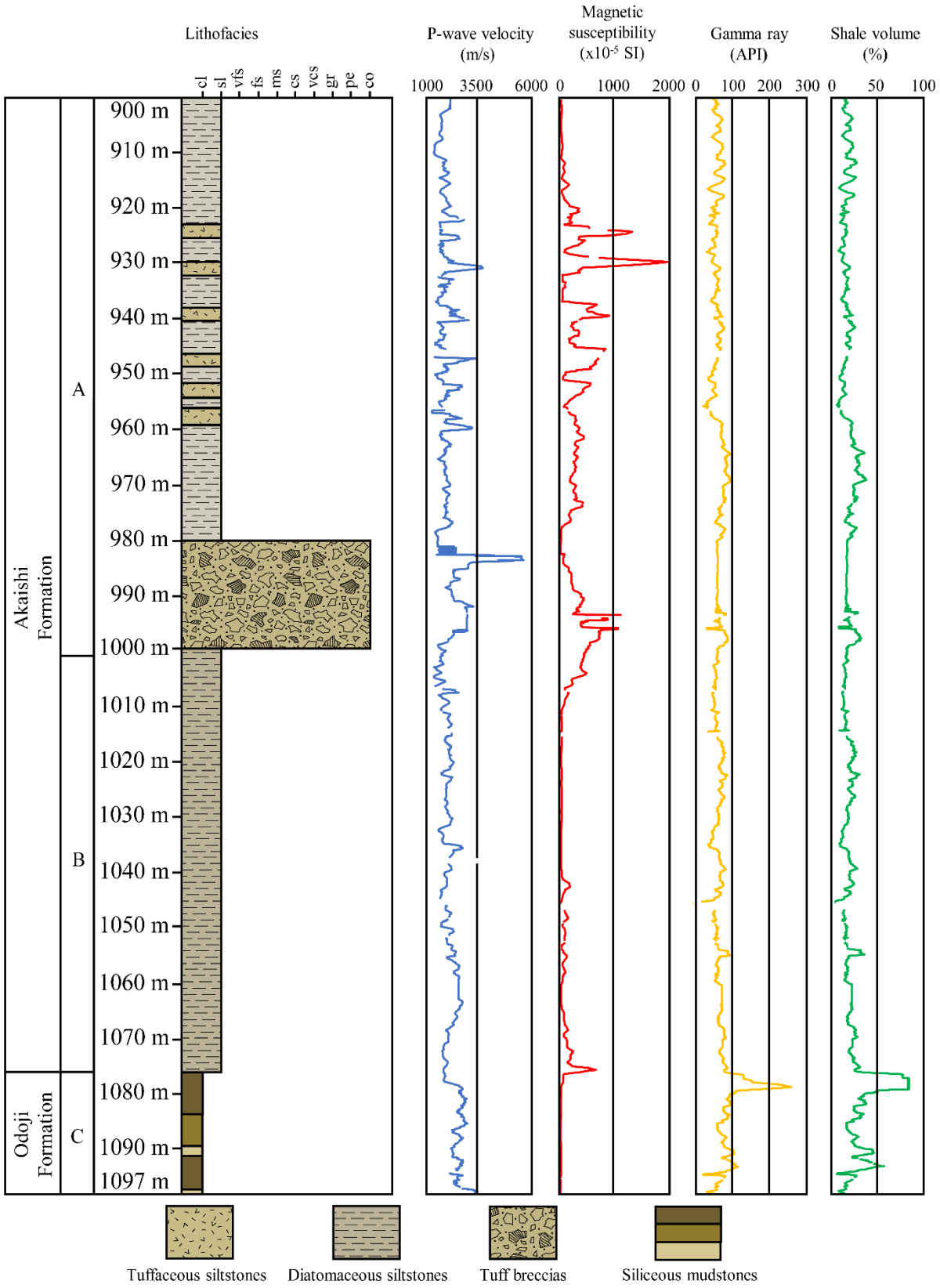

Figure 3.5. Columnar section of analyzed interval in the DTH27-1 well (left) and stratigraphic variations of the p-wave velocity log, magnetic susceptibility log, natural gamma ray log, and shale volume log. The grain size fraction abbreviations are as follows: cl, clay; sl, silt; vfs, very fine sand; fs, fine sand; ms, medium sand; cs, coarse sand; vcs, very coarse sand; gr, granule; pe, pebble; co, cobble.

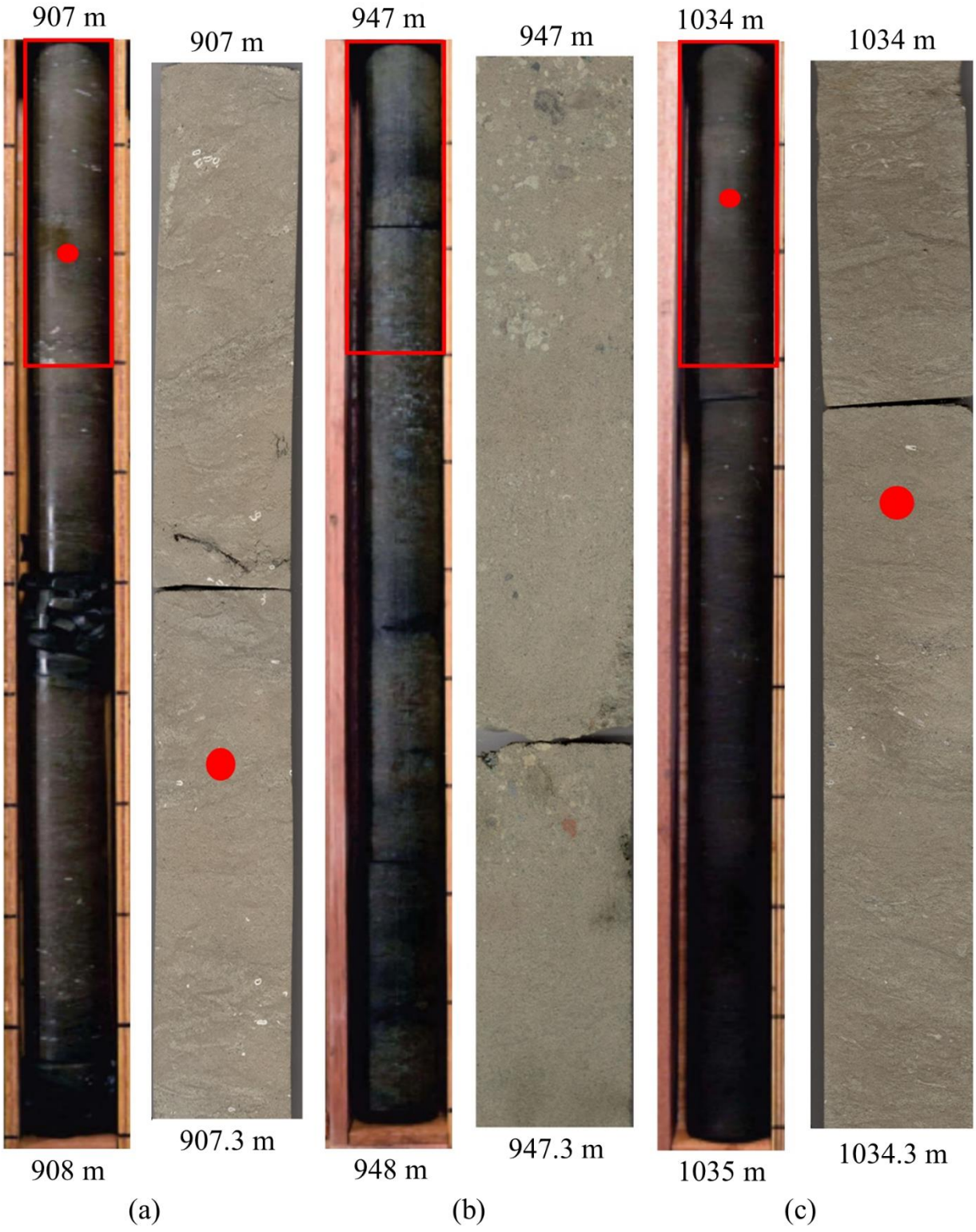

Figure 3.6. Photos of split-core sections of the Akaishi Formation at different depths. (a) Massive bioturbated diatomaceous siltstones from the upper part of the Akaishi Formation; (b) Tuffaceous siltstones from the upper part of the Akaishi Formation; (c) Massive bioturbated diatomaceous siltstones from the lower part of the Akaishi Formation. Red points indicate the positions of some of the analyzed samples.

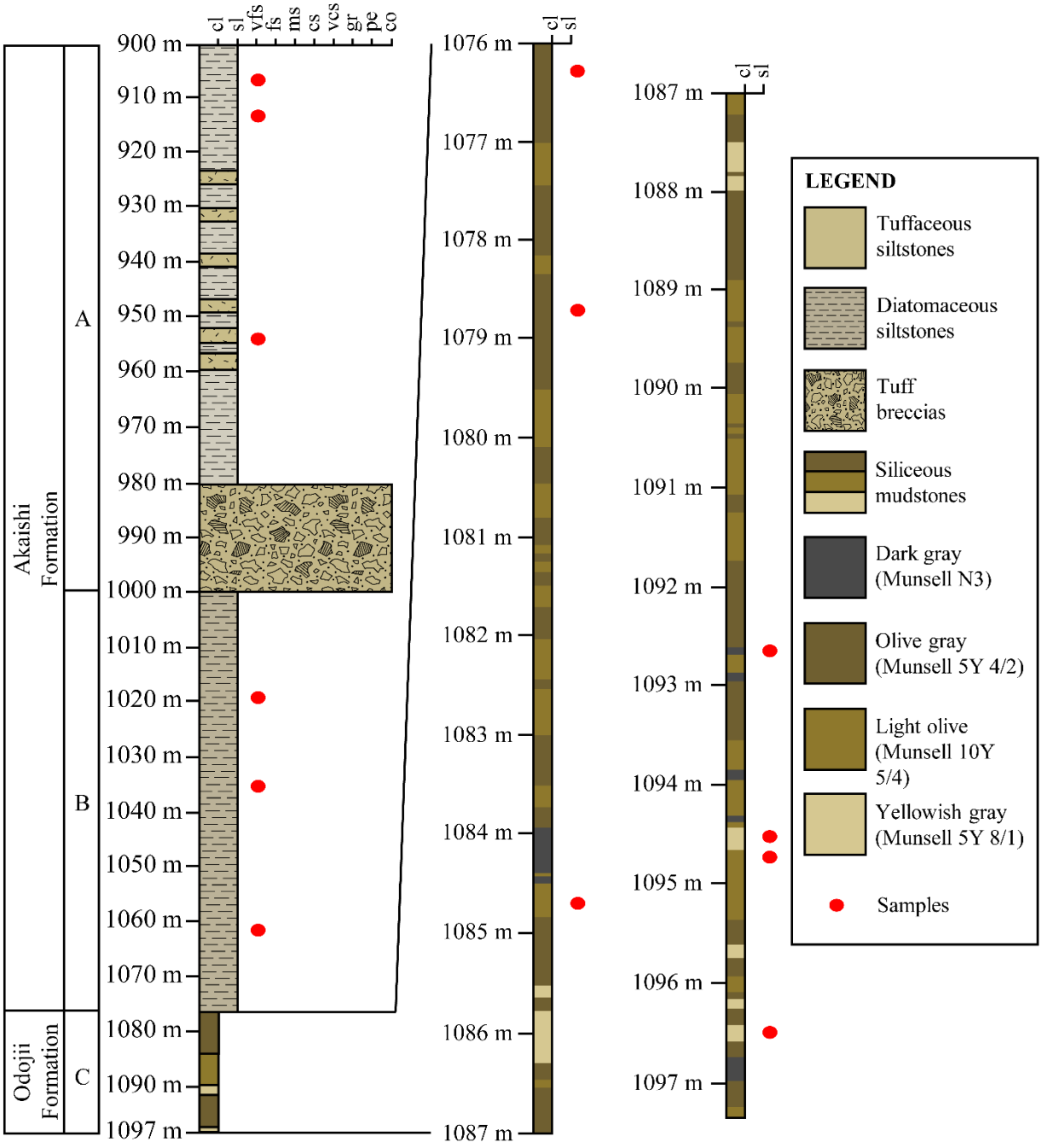

Figure 3.7. Lithostratigraphy of the analyzed interval in the DTH27-1 well. The left column is the stratigraphic column of the entire analyzed interval. The central and right columns show the lithofacies of the Odoji Formation in detail. The alternation of light and dark levels in the Odoji Formation is represented by the chromatic variations recognized during the core visual description. Red points in both the stratigraphic columns indicate the horizons of Rock-Eval samples. The grain size fraction abbreviations are as follows: cl, clay; sl, silt; vfs, very fine sand; fs, fine sand; ms, medium sand; cs, coarse sand; vcs, very coarse sand; gr, granule; pe, pebble; co, cobble.

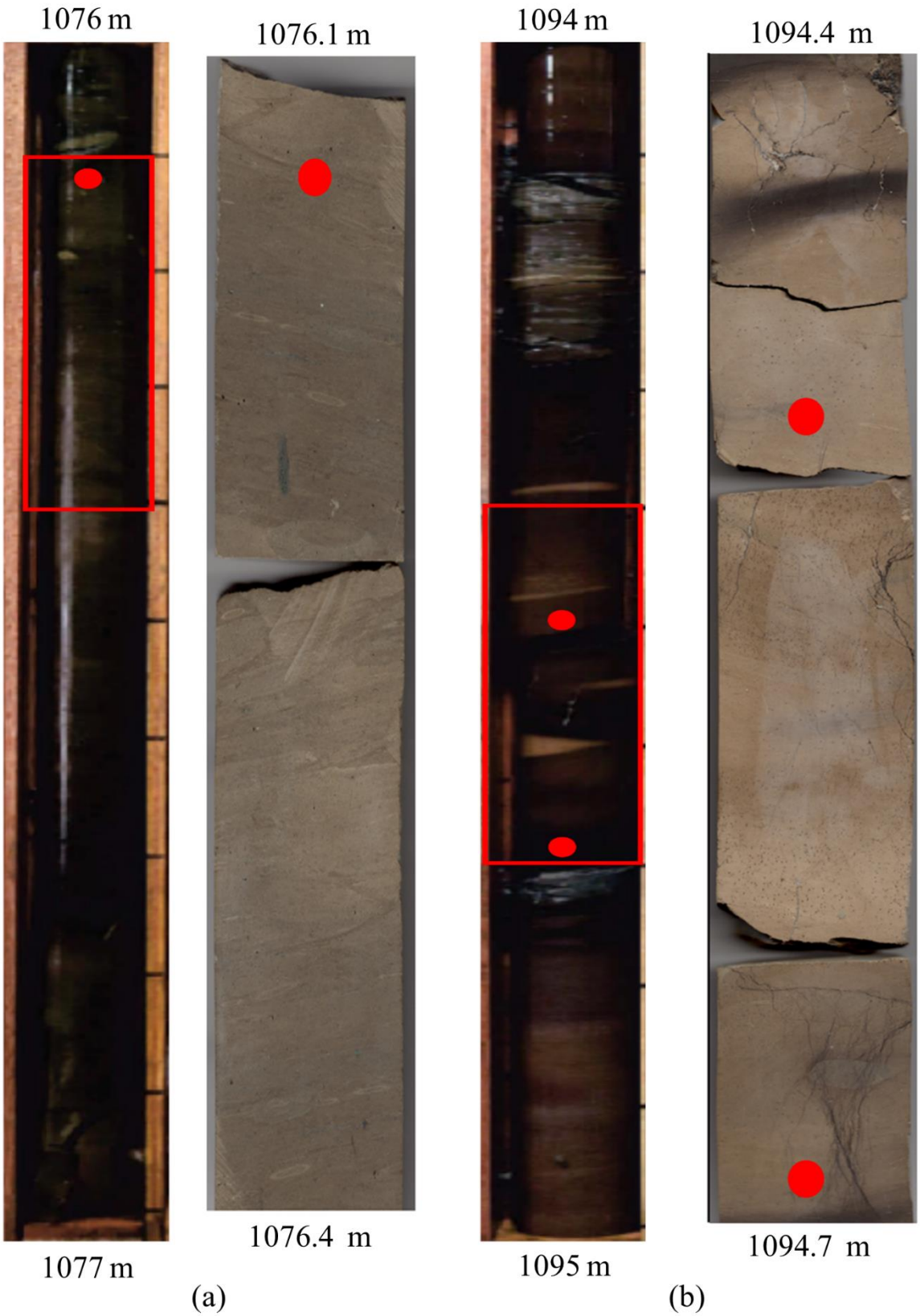

Fig. 3.8. Photos of split-core sections of the Odoji Formation. (a) Olive-gray siliceous mudstones from the upper part of the Odoji Formation; (b) Alternation of olive-gray and light olive siliceous mudstones from the lower part of the Odoji Formation. Red points indicate the positions of some of the analyzed samples.

3.4.1.2 Tanosawa and Odose Formations

The Tanosawa Formation, which ranges from 1097.4 m to 1467 m, is composed mostly of light gray andesitic lapilli tuffs (Figure 3.9). The lapilli tuffs are characterized by rounded centimetric clasts of mixed volcanic and sedimentary origin (Figure 3.11a). The lapilli tuffs are frequently interlayered by light gray tuffaceous siltstones levels with variable thickness from few meters to 10 meters (Figure 3.11b).

From 1440 m to 1467 m, the Tanosawa Formation is characterized by a lithological change from tuffaceous deposits to sedimentary deposits. This portion is composed of dark gray mudstones (Figure 3.11c), and by sandstones with gravel-sized clasts and rich in molluscan fragments (Figure 3.11d).

Geophysical parameters are variable in the two portions. P-wave velocity ranges from 2000 m/s to 4000 m/s in the tuffaceous siltstones levels, while it increases until 6500 m/s in the lapilli tuffs. On the other hand, the portions of mudstones and sandstones show a P-wave velocity of 4000 m/s and 3000 m/s, respectively (Figure 3.9). Magnetic susceptibility is very high in the lapilli tuffs and the tuffaceous siltstones, reaching values of 2500 (x 10^{-5}SI). On the other hand, the sandstones portion shows a positive value of magnetic susceptibility (100-200 x 10^{-5}SI); the mudstones portion shows low values. The gamma ray, except for the portion between 1100 m and 1120 m, is generally lower than 70 API degrees (average of 30–40 API degrees).

The Odose Formation is composed of sandstones and sandstones with gravel-sized clasts locally interlayered by dark coaly levels. Both sandstones and coaly levels are rich in woody fragments (Figures 3.10 and 3.11e).

The P-Wave velocity shows values between 1500 m/s and 4000 m/s. The Magnetic susceptibility is generally lower than 100 x 10^{-5}SI, except in one portion where it reaches 150 x 10^{-5}SI. Gamma ray response is higher than 50 API degrees in all the formation, except in some portions where the gamma ray is higher than 100 API degrees (Figure 3.10).

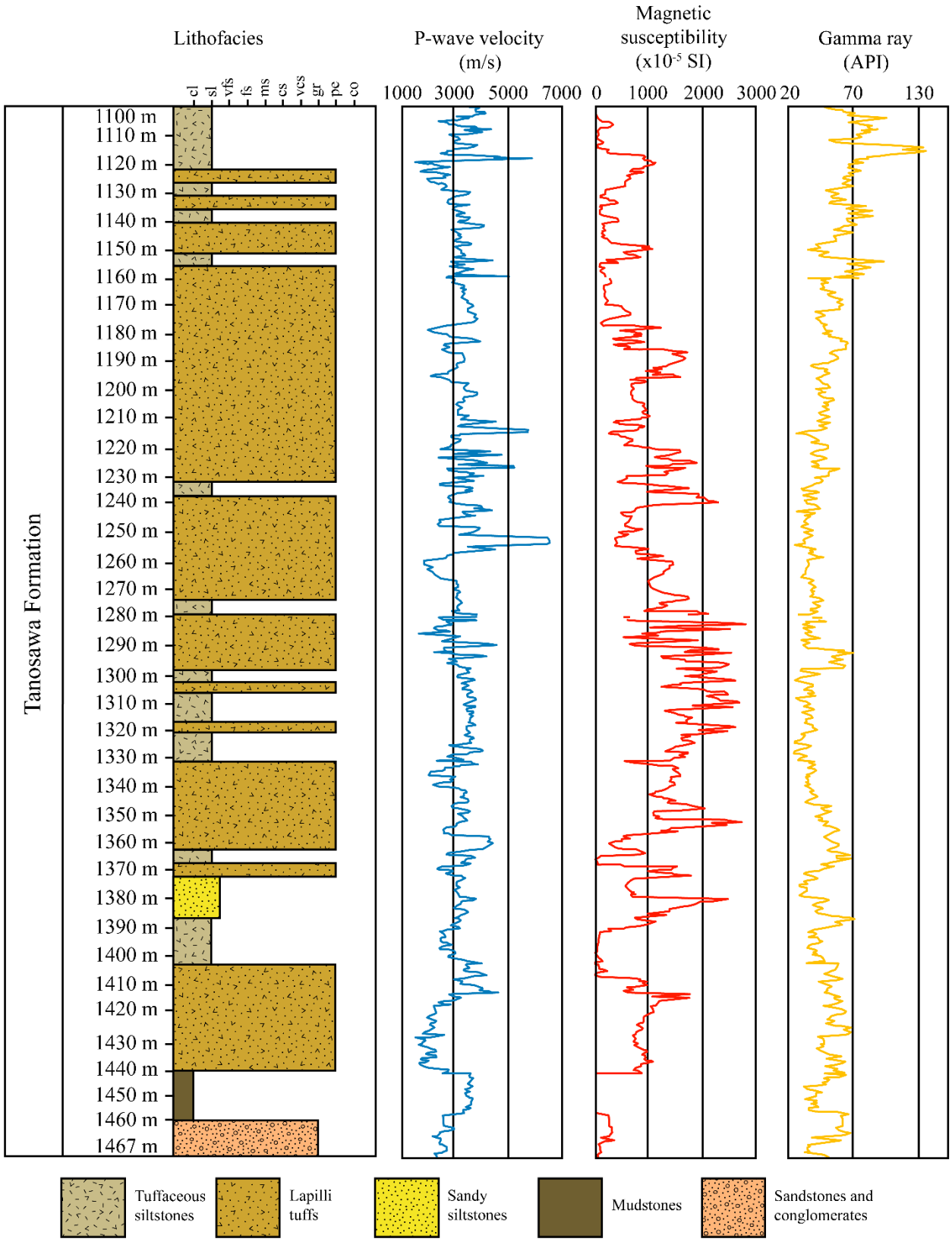

Figure 3.9. Columnar section of DTH27-1 well interval between 1100 m and 1467 m (left) and stratigraphic variations of the p-wave velocity log, magnetic susceptibility log, and natural gamma ray log. The grain size fraction abbreviations are as follows: cl, clay; sl, silt; vfs, very fine sand; fs, fine sand; ms, medium sand; cs, coarse sand; vcs, very coarse sand; gr, granule; pe, pebble; co, cobble.

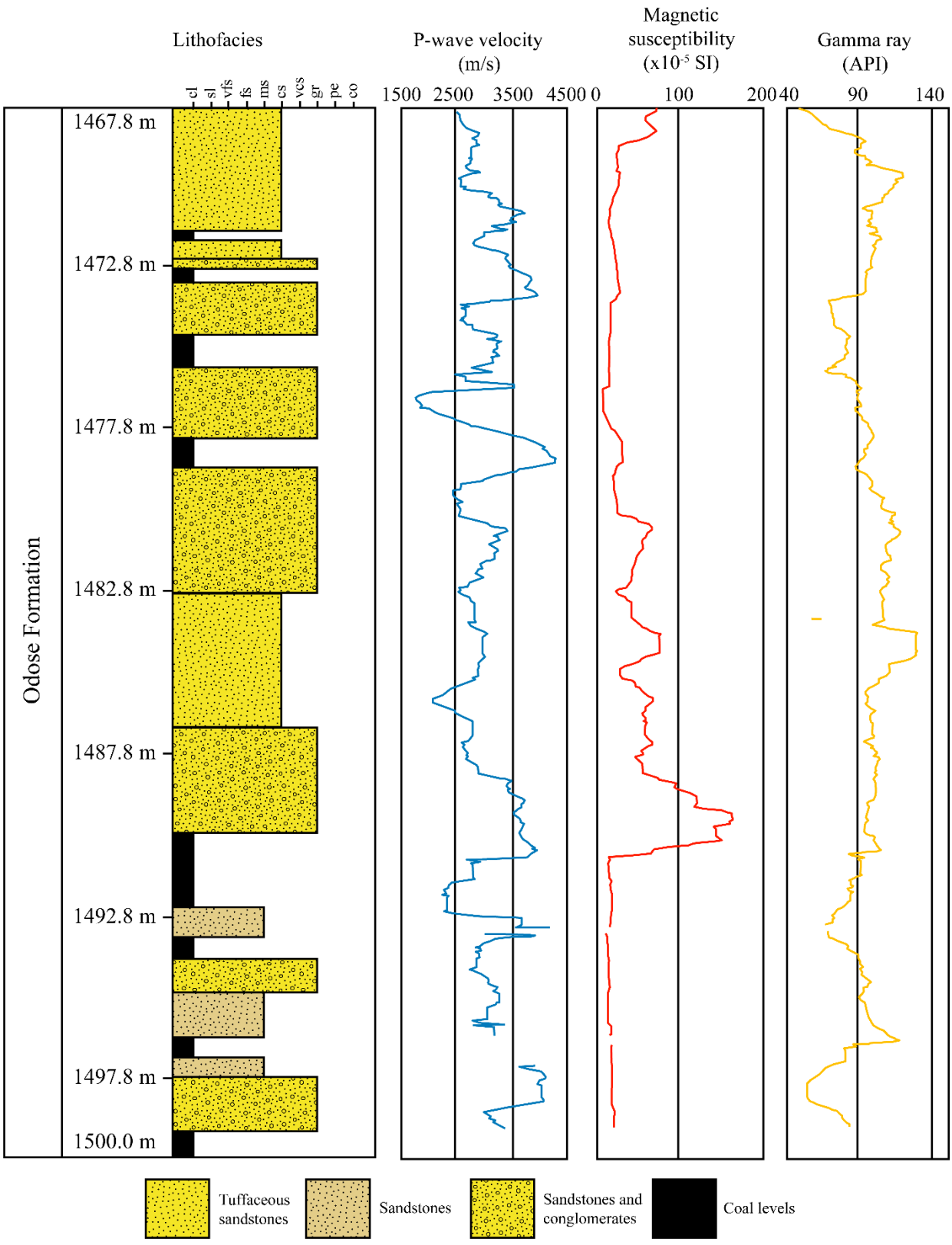

Figure 3.10. Columnar section of DTH27-1 well interval between 1467 m and 1500 m (left) and stratigraphic variations of the p-wave velocity log, magnetic susceptibility log, and natural gamma ray log. The grain size fraction abbreviations are as follows: cl, clay; sl, silt; vfs, very fine sand; fs, fine sand; ms, medium sand; cs, coarse sand; vcs, very coarse sand; gr, granule; pe, pebble; co, cobble.

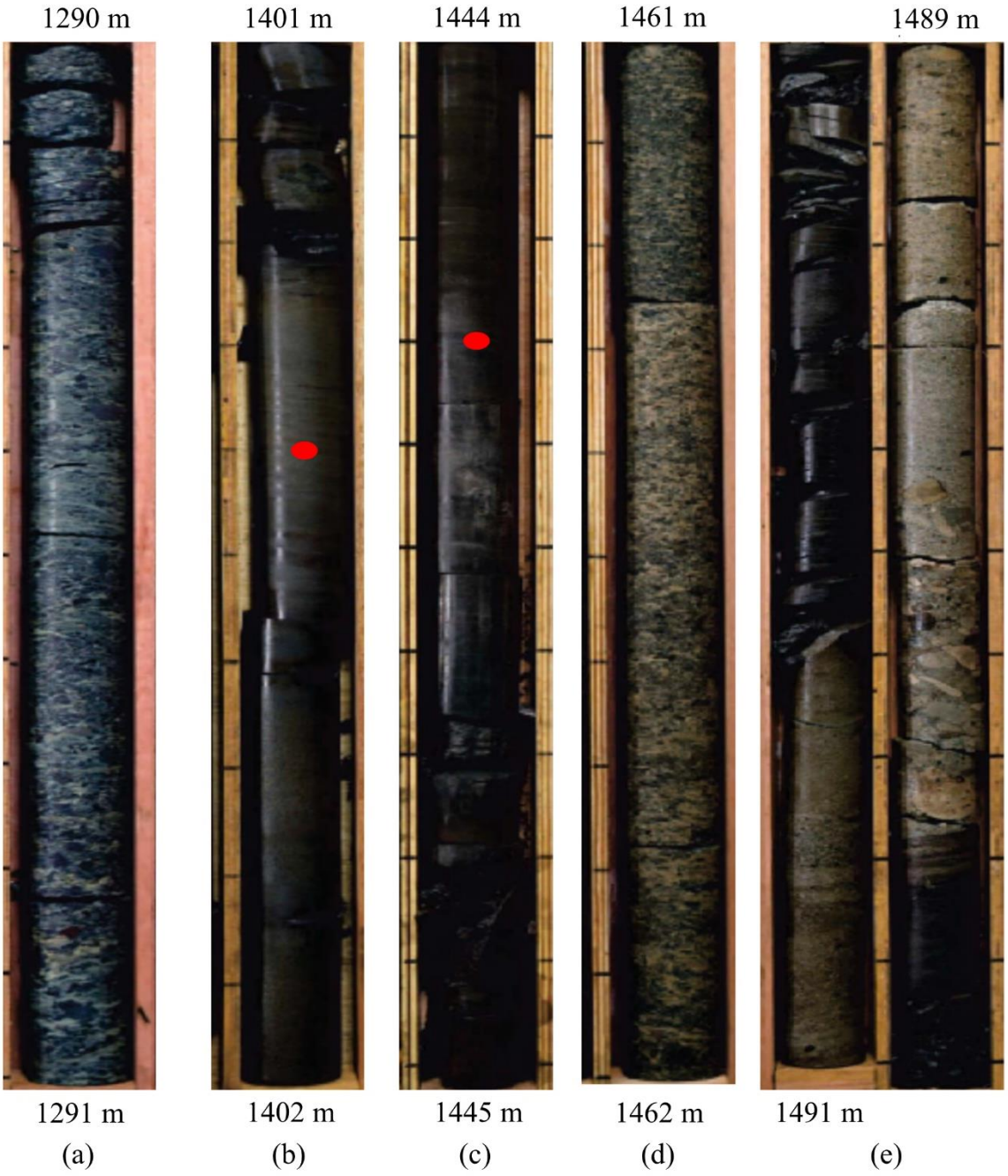

Figure 3.11. Photos of core sections of the Tanosawa and Odose Formations. (a) Lapilli tuffs from the Tanosawa Formation; (b) Tuffaceous siltstones from the Tanosawa Formation; (c) Mudstones from the lower part of the Tanosawa Formation; (d) Sandstones and conglomerates from the lower part of the Tanosawa Formation, (e) Tuffaceous sandstones and sandstones with conglomerates interlayered by coaly levels from the Odose Formation.

3.4.2 Organic Geochemistry

3.4.2.1 Rock-Eval pyrolysis

The Rock-Eval pyrolysis data for each sample of the studied formations are reported in Table 1; in Figures 3.12, 3.13, and 3.14 the variations of total organic carbon (TOC), and maximum temperature (T_{max}) are correlated to the natural gamma ray and shale (clay) volume variations. The shale (clay) volume was estimated through the equations of Asquith and Krygowski (2004) and Larianov (1969).

The TOC range of the Akaishi Formation was markedly lower than in the Odoji Formation. On the other hand, the TOC range of the Tanosawa was generally very low except for one sample with a higher TOC content. Lastly, the TOC range of the Odose Formation showed a large variability within different lithologies. Specifically, the coal horizons showed very high values of TOC compared to the sandstone horizons. The S1 values do not show a large variation in the Akaishi, Odoji, and Tanosawa Formations. In the Odose Formation, the S1values are generally low in the sandstones, while they are higher in the coal samples. The S2 values are considerably lower in the Akaishi Formation than in the Odoji Formation. In the Tanosawa Formation, S2 values are generally low, except for one sample. In the Odose Formation, S2 values are lower in the sandstones than in the coal horizons. The S3 values are somewhat low in all the analyzed formations. Lastly, the Akaishi Formation samples show low values of HI. The Odoji Formation is characterized by higher HI values, but its OI values are notably lower than in the Akaishi Formation. The Tanosawa Formation samples are generally characterized by low HI and OI values. In the Odose Formation, the coal samples are characterized by higher HI and lower OI values than the sandstones samples.

The T_{max} values of the Akaishi and the Odoji Formations show a minimal variation, and they are always lower than 435 °C. On the other hand, the Tanosawa and Odose Formation are characterized by an increase of T_{max} until values of 443 °C. According to Peters and Cassa (1994), T_{max} values lower than 435 °C, between 435 °C and 470 °C, and higher than 470 °C represent the immature, mature, and post-mature stages of thermal maturation, respectively. Therefore, the Akaishi and the Odoji Formations are immature for the hydrocarbon generation. On the other hand, the Tanosawa and Odose Formations show T_{max} ranges typical of the onset of the oil generation window.

3.4.2.2 CHNS elemental analysis

The nitrogen (TN) and sulfur (TS) contents from the CHNS elemental analysis of samples from the Akaishi and Odoji Formations are reported in Table 2 and Figure 3.15. The TN content of the Akaishi Formation is, on average, lower than in the Odoji Formation. Additionally, the TN content in the Odoji Formation shows a slight upward increase up to 0.19 wt%. The TOC/TN ratio in the

Akaishi Formation (<10) is lower than in the Odoji Formation (13–19). According to Meyers (1997), a TOC/TN ratio lower than 20 indicates that the organic matter originated prevalently from a marine environment. The TS content is variable in both the formations, but the Odoji Formation resulted, on average, richer in TS than the Akaishi Formation. The C/S ratio in the Akaishi Formation is a range of 0.08–1.00, while it is in a range of 0.88–2.66 in the Odoji Formation.

Table 1 Rock-Eval pyrolysis data of formations from the DTH27-1 well.

Sample Name	TOC (wt%)	S1 (mg/g)	S2 (mg/g)	S3 (mg/g)	T_{max} (°C)	S1+S2 (mg/g)	S2/S3	HI (mg/g)	OI (mg/g)
Akaishi Formation									
AK1	0.27	0.05	0.13	0.25	408	0.18	0.52	48	89
AK2	0.09	0.03	0.05	0.23	405	0.08	0.22	56	189
AK3	0.10	0.04	0.09	0.14	423	0.13	0.64	90	140
AK4	0.34	0.05	0.21	0.23	410	0.26	0.91	62	47
AK5	0.48	0.11	0.23	0.24	406	0.34	0.96	48	50
AK6	0.32	0.05	0.22	0.23	409	0.27	0.95	69	72
Odoji Formation									
OD1	2.61	0.07	4.70	0.34	412	4.77	13.82	180	23
OD2	1.69	0.32	6.04	0.29	409	6.36	20.82	357	17
OD3	1.74	0.23	5.66	0.36	415	5.89	15.72	325	21
OD4	2.83	0.31	13.37	0.44	415	13.68	30.38	472	16
OD5	1.57	0.41	7.11	0.66	421	7.52	10.77	453	42
OD6	2.03	0.28	8.81	0.30	409	9.09	29.36	434	15
OD7	0.81	0.14	3.61	1.20	413	3.75	3.00	413	148

Table 1 (Continued)

Sample Name	TOC (wt%)	S1 (mg/g)	S2 (mg/g)	S3 (mg/g)	T_{max} (°C)	S1+S2 (mg/g)	S2/S3	HI (mg/g)	OI (mg/g)
Tanosawa Formation									
TS1	2.66	0.16	5.34	0.51	433	5.50	10.47	201	19
TS2	0.29	0.02	0.20	0.18	435	0.22	1.10	69	62
TS3	0.11	0.03	0.08	0.11	433	0.11	0.72	73	100
TS4	0.18	0.04	0.20	0.15	430	0.24	1.30	111	83
TS5	0.14	0.03	0.12	0.80	432	0.15	0..15	86	86
Odose Formation									
OS1	0.94	0.06	1.41	0.17	443	1.47	8.29	150	18
OS2	3.03	0.13	8.64	0.30	438	8.77	28.8	285	10
OS3	0.38	0.03	0.45	0.15	438	0.48	3.00	118	39
OS4	0.85	0.06	1.39	0.20	440	1.45	6.95	164	24
OS5	1.31	0.06	1.89	0.18	442	1.95	10.5	144	14
OS6	15.96	2.55	77.77	0.74	429	80.32	105	487	5
OS7	9.98	0.74	37.97	0.58	433	38.71	65.46	380	6
OS8	24.62	5.14	101.41	0.87	430	106.55	116.56	412	4
OS9	18.80	2.57	85.17	0.88	429	87.74	96.78	453	5
OS10	0.48	0.05	0.62	0.16	443	0.67	3.875	129	33
OS11	42.01	7.08	141.6	1.36	432	148.68	104.11	337	3

Abbreviations: HI, hydrogen index (mg hydrocarbon (S2)/g TOC); OI, oxygen index (mg CO2 (S3)/g TOC); S1, low hydrocarbon yield (mg hydrocarbon/g rock); S2, high hydrocarbon yield (mg hydrocarbon/g rock); S3, CO2 (mg CO2/g rock); S1 + S2, Genetic source potential; S2/S3, hydrocarbon type index; T_{max}, Maximum temperature; TOC, total organic carbon; wt%, weight percent.

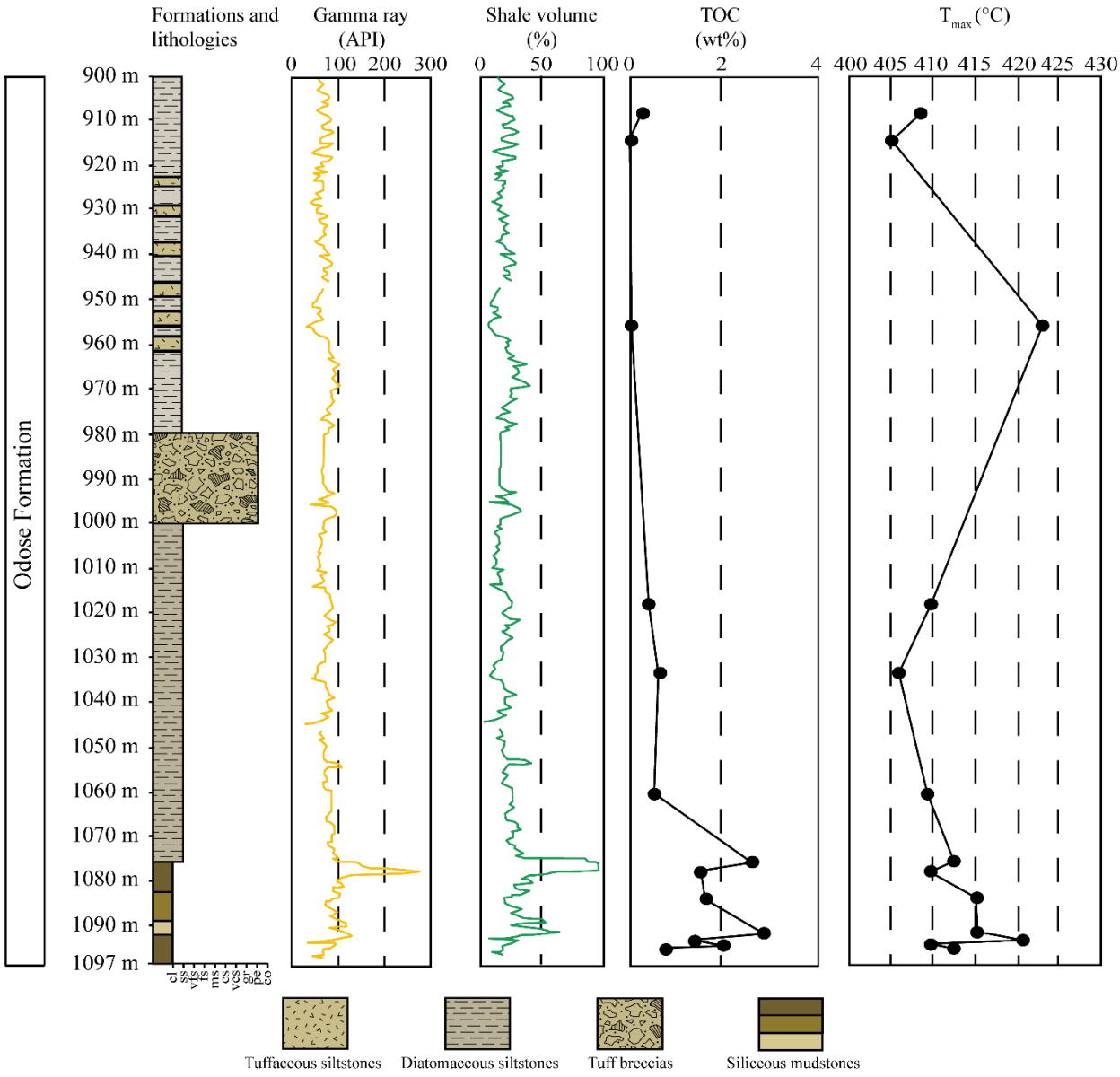

Figure 3.12. Stratigraphic variations of the natural gamma ray log, shale volume log, total organic carbon (TOC), and maximum temperature (T_{max}) in the Akaishi and Odoji Formations. The grain size fractions abbreviations are as follows: cl, clay; sl, silt; vfs, very fine sand; fs, fine sand; ms, medium sand; cs, coarse sand; vcs, very coarse sand; gr, granule; pe, pebble; co, cobble.

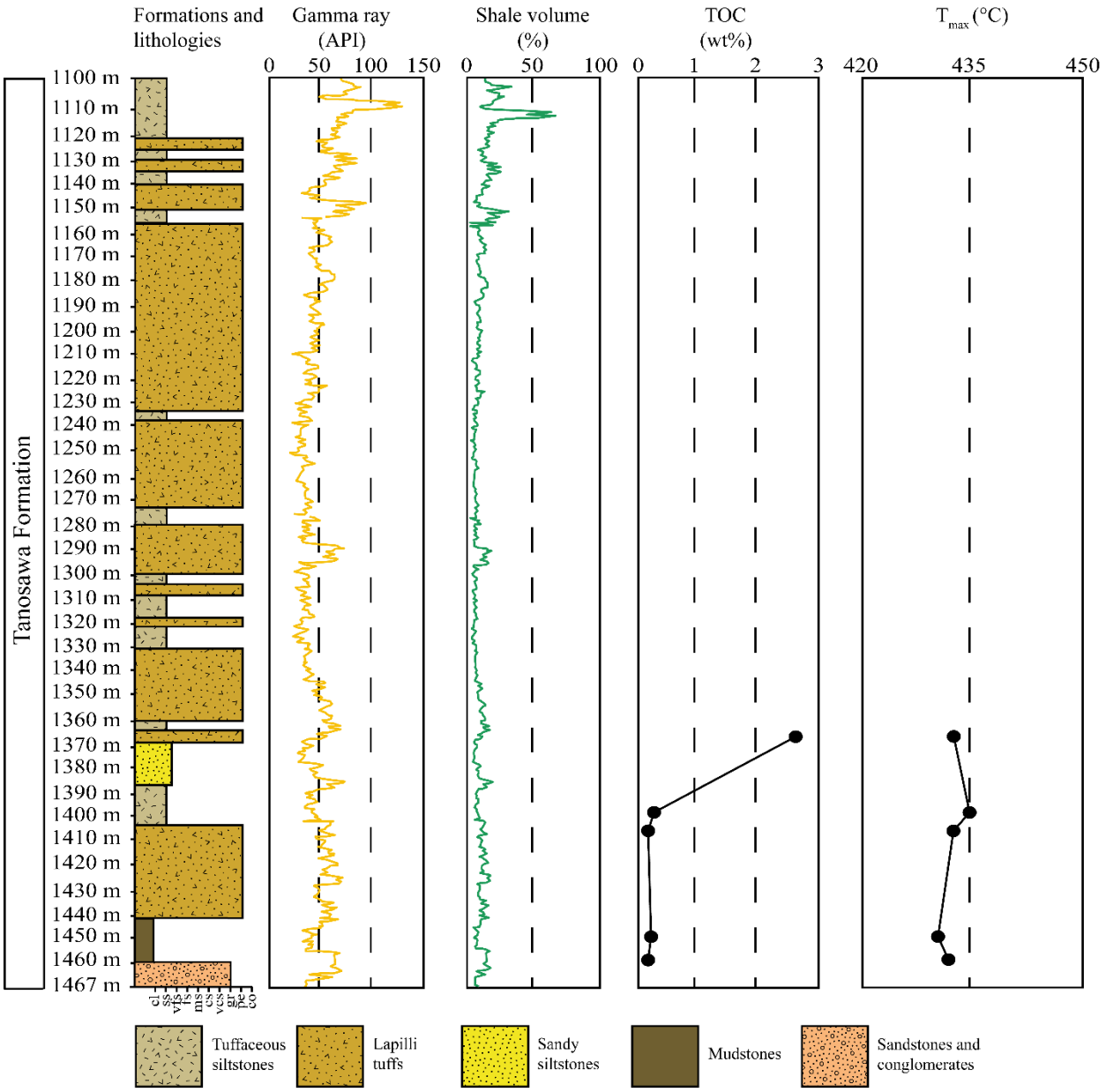

Figure 3.13. Stratigraphic variations of the natural gamma ray log, shale volume log, total organic carbon (TOC), and maximum temperature (T_{max}) in the Tanosawa Formation. The grain size fractions abbreviations are as follows: cl, clay; sl, silt; vfs, very fine sand; fs, fine sand; ms, medium sand; cs, coarse sand; vcs, very coarse sand; gr, granule; pe, pebble; co, cobble.

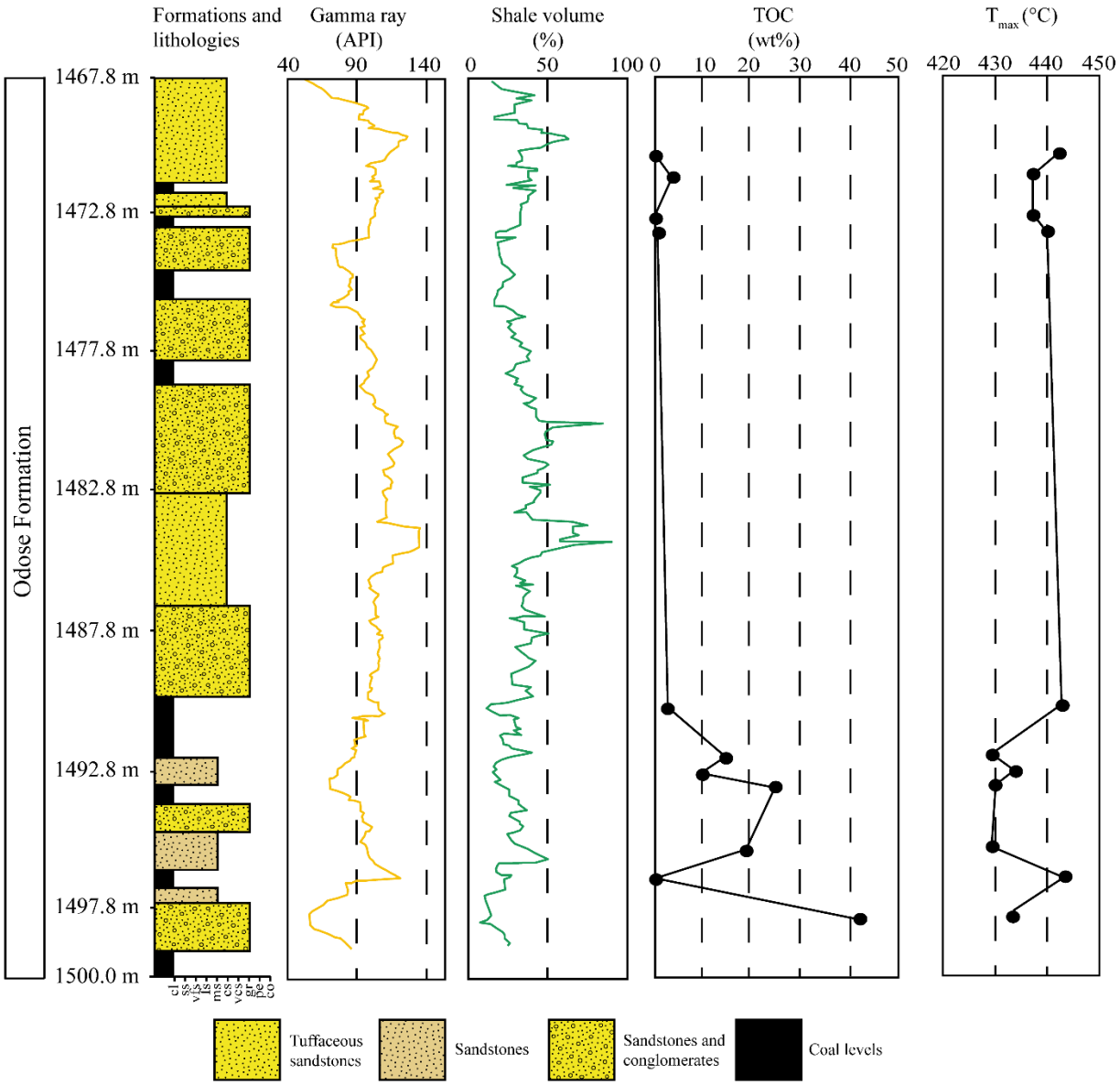

Figure 3.14. Stratigraphic variations of the natural gamma ray log, shale volume log, total organic carbon (TOC), and maximum temperature (T_{max}) in the Odose Formation. The grain size fractions abbreviations are as follows: cl, clay; sl, silt; vfs, very fine sand; fs, fine sand; ms, medium sand; cs, coarse sand; vcs, very coarse sand; gr, granule; pe, pebble; co, cobble.

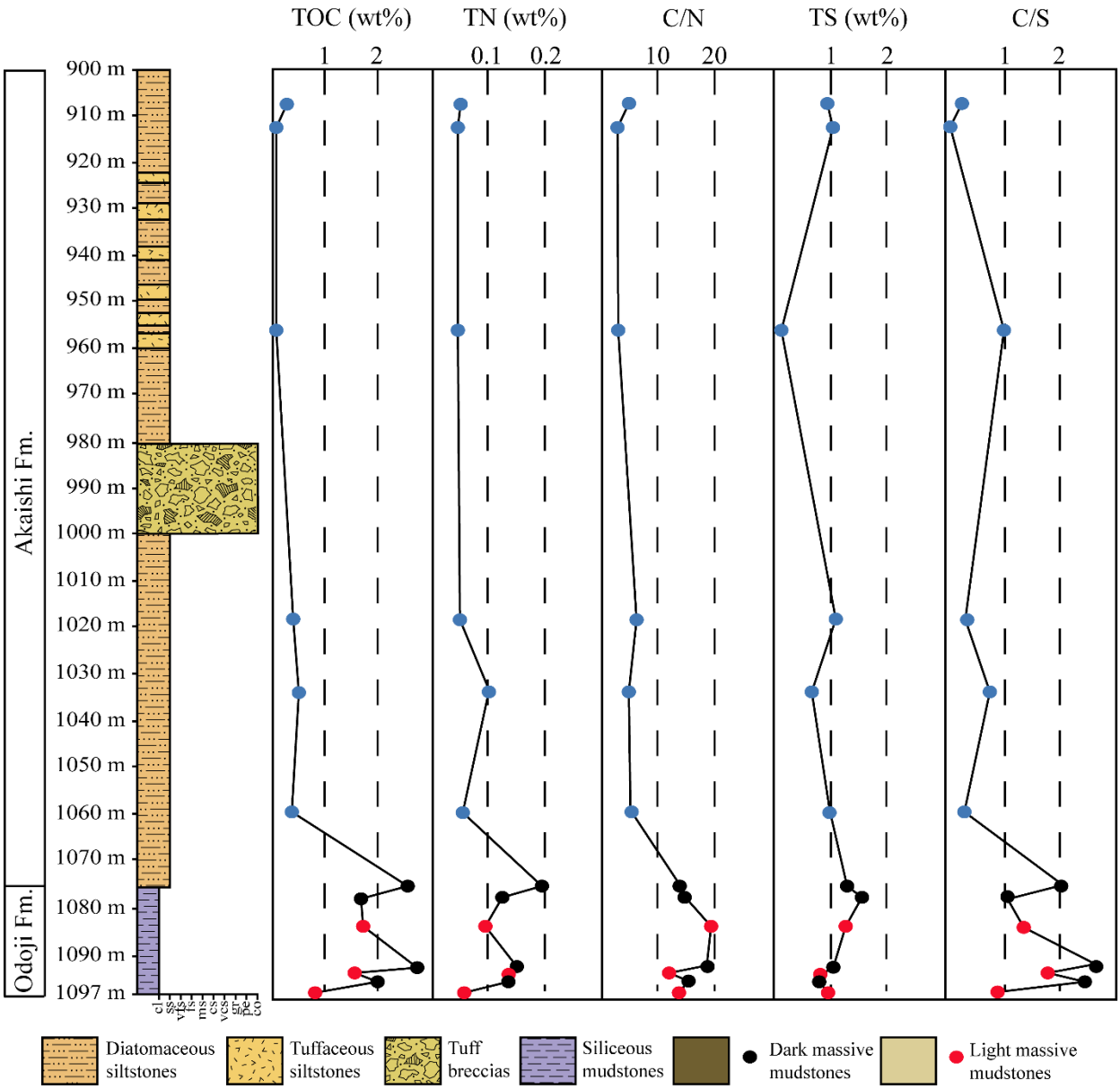

Figure 3.15. Vertical distributions of TOC, TN, and TS contents and C/N and C/S ratios of the Akaishi and the Odoji Formations from the Tsugaru Basin area. The grain size fraction abbreviations are as follows: cl, clay; sl, silt; vfs, very fine sand; fs, fine sand; ms, medium sand; cs, coarse sand; vcs, very coarse sand; gr, granule; pe, pebble; co, cobble.

3.4.3 Inorganic Geochemistry

3.4.3.1 X-Ray Fluorescence

The results of major oxides analysis of the Akaishi and the Odoji Formation are reported in Table 2. In both the formations, the SiO_2 is the most abundant oxide. However, the Odoji Formation is richer in SiO_2 than the Akaishi Formation. The detrital SiO_2 was calculated with the equation of Leinen (1977): detrital $SiO_2 = 4.33Al + 1.36Mg^2$; the biogenic SiO_2 was calculated subtracting the detrital SiO_2 from the total SiO_2.

Other oxides such as Al_2O_3, Fe_2O_3, CaO, MgO, K_2O, and Na_2O are present at variable concentrations in both the formations. However, the Al_2O_3, Fe_2O_3, K_2O, and Na_2O are more abundant in the Akaishi Formation than in the Odoji Formation. The less abundant oxides in both the formations are TiO_2, P_2O_5, and MnO.

Based on the ternary plot of SiO_2, Al_2O_3, and CaO of Ross and Bustin (2009), the Akaishi and the Odoji Formations are variably enriched in SiO_2 (Figure 3.16). The presence of biogenic and detrital SiO_2 indicates that the Si element is a component of biogenic quartz and detrital quartz, but also forms clay minerals with other elements such as Al, K, and Ti (Brumsack, 2006). All the samples have a K_2O/Al_2O_3 ratio lower than 0.3, indicating a prevalence of clay minerals on Feldspars (Cox and Lowe, 1995).

The variable amounts of Fe_2O_3, CaO–MgO, and Na_2O can be associated respectively to the presence of pyrite, calcite and dolomite, and feldspars. On the other hand, the P_2O_5 of the Middle-Late Miocene sediments of the Japan Sea is, generally, associated with apatite minerals.

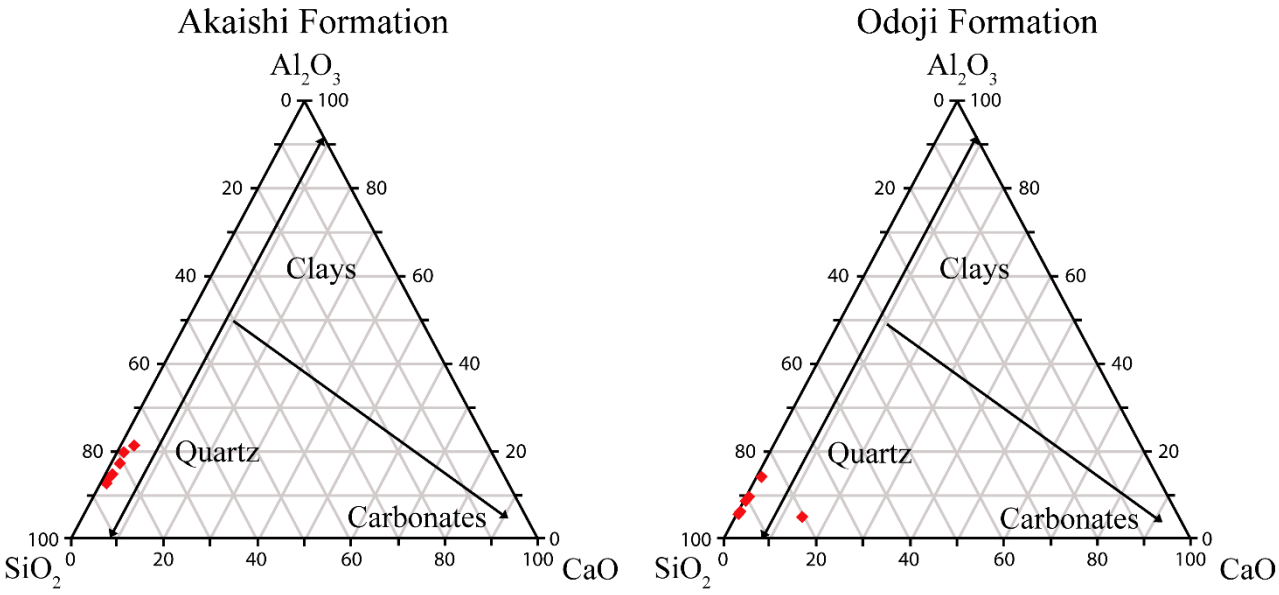

Figure 3.16. Ternary diagrams showing relative proportions of major compositions of SiO_2 (quartz), Al_2O_3 (clays), and CaO (carbonates). (a) Composition of the Akaishi Formation; (b) Composition of the Odoji Formation (modified from Ross and Bustin, 2009).

3.4.3.2 Pyrite morphology and size

Observation of pyrite in reflected light showed that the framboidal pyrite is the most abundant type (Figure 3.17); euhedral pyrites are, generally, absent or rare. Framboidal pyrite is absent in the Akaishi Formation and variably abundant in the Odoji Formation (Table 3). The framboidal pyrite morphologies in the Odoji Formation's samples are shown in Figure 3.17. Single (Figure 3.17a–d) and aggregates of framboids (Figure 3.17e–f) are present. Additionally, the framboids show signs of

secondary pyrite crystallization on the original framboidal structure (Figure 3.17). The mean framboidal pyrite size is larger than 5 μm (range of 7.2–10.32 μm) in all the observed samples (Figures 3.17 and 3.18; Table 3).

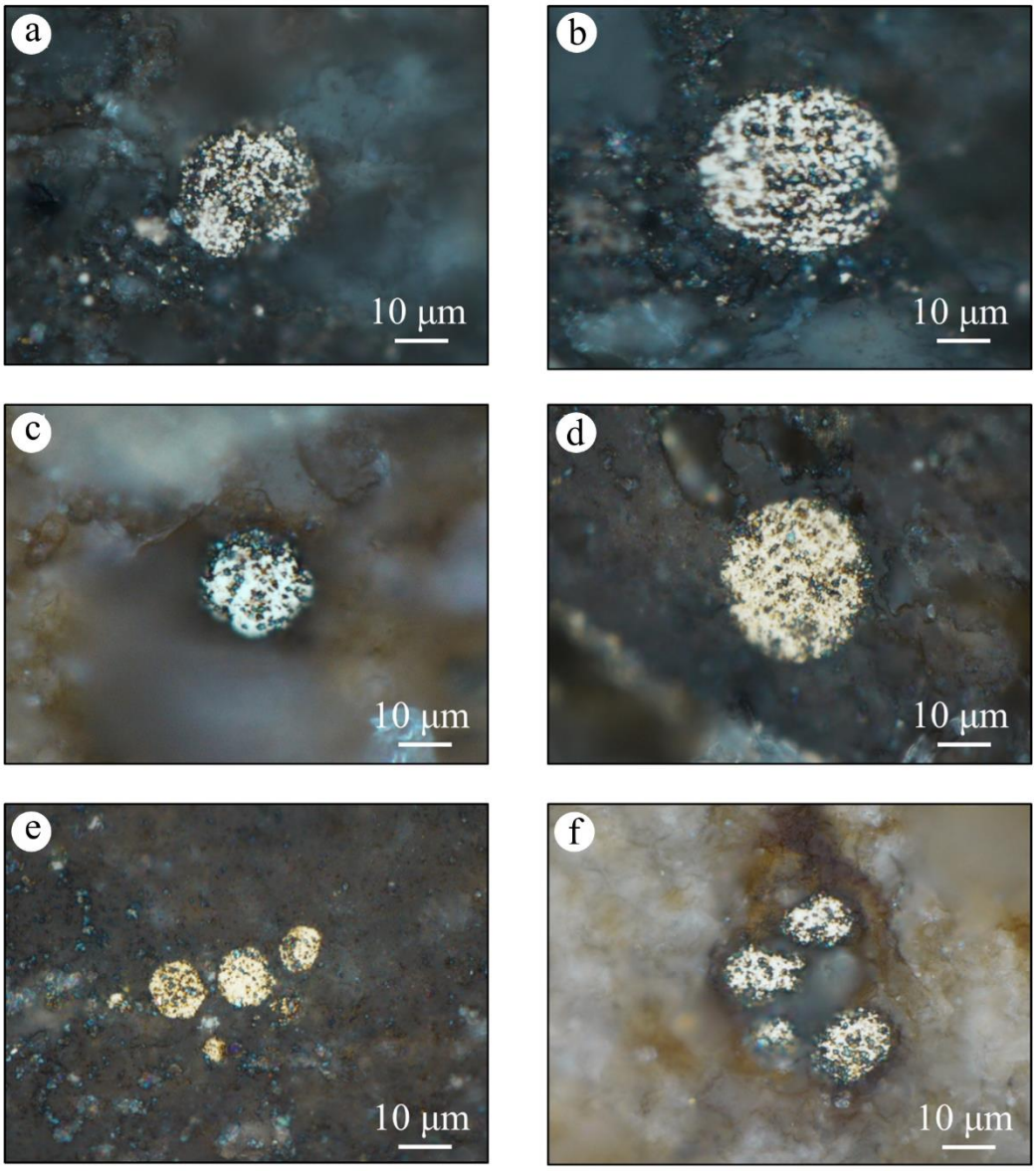

Figure 3.17. Microscopic features of framboidal pyrite from the *Odoji Formation* under reflected-light microscopy. (a–d) Examples of single framboids; (e–f) Examples of aggregates of framboids.

Table 2 TOC, TN, TS and major elements abundances of the Akaishi and the Odoji Formations from DTH27-1 well

Sample Elements wt%	SiO_2	$BSiO_2$	$DSiO_2$	TiO_2	Al_2O_3	Fe_2O_3	MgO	CaO	K_2O	Na_2O	P_2O_5	MnO	TOC	TN	TS	C/N	C/S
AK1	73.41	42.11	32.29	0.42	12.95	3.38	1.98	1.62	2.59	2.29	0.06	0.04	0.27	0.05	0.94	5.33	0.29
AK2	65.52	24.31	41.21	0.33	16.61	5.71	3.83	1.29	2.79	2.56	0.08	0.07	0.09	0.04	1.08	2.57	0.08
AK3	75.41	44.64	30.76	0.28	12.28	3.66	3.20	1.13	2.35	1.32	0.05	0.07	0.10	0.04	0.10	2.33	1.00
AK4	75.25	48.04	27.20	0.46	11.17	4.35	1.96	1.29	1.78	2.09	0.10	0.04	0.34	0.05	1.13	6.80	0.31
AK5	64.40	19.98	44.42	0.45	18.14	6.04	3.47	2.64	2.25	1.31	0.07	0.00	0.48	0.10	0.65	4.80	0.75
AK6	66.39	30.89	35.49	0.51	14.19	8.09	3.63	1.70	1.81	2.20	0.07	0.04	0.32	0.06	0.98	5.12	0.33
OD1	71.01	41.52	29.49	0.33	12.05	5.12	2.28	1.20	2.10	1.60	0.23	0.00	2.61	0.19	1.28	13.74	2.02
OD2	78.70	57.75	20.94	0.36	8.66	3.63	1.35	0.77	1.50	1.48	0.13	0.03	1.69	0.12	1.57	14.20	1.08
OD3	84.78	70.91	13.86	0.22	5.74	2.20	0.87	0.75	0.96	1.25	0.13	0.00	1.74	0.09	1.27	18.91	1.37
OD4	80.60	61.36	19.23	0.26	7.86	2.65	1.48	0.64	1.26	1.16	0.10	0.00	2.83	0.15	1.05	19.19	2.67
OD5	68.35	57.89	10.45	0.17	4.28	1.52	0.79	12.33	0.70	0.10	9.12	0.04	1.57	0.13	0.88	12.66	1.83
OD6	86.52	73.23	13.29	0.19	5.50	1.64	0.84	0.63	0.73	0.90	0.08	0.00	2.03	0.13	0.84	15.62	2.42
OD7	91.59	84.68	6.91	0.08	2.77	1.65	0.68	0.27	0.44	0.68	0.03	0.00	0.81	0.06	0.93	13.28	0.88

Note: $BSiO_2$ = Biogenic Silica; $DSiO_2$ = Detrital Silica; TOC = Total Organic Carbon; TN = Total Nitrogen; TS = Total Sulfur; C/N = Organic Carbon-Nitrogen ratio; C/S = Organic Carbon-Sulfur ratio; wt% = weight percent.

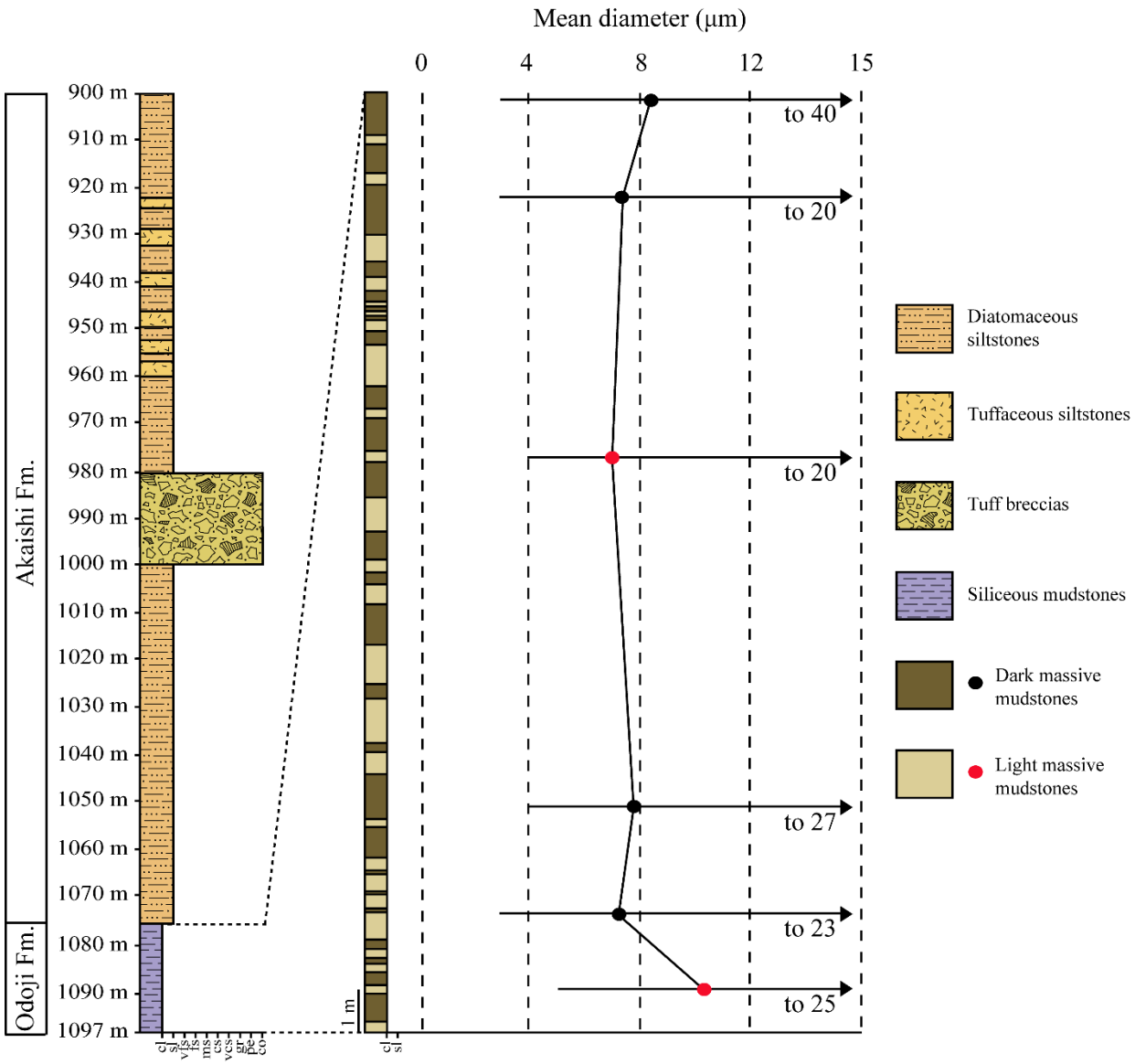

Figure 3.18. Vertical variations of the mean diameter of the framboidal pyrite in the Odoji Formation from the Tsugaru Basin area. The grain size fraction abbreviations are as follows: cl, clay; sl, silt; vfs, very fine sand; fs, fine sand; ms, medium sand; cs, coarse sand; vcs, very coarse sand; gr, granule; pe, pebble; co, cobble.

Table 3 Descriptive statistics of framboidal pyrite from the Odoji Formation.

Sample name	Mean diameter (μm)	Max Diameter (μm)	Min Diameter (μm)	Standard Deviation	Skewness	Measured framboids
OD1	8.53	40	3	6.74	2.71	123
OD2	7.57	20	3	4.98	2.61	108
OD3	7.08	20	4	2.92	2.50	67
OD4	7.98	27	4	3.30	2.64	155
OD5	7.18	23	3	2.83	2.22	104
OD6	10.32	25	5	4.37	1.40	50

3.5 Discussion

3.5.1 Kerogen type

A pseudo Van Krevelen diagram (Figure 3.19) was used to interpret the kerogen type in sediments of Akaishi, Odoji, Tanosawa, and Odose Formations (Peters, 1986). This diagram shows that the samples of the Akaishi and the Tanosawa Formations are generally characterized by the type III kerogen, which is associated with terrestrial organic matter. The kerogen type determination in the Akaishi Formation contrasts with the Jingu and Ujiié (1990) study's results, who identified a type II kerogen in the sediments of the Akaishi Formation. The marked shift from type II to type III kerogen in marine sediments indicates a degradation of the organic matter (Pratt, 1984; Tyson, 1995). The sediments of the Odoji Formation are mostly characterized by the type II kerogen. However, one sample deviates from the main trend, thereby suggesting a mixture between type II and type III kerogens. Lastly, the Odose Formation's samples show two different trends in the sandstones and the coals. The sandstones samples are mainly distributed in the area between the type II and type III kerogens, and their HI is lower than the coals and the Odoji Formation samples. This feature suggests that the sandstones are characterized by a consistent fraction of terrestrial organic matter. On the other hand, the high HI and low OI of the coal samples indicate a consistent fraction of marine organic matter.

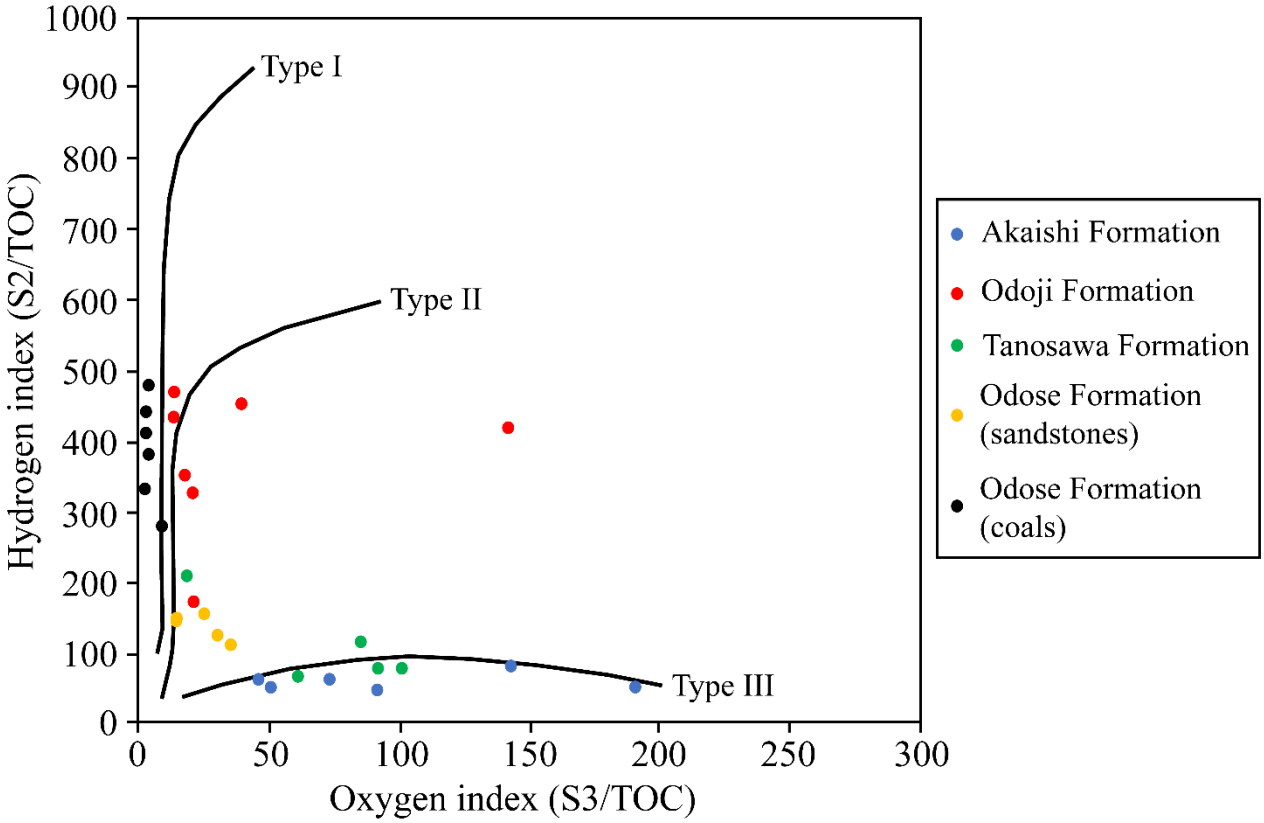

Figure 3.19. Hydrogen index (HI) vs oxygen index (OI) plot of the formations from the DTH27-1 well (modified from Peters, 1986).

3.5.2 Hydrocarbon Potential and Thermal Maturity

The hydrocarbon potential and thermal maturity of rocks from the DTH27-1 well were evaluated based on S1 and S2, TOC, and T_{max} values obtained from Rock-Eval pyrolysis. Furthermore, the TOC data of the various samples were compared with the classification of Tissot and Welte (1984) and Peters (1986) to evaluate the organic richness of these formations. According to this classification, the sedimentary rocks are poor when the TOC is lower than 0.5 wt%, fair when the TOC is in a range of 0.5–1.0 wt%, and good when the TOC is higher than 1.0 wt%. Based on this study's results, the Akaishi and the Tanosawa Formations are generally very poor in organic carbon (Figures 3.12 and 3.13). On the other hand, the Odoji Formation shows good/very good con

tent of organic carbon (Figure 3.12). Lastly, the sandstones and coals of the Odose Formation show respectively, a fair, and very good content of organic carbon (Figure 3.14).

Through the comparison of the TOC with the source potential (S1+S2), it was possible to consider whether the studied formations could be considered potential source rocks (Figure 3.20 and 3.21). Data show that Akaishi and Tanosawa Formations (except for one sample) have a low generative potential (Figure 3.20). The Odoji Formation has a fair to very good generative potential (Figure 3.20).

Lastly, the sandstones and the coals of the Odose Formation have respectively low and good to very good generative potentials (Figures 3.20 and 3.21).

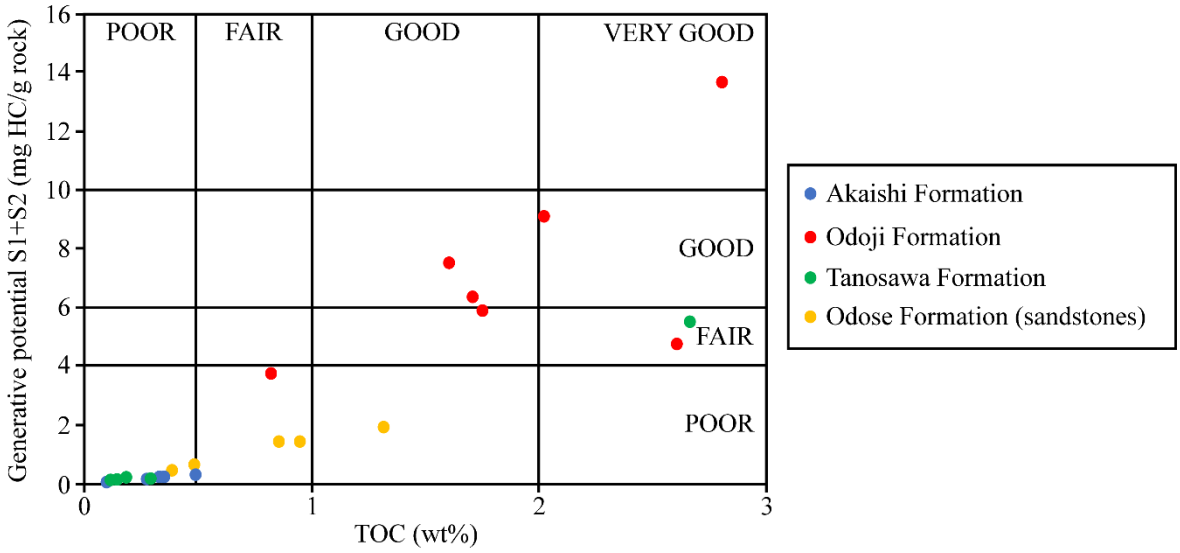

Figure 3.20. Plot of source potential (S1+S2) against TOC for the DTH27-1 well's formations. The lines separating the different fields are modified from Gottardi et al. (2019).

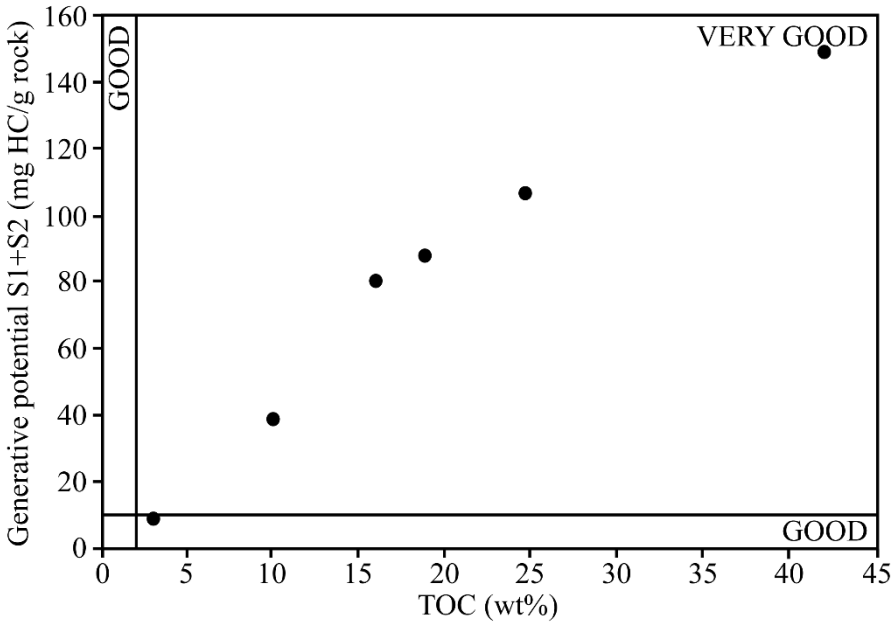

Figure 3.21. Plot of source potential (S1+S2) against TOC for the coal samples of the Odose Formation. Lines separating the different fields are modified from Gottardi et al. (2019).

Although our data indicated the Odoji Formation as a potential source rock, its T_{max} values were always lower than 435 °C (Figure 3.12), indicating that the Odoji Formation did not have the potential to expel hydrocarbons (Peters and Cassa, 1994). On the other hand, the Odose Formation coals have

T_{max} values around 435 °C or higher (Figure 3.14), suggesting the presence of a source rock horizon. However, no oil shows were found in the Odose Formation horizons of the DTH27-1 well.

T_{max} values from all the analyzed formations were used to calibrate a 1D burial/thermal model of the Tsugaru Basin with the Petro Mod software. Input data for the model were depths, thicknesses, and lithologies of formations of the DTH27-1 well. Data from the study of Aoyagi and Omokawa (1992) were used as ages of deposition. The surface temperature was set up between 20.50 °C (21 Ma) and 15.66 °C (Present). Heat flow varied from 100 mW/m^2 between 21 and 17.50 Ma to 65 mW/m^2 at 11 Ma, and finally to 50 mW/m^2 in the present; these values were chosen from typical heat flow trends in back-arc basins (Allen and Allen, 2013). Lastly, Sweeney and Burnham's equation (1990) was selected as the kinetic model. The resulting model is in Figure 3.22.

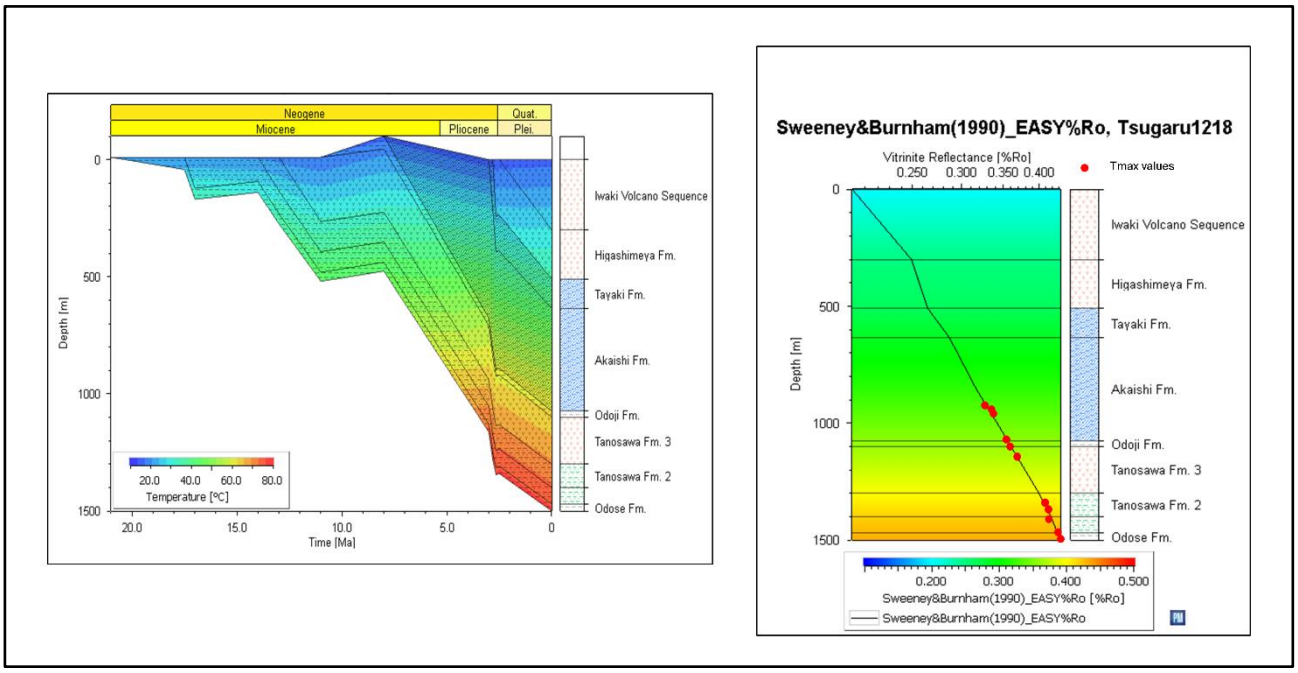

Figure 3.22. Left: 1-D burial and thermal history of the Tsugaru Basin performed with the kinetic model of Sweeney and Burhnam (1990). Right: thermal modeling calibrated with the Vitrinite Reflectance profile and the T_{max} values. The Tmax values were converted in Vitrinite Reflectance using the equation of Waseda (1996).

The 1D model shows a good fit with the T_{max} data and indicates an increase of the thermal maturity until 0.43% of Vitrinite Reflectance, at the bottom of the DTH27-1 well. This model suggests that the low degree of thermal maturity in the Tsugaru Basin is probably related to a limited burial depth of the studied formations. Therefore, at higher burial depths, the Odoji and the Odose Formations could reach the mature thermal stage.

3.5.3 Lithological and paleo-environmental controls on the organic richness

3.5.3.1 Lithological properties of sediments

Two important lithological factors that affect the preservation of organic matter in sediments are the grain size and porosity. According to Tissot and Welte (1984) and Allen and Allen (2013), the best conditions for organic matter preservation are achieved in fine grained and low porosity sediments. Low porosity and fine grain size can limit the circulation of water, the dissolution of oxygen inside the sediment pores, and the bacterial activity (Tissot & Welte, 1984). Our study revealed a marked difference in TOC content between the diatomaceous siltstones of Akaishi Formation and the siliceous mudstones of the Odoji Formation (Figures 3.12, 3.15 and 3.23); these sediments are generally characterized by different grain sizes and porosity. Both the grain size and porosity of the siliceous sediments were inherited from the initial condition of the deposition of the diatomaceous muds. Based on our lithological observations, sediments of the Odoji Formation are characterized by a smaller grain size than the Akaishi Formation. If the original diatomaceous mud of the Odoji Formation was characterized by a lower grain size, and low porosity, the inflow of oxygen from marine waters may have been limited. Therefore, the limited inflow of oxygen from marine waters possibly favored the preservation of organic particles from degradation, resulting in increased TOC content.

3.5.3.2 Source of the detrital fraction

The paleo-weathering intensity at the source and the provenance of the detrital fraction of sediments can be quantified through the interpretation of elemental geochemistry. The chemical index of alteration (CIA) of Nesbitt and Young (1982) is generally used to assess the degree of the chemical weathering and to reconstruct the paleoclimate at the source area (Zeng et al., 2015; Li et al., 2019). The CIA is expressed as: CIA = molar [(Al_2O_3) / (Al_2O_3+CaO*+Na_2O+K_2O)] x 100. The CaO* in this equation represents the CaO in silicate minerals (Nesbitt and Young, 1982, 1989). The CaO* is calculated with the following expression: CaO* = CaO-(10/3 x P_2O_5) (Cox et al., 1995). If the remaining mole fraction of CaO is higher than that of Na_2O, the CaO value is equal to the CaO*. Otherwise, the CaO* is equivalent to Na_2O (McLennan, 1993; Zeng et al., 2015). The CIA values are in a range of 66–84, and 65–84 in the Akaishi and Odoji Formations. These ranges suggest a moderate to high chemical weathering and a warm-humid climate at the source of the detrital fraction (Fedo et al., 1995). The CIA interpretation agrees with the plot SiO_2–(Al_2O_3+K_2O+Na_2O) (Figure 3.24).

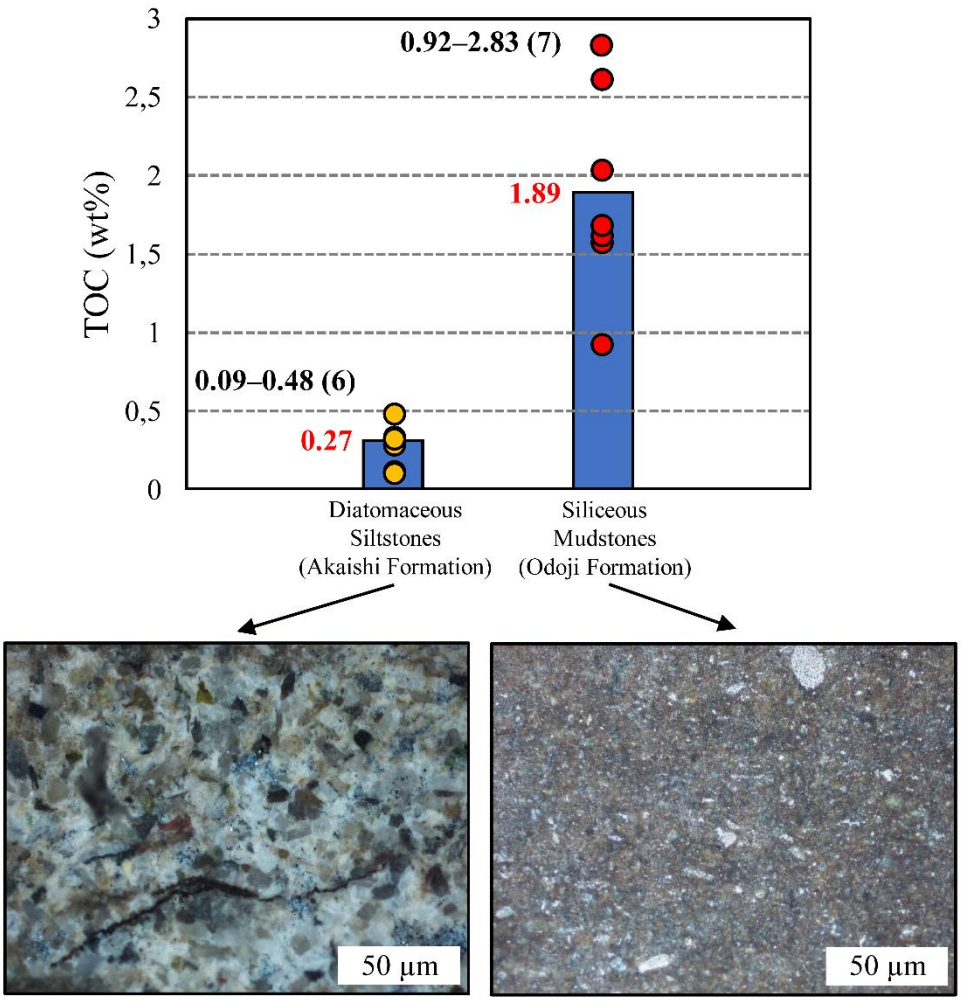

Figure 3.23. Graph showing a comparison of organic carbon content in the diatomaceous siltstones of the Akaishi Formation and the siliceous mudstones of the Odoji Formation. The data range and data number are reported in black, while the average TOC of the two formations is reported in red. In the lower part of the figure, × 10 magnified photos are shown and are representative of the grain size variation in the two formations.

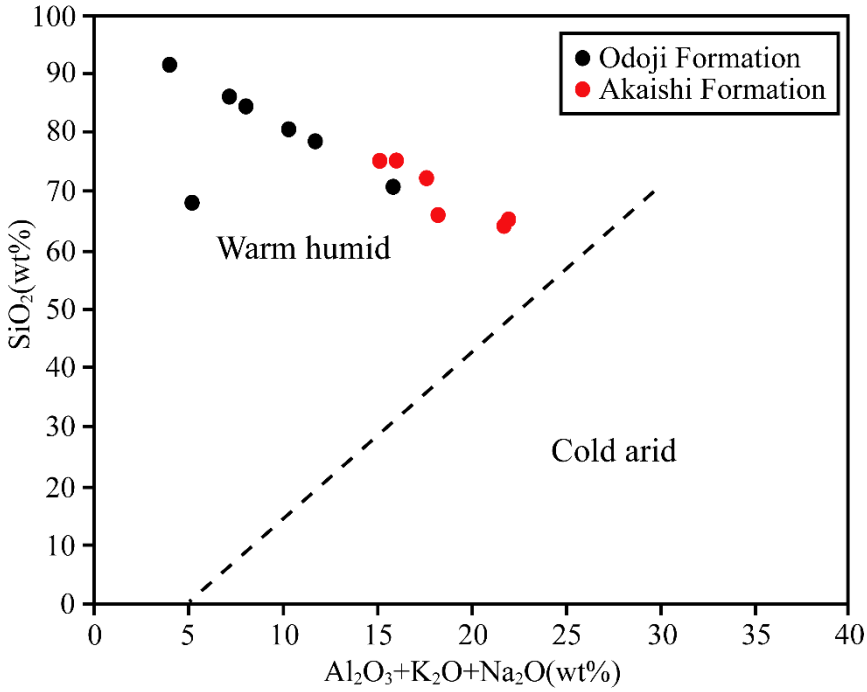

Figure 3.24. Plot of SiO_2 versus $Al_2O_3+K_2O+Na_2O$ for the discrimination of paleoclimate conditions (modified from Chen et al., 2020).

The provenance of detrital fraction in the Akaishi and Odoji Formations can be inferred from the Al_2O_3/TiO_2 ratio (Wang et al., 2017). According to Hayashi et al. (1997), low Al_2O_3/TiO_2 ratios (3–8) indicate a mafic source, moderate Al_2O_3/TiO_2 (8–21) ratios indicate an intermediate source and high Al_2O_3/TiO_2 (21–70) indicate a felsic source. The Al_2O_3/TiO_2 ratio is in a range of 24–50 and 24–36, respectively, in the Akaishi and the Odoji Formations. These values indicate that the detrital fraction originated from a felsic source. Further insights about the provenance of detritus were derived from the diagram of Roser and Korsch (1988), which allows the discrimination of provenance in terms of tectonic setting (Figure 3.25). This diagram shows that all the analyzed samples are in the field of felsic composition, and most of them fall in the quartzose sedimentary provenance field. These results indicate that the detrital fraction of sediments originated in a passive continental margin or recycled orogenic provinces (Roser and Korsch, 1988).

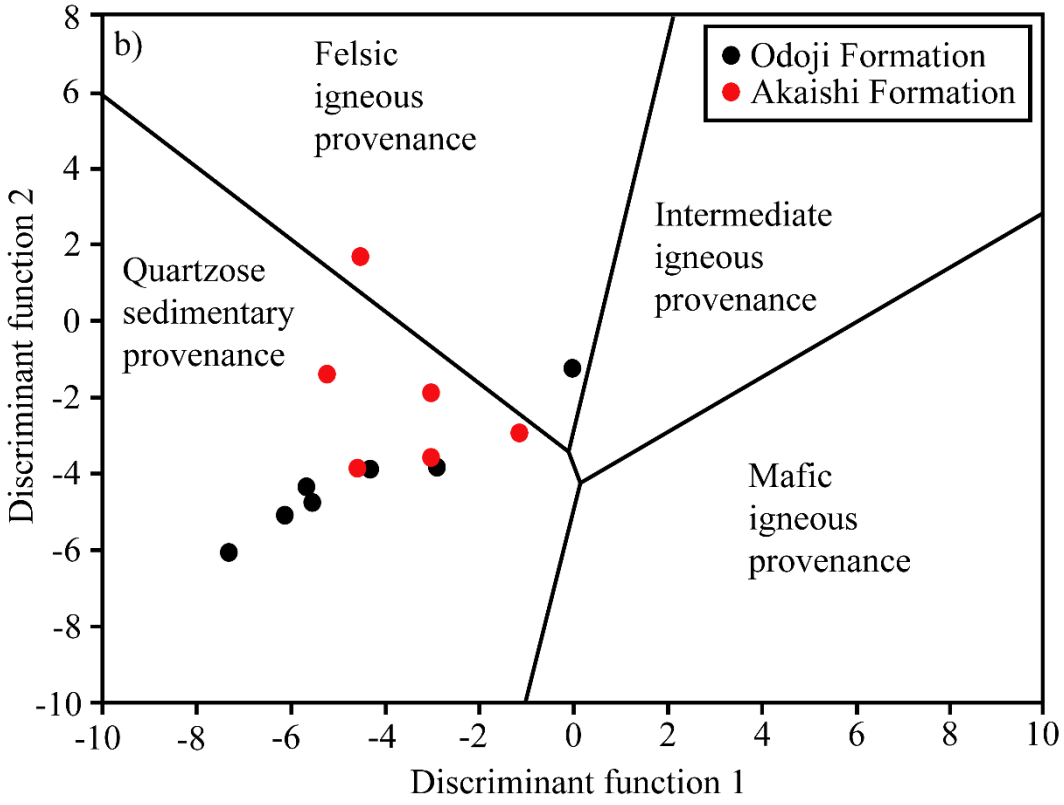

Figure 3.25. Provenance discrimination diagrams for the Akaishi, Odoji, and Onnagawa Formations. F1 = (−1.773×TiO_2%) + (0.607×Al_2O_3%) + (0.76×Fe_2O_{3T}%) + (−1.5×MgO%) + (0.616×CaO%) + (0.509×Na_2O%) + (−1.22 × K_2O%) + (−9.09). F2 = (0.445×TiO_2%) + (0.07×Al_2O_3%) + (−0.25×Fe_2O_{3T}%) + (−1.142×MgO%) + (0.438×CaO%) + (0.432×Na2O%) + (1.426×K_2O%) + (−6.861). After Roser & Korsch (1988).

Kimura et al. (2004) hypothesized that the terrigenous detritus of Middle-Late Miocene formations of northwestern Honshu originated from the continental rocks of the Asian continent and was transported from the continent by the Asian monsoon. Therefore, the detrital fraction variation was related to the variation in the intensity of the Asian monsoon. By observing detrital oxides (detrital SiO_2, Al_2O_3, K_2O, TiO_2, and Na_2O), it is possible to notice a gradual increase of the detrital fraction from the main part of the Odoji Formation to the Akaishi Formation (Figure 3.26). Some studies (Zachos et al., 2001; Wan et al., 2007; Clift et al., 2014; Tada et al., 2016) documented an increase of the Asian monsoon activity around 8 Ma. This event finds a good correlation with the timing of the deposition of the Akaishi Formation and suggests a relationship between the increase of the detrital fraction and the Asian monsoon's activity. Other studies (Tada, 1991, 1994) hypothesized a potential riverine input of detrital material from the land areas located in northeastern Honshu. A study from Nakajima (2017) indicated the presence of several continental granite deposits in the Kitakami and Abukuma areas. If the hypothesis of Tada (1991, 1994) is true, the increase of the detrital fraction in the Akaishi Formation may be related to an increase in the river sediment supply.

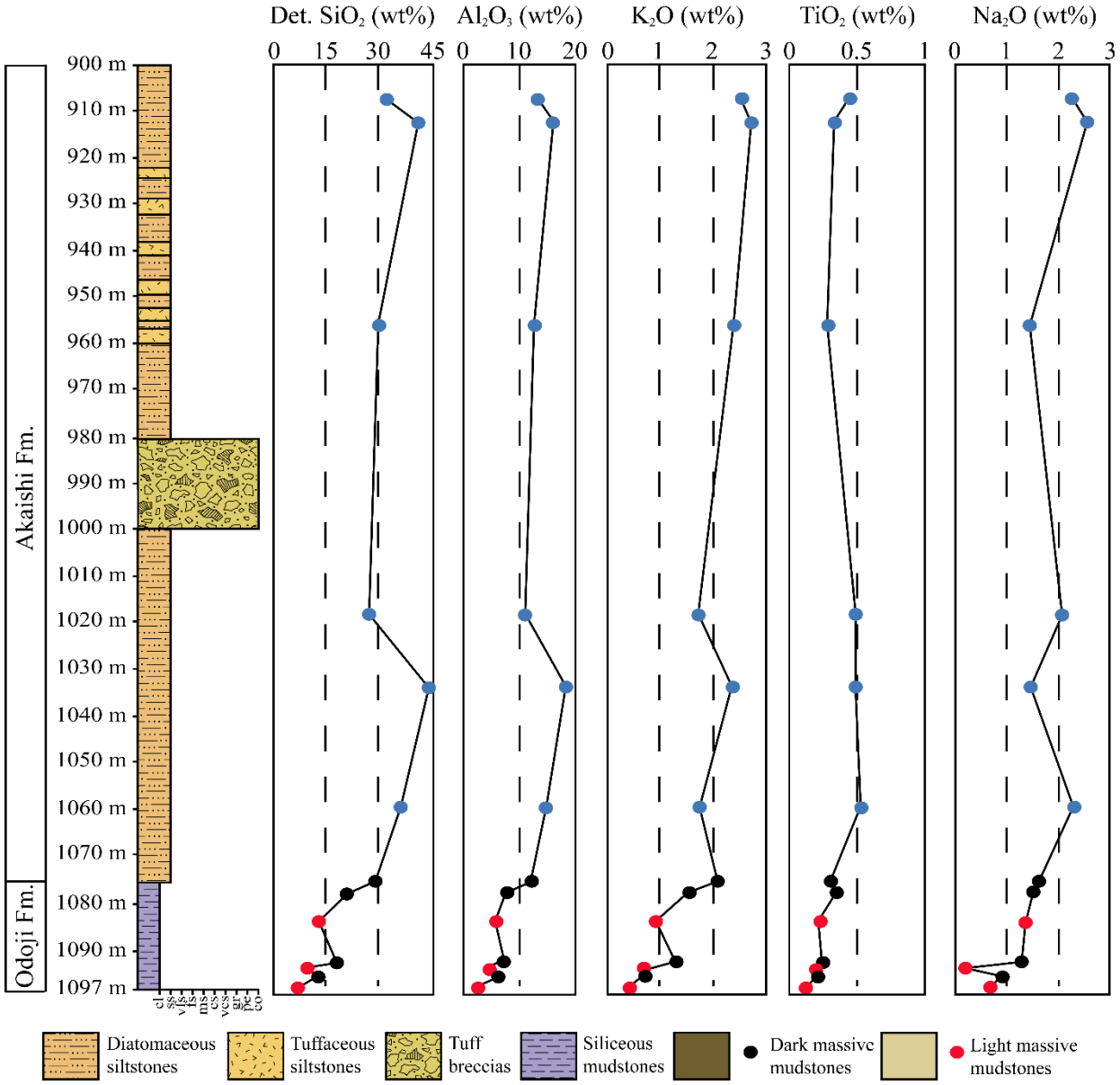

Figure 3.26. Vertical distribution of detrital SiO_2, Al_2O_3, K_2O, TiO_2, and Na_2O contents of the Akaishi and the Odoji Formations from the Tsugaru Basin area. The grain size fraction abbreviations are as follows: cl, clay; sl, silt; vfs, very fine sand; fs, fine sand; ms, medium sand; cs, coarse sand; vcs, very coarse sand; gr, granule; pe, pebble; co, cobble.

Several studies (Piper and Isaacs, 1984; Waseda et al., 1995; Ross and Bustin, 2009; Zeng et al., 2015) suggested that the influx of detrital minerals, such as clay minerals, plays an important role for the dilution and preservation of organic carbon. However, Bohacs et al. (2005) reported that an excessive influx of detrital minerals causes an excessive dilution of organic carbon. The influence of the detrital minerals on the preservation of TOC can be evaluated, correlating the detrital SiO_2, Al_2O_3, and K_2O contents with the TOC. The plots in Figure 3.27 indicate a moderate positive correlation between the detrital oxides and the TOC in the Odoji Formation. On the other hand, there is no

correlation between the TOC and the oxides in the Akaishi Formation. These results indicate a possible influence of clay minerals on the preservation of TOC in the Odoji Formation.

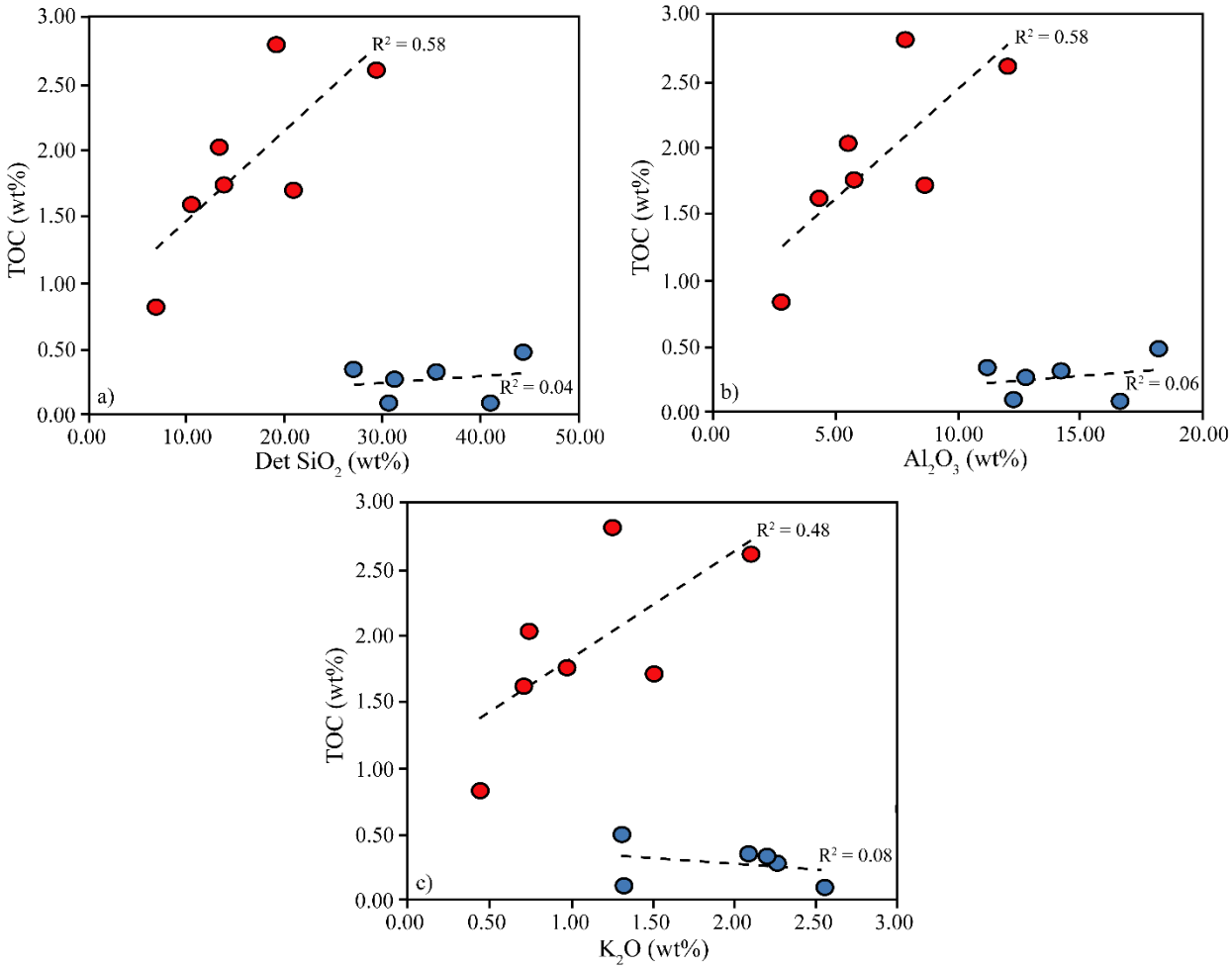

Figure 3.27. Cross plots of detrital SiO_2 (wt%), Al_2O_3 (wt%), and K_2O (wt%) versus total organic carbon (TOC) (wt%) of the samples from the Akaishi and the Odoji Formations. Red and blue points are respectively, the samples of the Akaishi and the Odoji Formations.

3.5.3.3 Paleoproductivity

The Middle-Late Miocene period in the Japan Sea is considered a period of intense surface water bio-productivity (Koizumi and Yamamoto, 2018). The broad diffusion of diatoms in areas of upwelling rich in nutrients (nitrogen, phosphorus, silica) favored the deposition of siliceous and diatomaceous sediments rich in biogenic silica (Aoyagi and Omokawa, 1992; Koizumi and Yamamoto, 2018). The TOC/TN ratios always lower than 20 in both the Akaishi and the Odoji Formations (Table 2), and the generally positive correlation between the TOC and the TN (Figure 3.28a) confirm that the siliceous sediments were mostly composed of marine diatomaceous organic matter (Meyers, 1997).

Various studies (Tada, 1991, 1994; Yamamoto and Watanabe, 1995; Yamamoto et al., 1999) correlated the biogenic silica variations with the paleoproductivity. The biogenic silica concentration in the sediments of the Odoji Formation is generally very high, indicating a high paleoproductivity during the deposition (Table 2). On the other hand, the Akaishi Formation is characterized by lower contents of the biogenic silica and by the increase of the detrital silica (Table 2). However, Tada et al. (1986) demonstrated that the decrease of biogenic silica was not related to a decrease of the paleoproductivity, but a continuous increase in detrital input since the early Late Miocene.

The plot of biogenic silica against TOC revealed a moderate negative correlation between these two elements in the Odoji Formation, and no correlation in the Akaishi Formation (Figure 3.28b). Tada (1994), Waseda et al. (1995), and Bohacs et al. (2005) recognized a similar negative correlation in the Japan Sea siliceous sediments and some sections of the Monterey Formation, in California. According to Bohacs et al. (2005), in areas of intense upwelling, the production of large volumes of biogenic silica can cause a biogenic dilution, which results in minor contents of organic matter in the sediments. Therefore, the TOC accumulation is favored in conditions of moderate bio-productivity, when the auto-dilution by biogenic silica is limited. The auto-dilution by biogenic silica possibly explains the negative correlation between the TOC and the biogenic silica in the Odoji Formation. On the other hand, the lack of correlation between the biogenic silica and the TOC in the Akaishi Formation, suggests that even if the paleo-productivity was high, the final TOC was probably affected by redox condition in the bottom water.

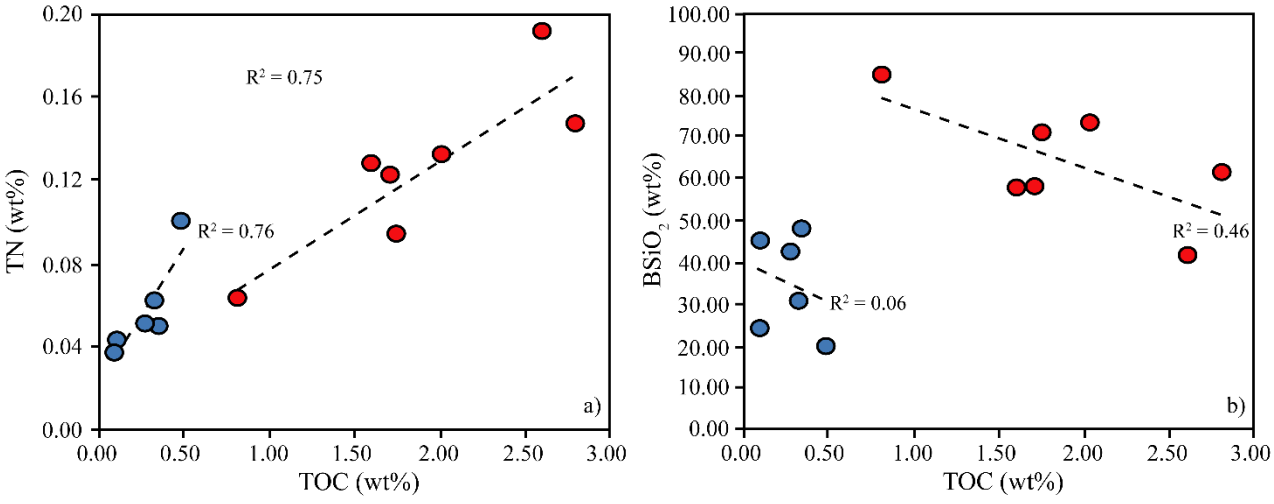

Figure 3.28. Cross plots of TN (wt%), and biogenic SiO_2 (wt%) versus total organic carbon (TOC) (wt%) of the samples from the Akaishi and the Odoji Formations.

3.5.3.4 Redox condition in the bottom waters

Paleoredox conditions of the Akaishi and Odoji Formations were reconstructed based on the lithological features of sediments, such as bioturbation and development of laminations. Various studies (Savrda and Bottjer, 1986; Tada et al., 1986; Tsuji et al., 1991; Waseda et al., 1995) associated the occurrence of bioturbations and the lack of development of laminations with the establishment of oxic/dysoxic conditions in the bottom water. On the other hand, the development of laminations is indicative of low oxygen marine environments (anoxic/euxinic) (Demaison and Moore, 1980). In this context, the moderate to high bioturbation in the Akaishi Formation suggests oxic conditions in the bottom water (Figure 3.6a); the massive facies with sparse bioturbation in the Odoji Formation possibly indicate a moderate presence of oxygen in the bottom water (Figure 3.8).

The framboidal pyrite size and the C-S relationship provide a useful method to identify the redox conditions and corroborate the lithological observations. According to several studies (Wilkin et al., 1996; Lyons and Severmann, 2006; Wei et al., 2016; Liu et al., 2019), framboidal pyrite formed in oxic/dysoxic condition is generally larger than 5 μm. The plot of Figure 3.29a and the data of Table 3 indicate that the framboidal pyrite size of the Odoji Formation's samples is always larger than 5 μm. On the other hand, the absence of framboidal pyrite in the Akaishi Formation is in agreement with the hypotheses of Takahashi et al. (2015) and Wignall et al. (2015) studies, who associated the absence of framboidal pyrite to the establishment of oxic conditions. The C-S diagram shows that most of the samples are in the area of normal marine oxygenated conditions (Figure 3.29b). However, some samples from both the Akaishi and the Odoji Formations do not follow this trend. The trend of the Akaishi Formation can be explained with the presence of sulfur not included in pyrite minerals. On the other hand, the trend of the Odoji Formation was influenced by the limited input of reactive Fe. Specifically, the amount of Fe was not enough to form pyrite minerals in combination with the sulfur.

According to several studies (Demaison and Moore, 1980; Glenn and Arthur, 1985; Tyson, 1995; Katz, 2005), the redox condition is one of the main factors affecting the preservation of the organic carbon. Based on this study's data, the Akaishi Formation is characterized by lower organic carbon contents than the Odoji Formation (Figure 3.23). Additionally, the HI-OI diagram showed that the samples of the Akaishi Formation are characterized by type III kerogen (Figure 3.19). This feature indicates that the organic matter of the Akaishi Formation's samples was degraded and could explain the low values of TOC. On the other hand, the good content of TOC in the Odoji Formation indicates that the organic matter was preserved from the degradation.

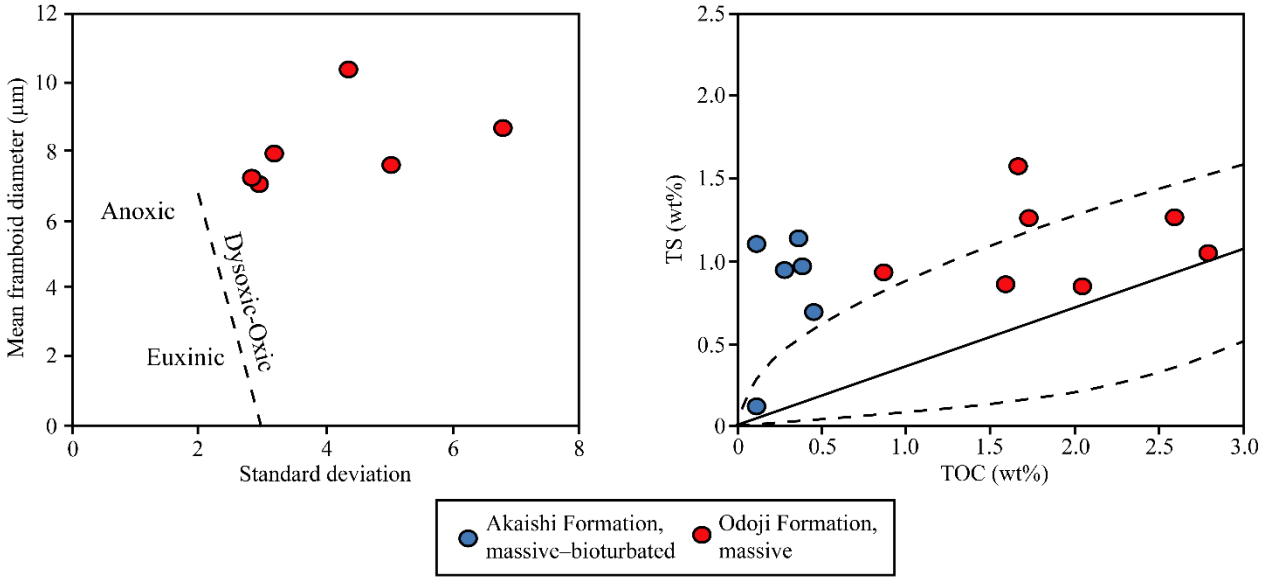

Figure 3.29. (a) Mean diameter versus standard deviation plot of framboidal pyrite data of the Odoji Formation (modified from Wilkin et al., 1996); (b) Crossplot of sulfur and organic carbon in sediments of the Akaishi and the Odoji Formations. The outlined area denotes the region of normal marine sediments (after Berner and Raiswell, 1983).

3.6 Conclusions

The sedimentological and geochemical characterization of DTH27-1 well's formations allowed us to evaluate the source rock potential and the thermal evolution of the Tsugaru Basin area and hypothesize the paleoenvironmental conditions in the Middle-Late Miocene.

Rock-Eval pyrolysis analysis of the Miocene succession revealed two formations with a good TOC range and generative potential, the siliceous mudstones of the Odoji Formation, and the coal levels of the Odose Formation. On the other hand, the Akaishi and Tanosawa Formations were poor in organic carbon and had low generative potential. T_{max} ranges and paleotemperature through thermal modeling indicated that the Odoji Formation is immature for the generation of hydrocarbons, while the Odose Formation is in the early oil window. The general low thermal maturity in the Tsugaru Basin area is related to a limited burial of the Miocene succession than to a geothermal gradient anomaly.

Analysis of the detrital oxides revealed that a moderate to high paleo-weathering in the Middle-Late Miocene period was active at the source of the detrital fraction. The felsic composition of this fraction suggested that the source of the detrital fraction derived from continental areas located on the Asian continent and in northeastern Honshu. In the first case, the Asian monsoon had a primary

role in the transport of the detrital fraction from Asia to the paleo-Japan Sea. This hypothesis suggests a relationship between the monsoon activity and the detrital fraction content in the Japan Sea's sediments. In the second case, the detrital fraction is derived from a riverine source. Therefore, the detrital fraction content was related to the intensity in the riverine supply. The variation of detrital fraction shows a good correlation with the TOC in the Odoji Formation samples, indicating that dilution of organic matter by detritus probably favored the preservation of the organic carbon.

The high concentrations of the biogenic SiO_2 in the Akaishi and the Odoji Formations indicated high primary productivity of the diatoms in the surface water. The high productivity favored the input of large amounts of organic matter in the water column, which compensated for the degradation process of the oxidizing water column during the deposition of the Odoji Formation. In other cases, the large amounts of deposited biogenic silica generated an auto-dilution process that reduced the organic carbon content even during the low-oxygen intervals.

The massive and bioturbated facies and the morphology of the framboidal pyrite indicate that an oxidizing water column characterized the Tsugaru Basin area. The intense degradation process active in the water column, negatively affected the TOC of the Akaishi Formation, resulting in a marked difference in the TOC content between the Akaishi and the Odoji Formations. The grain size and porosity of the Akaishi Formation's siltstones possibly favored the inflow of oxygenated waters from the water column, facilitating the process of degradation of the organic matter.

CHAPTER 4

Sedimentary and geochemical characterization of the Middle-Late Miocene siliceous formations in the Akita Basin. Japan

4.1 Introduction

Akita region is considered one of the most important areas for hydrocarbons exploration in Japan, and the Middle-Late Miocene siliceous formations were targeted by several studies of both academia and Oil & Gas industry. These formations have a potential for the generation of hydrocarbons, and they were explored for both conventional and, more recently, unconventional oil and gas exploration and production (Aoyagi and Omokawa, 1992; Waseda et al., 1995; Yokoi et al., 2013; Yokoi and Tsuji, 2015). Besides their importance for hydrocarbon exploration, the outcrops of these formations throughout all the Akita Prefecture offer the chance to interpret the Akita Basin's sedimentary and paleoenvironmental evolution in the Middle-Late Miocene. Several studies (Tada, 1991; Tsuji et al., 1991; Sugii, 1998) highlighted the importance of lithofacies variations like the occurrence of laminations or the degree of bioturbation. The lithofacies data were interpreted to define the paleo-redox conditions of the Japan Sea in the Middle Miocene.

Other studies (Yamamoto and Watanabe, 1994; Yamamoto et al., 1999; Kimura et al., 2004) attempted to interpret the paleoenvironmental conditions through bulk compositional analysis. Although these data provided a robust background about the paleoenvironmental evolution of the Japan Sea in the Middle-Late Miocene, they did not include complete data about the influence of these conditions on the preservation and accumulation of organic matter in these sediments. Additionally, previous studies were mostly focused on selected study areas throughout the Akita region. Because the results and models of these studies are local, it is not easy to extend the authors' interpretations to each area of northwestern Honshu. Therefore, to interpret the Japan Sea's paleo-oceanographic condition in the Middle-Late Miocene, it is necessary to investigate the Middle-Late Miocene formations throughout all the regions of northwestern Honshu.

This chapter is focused on the Onnagawa and the Iwaya Formations outcropping respectively in the Sugisawa and Gotanzawa areas, in the central-northern Akita Prefecture (Figure 4.1). Samples from different outcropping sections were analyzed with the Rock-Eval pyrolysis method to define the source rock potential and the thermal maturity of these formations. Subsequently, sedimentological and geochemical investigations were conducted on the siliceous sediments to assess the paleo primary productivity, the redox conditions in the bottom water, and the detrital matter input in the Akita region.

Additionally, it was considered the influence of these factors on preserving the organic matter in these sediments.

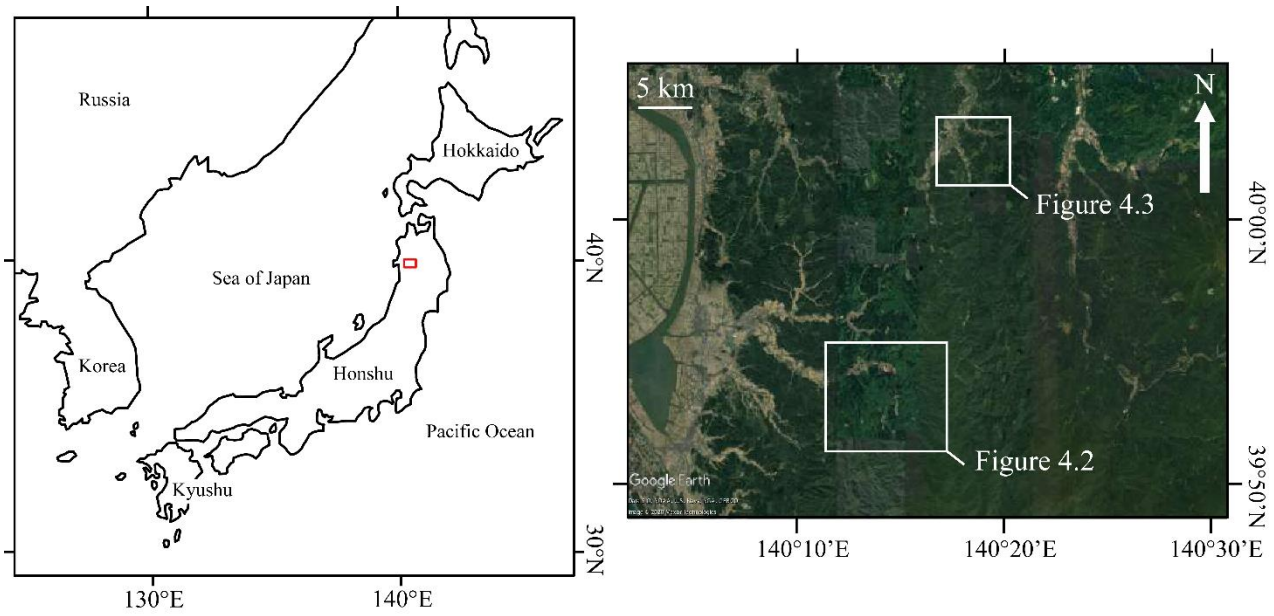

Figure 4.1. Location map showing the Sugisawa and Gotanzawa areas (from Google Earth Pro: Image © 2020 Maxar Technologies, Data SIO, NOOA, U.S. Navy, NGA, GEBCO).

4.2 Geological Setting

The Sugisawa and Gotanzawa areas are in the central-northern part of the Akita Prefecture (Figure 4.1). General geological maps of the two study areas are shown in Figures 4.2 and 4.3. Both the areas comprise geological succession, correlated for age and lithologies (Figure 4.4). These stratigraphic successions are correlated with the one outcropping at the Oga Peninsula, traditionally considered the reference for the Akita region (Koizumi et al., 2009).

The base of the Miocene successions is represented in both the areas by the Early Miocene Omata Formation. This formation is composed of pyroclastic and volcanoclastic rocks, non-marine deposits, and lacustrine sediments (Sumi and Moritani, 1972; Ingle et al., 1990; Kano et al., 2011). These volcanic deposits are associated with the initial extension and rifting in the Japan Sea region. The Omata Formation is overlaid by the Early-Middle Miocene Torisagawa and Utto Formations in Sugisawa (Kano et al., 2011), and the Makibuchi and Kirinai Formations in Gotanzawa (Sumi and Moritani, 1972). These formations are composed mainly of pyroclastic and volcanoclastic rocks, occasionally interfingered by sandstones and conglomerates, and marine deposits (Sumi and Moritani, 1972; Kano et al., 2011). The marine deposits in this interval are considered the evidence of marine

flooding and marked the beginning of a phase of subsidence, which brought to the formation of the Japan Sea (Iijima et al., 1988).

Substrate units are followed by the deposition, during the Middle-Late Miocene, of siliceous sediments, generally enriched in the diatomaceous organic component. Middle-Late Miocene geological record is represented in the Sugisawa and Gotanzawa areas by the Onnagawa and the Iwaya Formation, respectively (Sumi and Moritani, 1972; Iijima et al., 1988; Tada, 1991; Ujiié, 1995). The Onnagawa and Iwaya Formations overlies respectively, the Kitanomatasawa and the Osarubegawa Formations (Sumi and Moritani, 1972; Kano et al., 2011). These formations are composed of acid rocks accompanied by basalts and andesites, mudstones, and terrigenous sediments (Sumi and Moritani, 1972; Kano et al., 2011).

The deposition of siliceous sediments was associated with a rapid phase of subsidence that caused the deepening of the sea at bathyal depths (Iijima et al., 1988; Tada, 1991; Tada, 1994). According to the biostratigraphic data of Koizumi and Matoba (1989) and Hibi (2020), the Onnagawa and Iwaya Formations deposited between 13 Ma and 10. Various studies (Ingle et al., 1990; Tada, 1991; Aoyagi and Omokawa, 1992; Tada, 1994) indicated that these deposits reflected an increase in primary bio-productivity and an oxygen-deficient condition in the bottom waters. Studies from Tada (1994) and Matsuzaki et al. (2018) suggested that the presence of oxygen-deficient conditions in the bottom waters was influenced by the inflow of Oxygen Minimum Zone (OMZ) water from the North Pacific, through a 500 to 1000 m deep sill. Additionally, Yamamoto et al. (1999) indicated a reduction in the flux of terrigenous sediments to the basinal areas.

During the Late Miocene and the Early Pliocene, a marine regression occurred with a compressional tectonic uplift. The compressional phase started at 7 Ma and caused the progressive shoaling of the sill that connected the Japan Sea with the North Pacific (Tada, 1994; Matsuzaki et al., 2018). The shoaling of the sill limited the inflow of OMZ water from the North Pacific, causing the establishment of oxygenated conditions in the bottom waters (Ingle et al., 1990). The geological record in this period is represented by the deposition of the Funakawa Formation in Akita Prefecture and the Akaishi Formation in Aomori Prefecture (Iijima et al., 1988; Tada, 1991; Jingu and Ujiié, 1990). These formations are composed respectively by mudstones and diatomaceous siltstones with intercalated tuffs and tuffaceous sediments. Additionally, Yamamoto et al. (1999) reported that the increase in the flux of terrigenous sediments resulted in the dilution of diatomaceous deposits.

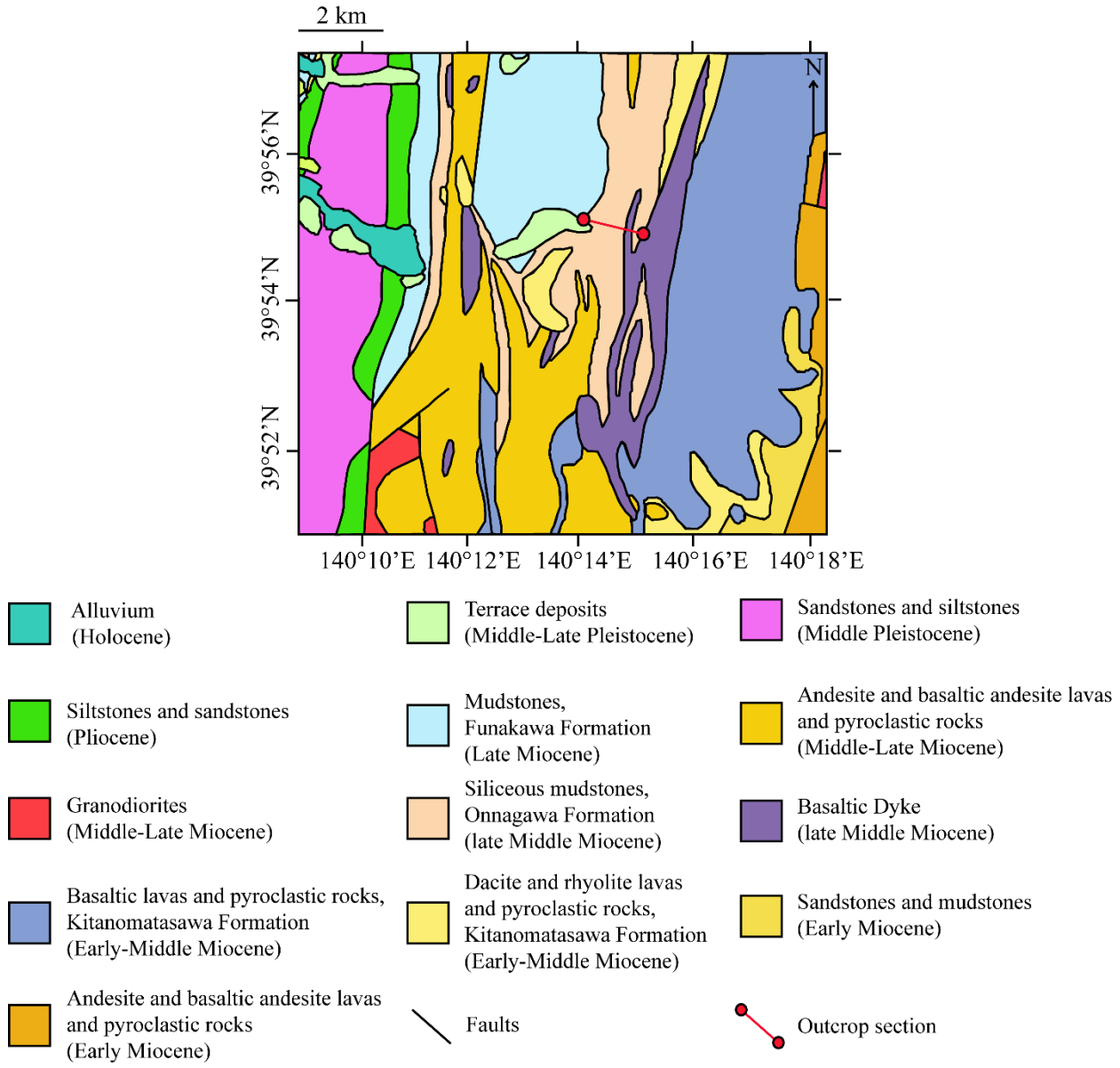

Figure 4.2. Geological map of the Sugisawa area with the outcropping formations and main tectonic elements. The red line indicates the sampling section of the Onnagawa Formation examined in this study. Redrawn from the "Seamless Digital Geological Map" of the Geological Survey of Japan Web Page (https://gbank.gsj.jp/geonavi/geonavi.php#12,40.62056,140.26143).

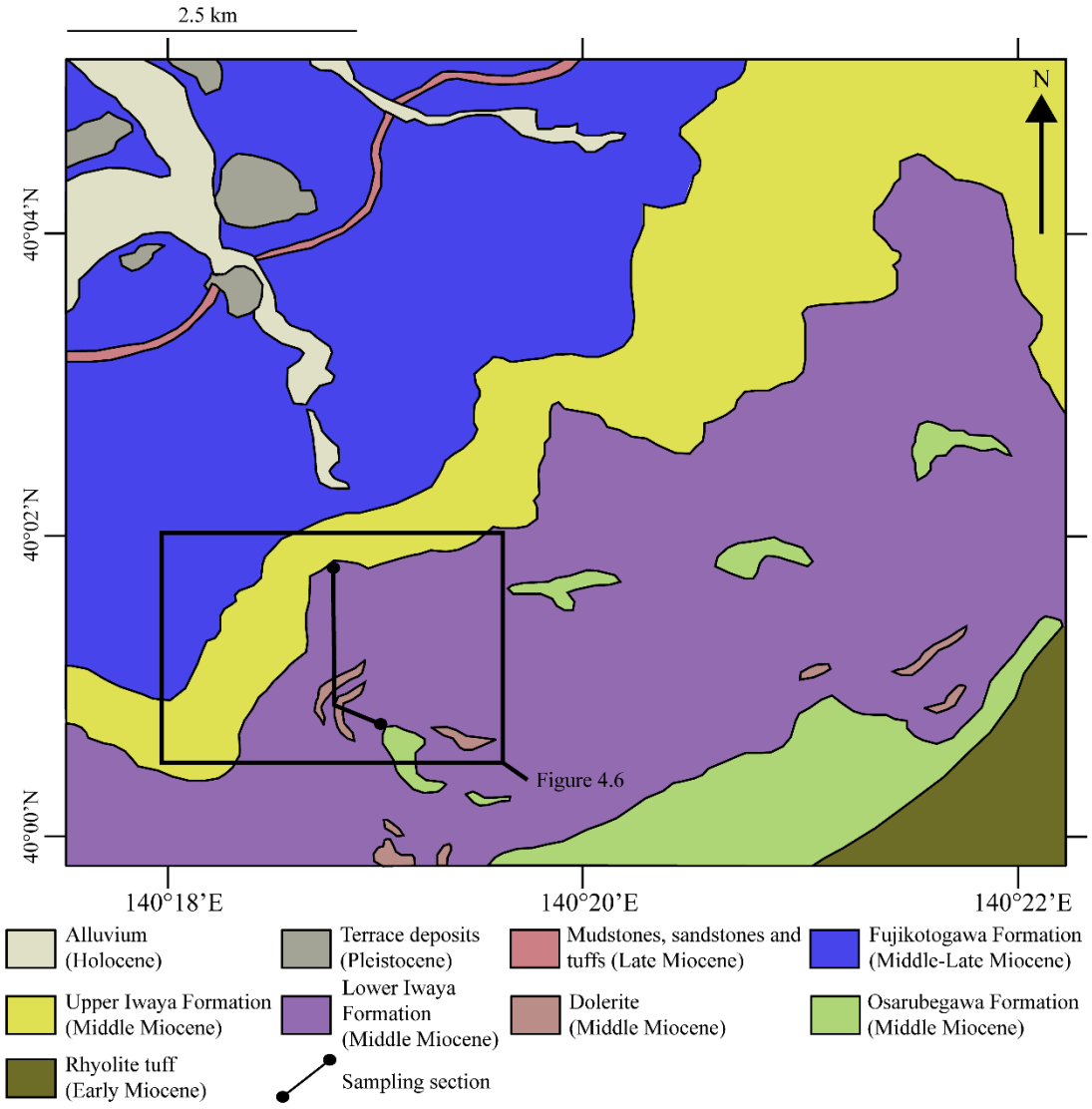

Figure 4.3. Geological map of the Kamikoani Village area, including Gotanzawa with the outcropping formations and main tectonic elements. The black line indicates the sampling section of the Iwaya Formation examined in this study. Resized and redrawn from the 1:50000 scale Yonaizawa geological map (Sumi and Moritani, 1972).

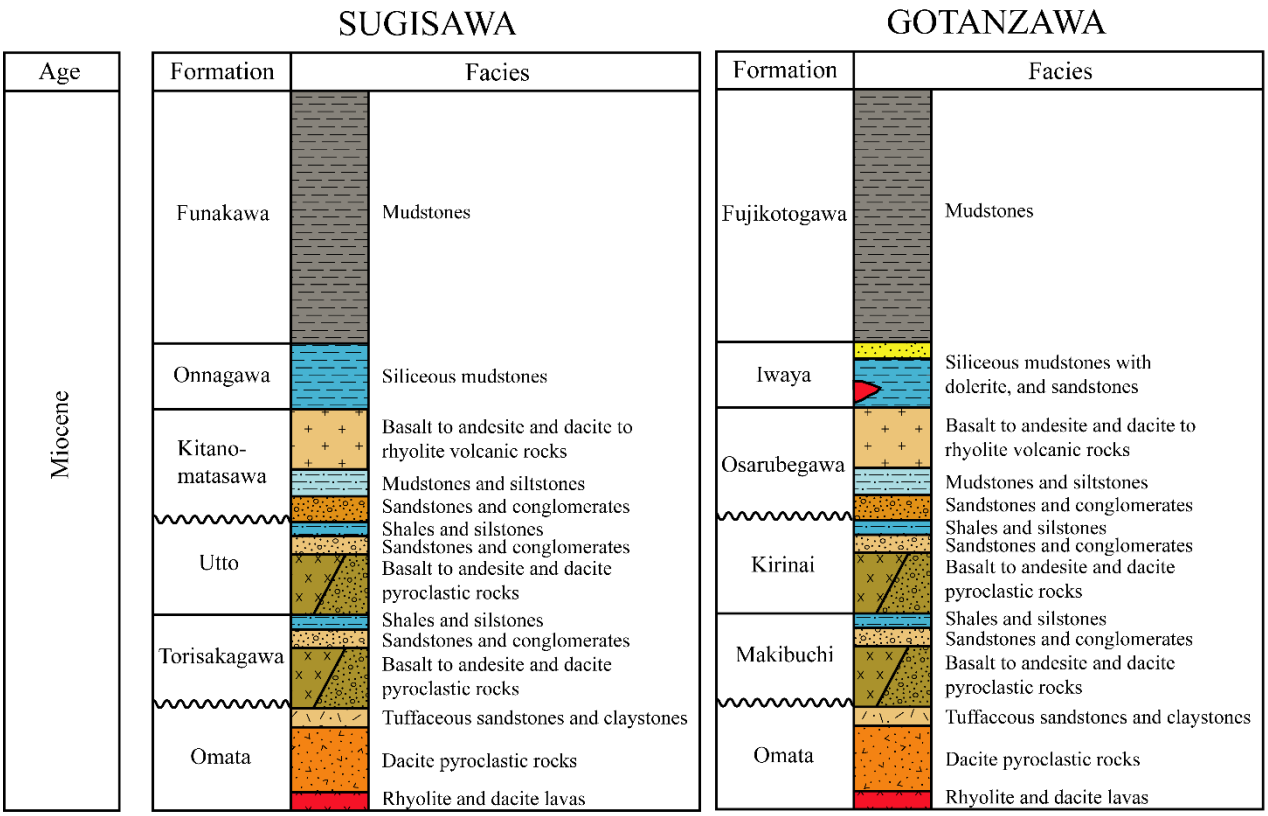

Figure 4.4. Schematic columnar section of the Miocene succession in the Sugisawa and Gotanzawa areas (modified from Sumi and Moritani, 1972 and Kano et al., 2011).

4.3 Materials

A total of thirty-nine samples were collected, lithologically described, and used for the analysis. All the samples were stored in plastic bags to preserve them from contamination and oxidation. Eighteen samples from the Onnagawa Formation were collected during a sampling campaign in the Gojome-Sugisawa area in 2017, along the outcrops of the Babame River (Figure 4.2). The samples were projected, at different heights, on a compiled stratigraphic column of the outcrop section (Figure 4.5). Twenty-one samples from the Iwaya Formation were collected along a sampling route in the Gotanzawa area, near the Kamikoani Village during a sampling campaign in 2019 (Figures 4.3 and 4.6). The analyses of the samples were performed with the following workflow:

(1) Sugisawa: all the samples analyzed with the Rock-Eval pyrolysis, CHNS, and XRF. The framboidal pyrite of eight samples was observed through reflection microscopy;

(2) Gotanzawa: all the samples analyzed with the Rock-Eval pyrolysis. The framboidal pyrite of ten samples was observed through reflection microscopy.

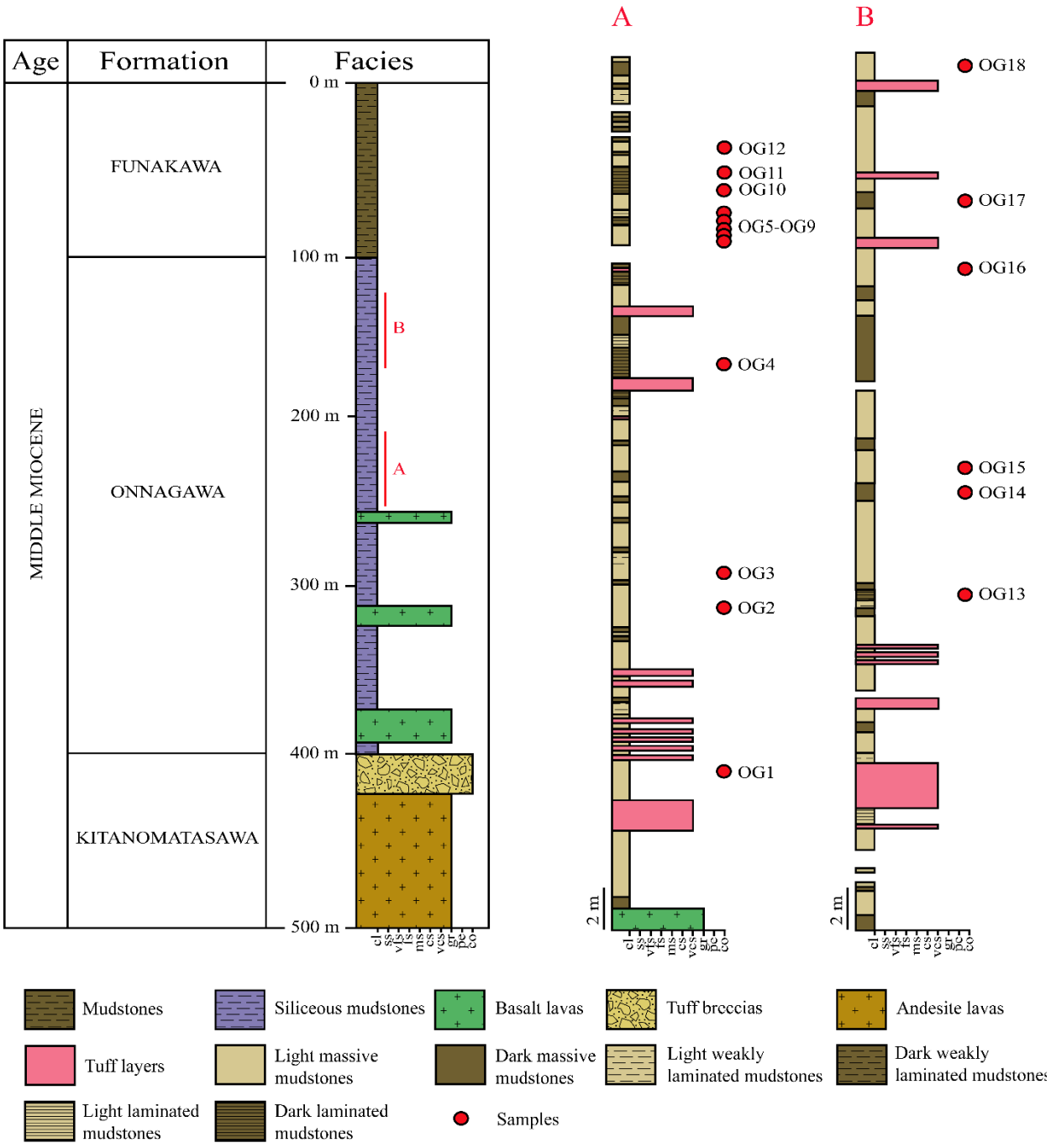

Figure 4.5. Stratigraphic columns of the formations outcropping along the sampling section in the Sugisawa area. The left column includes all the formations from the Middle Miocene to the Late Miocene. The central and right columns show the lithofacies of the Onnagawa Formation. Red points indicate the position of the samples analyzed in this study. The grain size fraction abbreviations are as follows: cl, clay; sl, silt; vfs, very fine sand; fs, fine sand; ms, medium sand; cs, coarse sand; vcs, very coarse sand; gr, granule; pe, pebble; co, cobble.

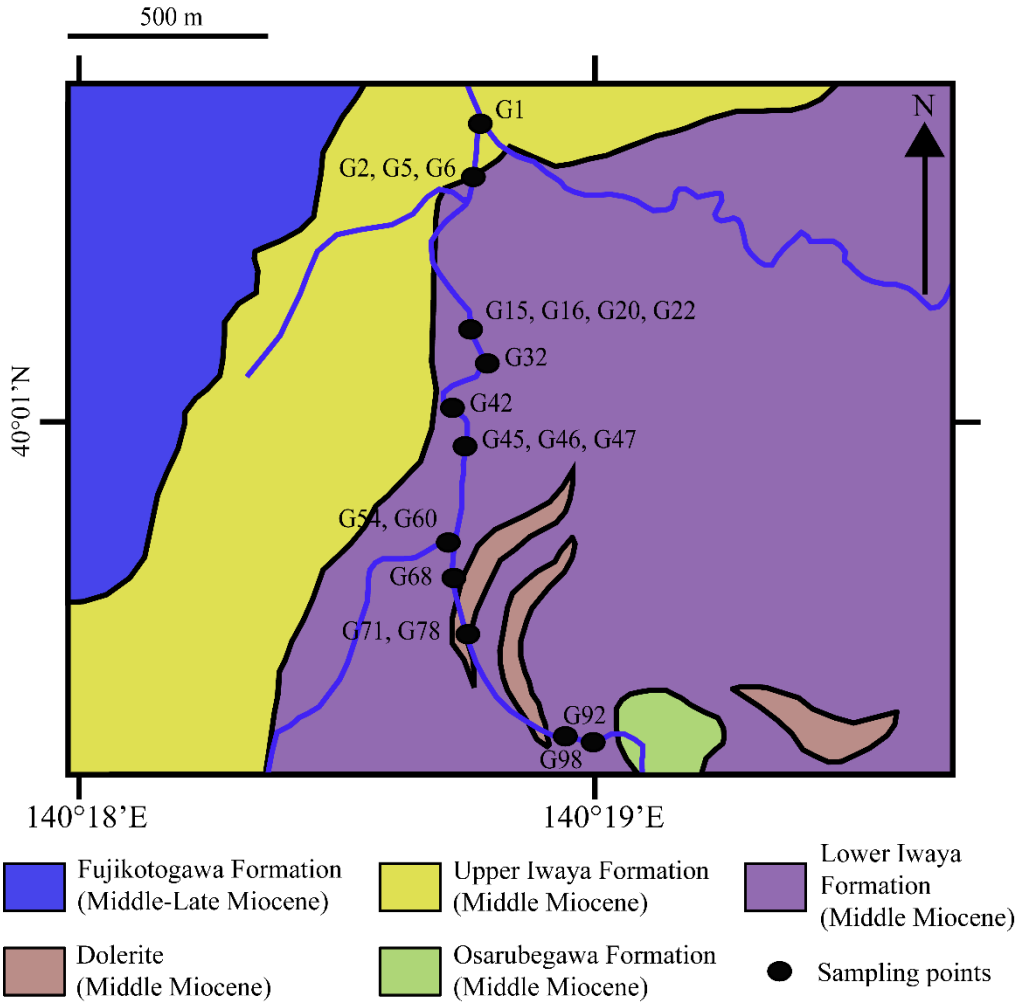

Figure 4.6. Geological map of the Kamikoani Village area, including Gotanzawa with the outcropping formations and main tectonic elements. The black points indicate the sampling locations and the name of the samples analyzed in this study. Resized and redrawn from the 1:50000 scale Yonaizawa geological map (Sumi and Moritani, 1972).

4.4 Results

4.4.1 Lithofacies description

The samples of the Onnagawa and Iwaya Formations are composed mostly of siliceous hard mudstones, and they show rhythmical alternations of light and dark levels (Figure 4.7). The Onnagawa Formation's mudstones are characterized by a color variation from dark brown-dark grey in the dark to pale brown in the light levels. On the other hand, the Iwaya Formation is characterized by a color variation from dark grey in the dark to brow grey in the light levels. The thickness of the dark and light levels varies from few centimeters to a few meters in both the formations. The frequency of light and dark levels is comparable in the Onnagawa Formation, while the frequency of

dark levels is higher than the light levels in the Iwaya Formation (Hibi, 2020). The Onnagawa Formation of the Sugisawa area is characterized by the occurrence of both massive and laminated sediments. Laminations are parallel, 5–7 millimeters thick, and less than 1 millimeter spaced (Figure 4.7 a-b). On the other hand, the Iwaya Formation is characterized exclusively by massive sediments (Figure 4.7 c-d).

Figure 4.7. Photos of sampling outcrops in the Sugisawa and Gotanzawa areas. (a) Alternations of light and dark massive mudstones of the Onnagawa Formation; (b) Alternations of light and dark laminated mudstones of the Onnagawa Formation; (c-d) Alternations of light and dark massive mudstones of the Iwaya Formation.

4.4.2 Organic Geochemistry

4.4.2.1 Pyrolysis Rock-Eval

The Rock-Eval pyrolysis data for each sample of the studied formations are reported in Table 4, while in Figures 4.8 and 4.9 are reported the vertical distributions of the total organic carbon (TOC) and maximum temperature (T_{max}).

Based on the Rock-Eval pyrolysis data, the Onnagawa and the Iwaya Formations are variably enriched in TOC. The TOC shows an increasing trend from the light to dark-colored samples in the Iwaya Formation (Figure 4.8). However, the same trend was not recognized in the Onnagawa Formation (Figure 4.9). The ranges of values of the S1, S2, and S3 are comparable in the two formations (Table 4). values do not show a significant variation in the two formations. High HI and low OI characterize all the samples of the Onnagawa Formation; in the Iwaya Formation, the low TOC samples are characterized by lower HI and higher OI than the samples with high TOC values (Table 4).

The T_{max} values of the Onnagawa and Iwaya Formations show a minimal variation, and, except for one sample, they are always lower than 435 °C (Table 4, Figures 4.8 and 4.9). Therefore, both the formations are immature for hydrocarbons generation.

4.4.2.2 CHNS elemental analysis

CHNS elemental analysis data of samples from *Onnagawa Formation* are reported in Table 5, while in Figure 4.10 are reported the vertical distributions of the total nitrogen and sulfur, and TOC/TN and TOC/TS ratios. The nitrogen content is very low in all the analyzed samples, but it tends to increase slightly upward (Figure 4.10). However, the nitrogen variations do not show a relationship with the lithofacies changes. The TOC/TN ratio is lower than 20 in most of the samples, but it never exceeds the value of 30 (Figure 4.10).

The sulfur content is lower than 1 wt%, except in two samples where it exceeds 1 wt%. The sulfur contents, as well as the TOC/TS ratio, are variable along with the stratigraphy, but they did not show any relationship with the lithofacies changes (Figure 4.10).

Table 4 Rock-Eval pyrolysis data of the Onnagawa and Iwaya Formations.

Sample Name	TOC (wt%)	S1 (mg/g)	S2 (mg/g)	S3 (mg/g)	T_{max} (°C)	S1+S2 (mg/g)	S2/S3	HI (mg/g)	OI (mg/g)
OG1	0.57	0.09	3.18	0.13	413	3.27	24.40	558	23
OG2	0.71	0.11	3.41	0.23	410	3.52	14.80	480	14
OG3	0.79	0.22	3.76	0.60	400	3.98	6.20	476	16
OG4	0.94	0.18	4.36	0.20	409	4.54	21.80	464	21
OG5	1.11	0.10	5.87	0.24	401	5.97	24.40	529	9
OG6	1.36	0.40	7.92	0.13	402	8.32	60.90	582	10
OG7	1.21	0.26	6.24	0.13	406	6.50	48.00	516	11
OG8	0.85	0.38	5.20	0.11	404	5.58	52.00	612	13
OG9	1.41	0.38	8.47	0.16	405	8.85	52.90	601	11
OG10	0.79	0.32	5.57	0.13	406	5.89	42.80	705	16
OG11	2.10	0.54	12.74	0.24	404	13.28	53.10	607	11
OG12	1.12	0.37	6.20	0.12	403	6.57	51.60	554	11
OG13	1.41	0.54	8.25	0.15	411	8.79	55.00	585	11
OG14	1.62	0.20	8.08	0.16	410	8.28	50.50	499	10
OG15	0.78	0.29	4.80	0.13	401	5.09	36.90	615	17
OG16	1.36	0.15	6.52	0.14	411	6.67	46.50	479	10
OG17	1.95	0.23	8.85	0.22	408	9.08	40.20	454	11
OG18	1.85	0.22	8.36	0.16	402	8.58	52.20	454	9

Table 4 (Continued).

Sample Name	TOC (wt%)	S1 (mg/g)	S2 (mg/g)	S3 (mg/g)	T_{max} (°C)	S1+S2 (mg/g)	S2/S3	HI (mg/g)	OI (mg/g)
G1	1.47	0.11	5.29	0.31	407	5.40	17.06	360	21
G2	1.30	0.25	5.84	0.15	403	6.09	38.93	449	12
G5	0.56	0.04	1.40	0.28	418	1.44	5.00	245	50
G6	1.68	0.26	9.30	0.14	413	9.56	66.42	554	8
G15	1.62	0.20	6.83	0.29	410	7.03	23.55	422	14
G16	1.71	0.59	6.37	0.24	410	6.96	26.54	505	11
G20	1.47	0.22	6.07	0.21	405	6.29	28.90	413	14
G22	2.30	0.38	9.94	0.16	407	10.32	62.12	432	7
G32	1.46	0.29	5.92	0.15	407	6.21	39.46	405	10
G42	1.11	0.20	4.55	0.08	407	4.75	56.87	410	7
G45	1.14	0.10	3.88	0.14	409	3.98	27.71	340	7
G46	0.47	0.06	0.94	0.38	427	1.00	2.47	200	81
G47	1.73	0.20	5.79	0.23	406	5.99	25.17	335	13
G54	0.46	0.03	0.61	0.33	428	0.64	1.84	133	72
G60	0.83	0.03	1.63	0.21	420	1.66	7.76	196	25
G68	0.65	0.03	1.05	0.19	422	1.08	5.52	162	29
G71	3.00	0.21	7.63	0.37	413	7.84	20.62	231	11
G78	1.50	0.04	2.70	0.70	429	2.74	3.85	180	47
G92	1.70	0.08	5.43	0.18	417	5.51	30.16	319	11
G98	0.27	0.05	2.36	0.09	441	2.41	26.20	133	33

Abbreviations: HI, hydrogen index (mg hydrocarbon (S2)/g TOC); OI, oxygen index (mg CO2 (S3)/g TOC); S1, low hydrocarbon yield (mg hydrocarbon/g rock); S2, high hydrocarbon yield (mg hydrocarbon/g rock); S3, CO2 (mg CO2/g rock); S1 + S2, Genetic source potential; S2/S3, hydrocarbon type index; T_{max}, Maximum temperature; TOC, total organic carbon; wt%, weight percent.

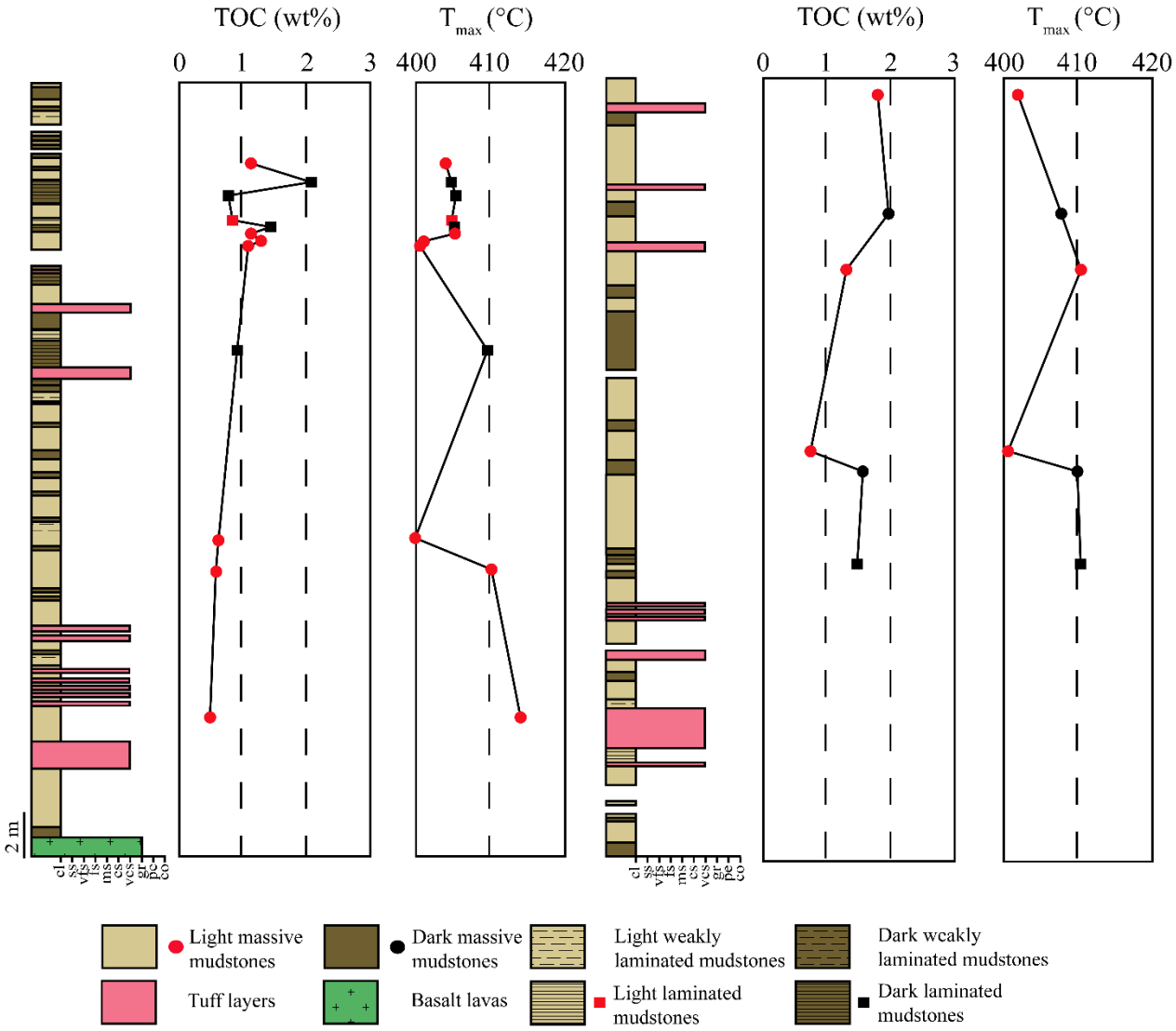

Figure 4.8. Vertical distributions of the TOC and T_{max} in the Onnagawa Formation. The grain size fraction abbreviations are as follows: cl, clay; sl, silt; vfs, very fine sand; fs, fine sand; ms, medium sand; cs, coarse sand; vcs, very coarse sand; gr, granule; pe, pebble; co, cobble.

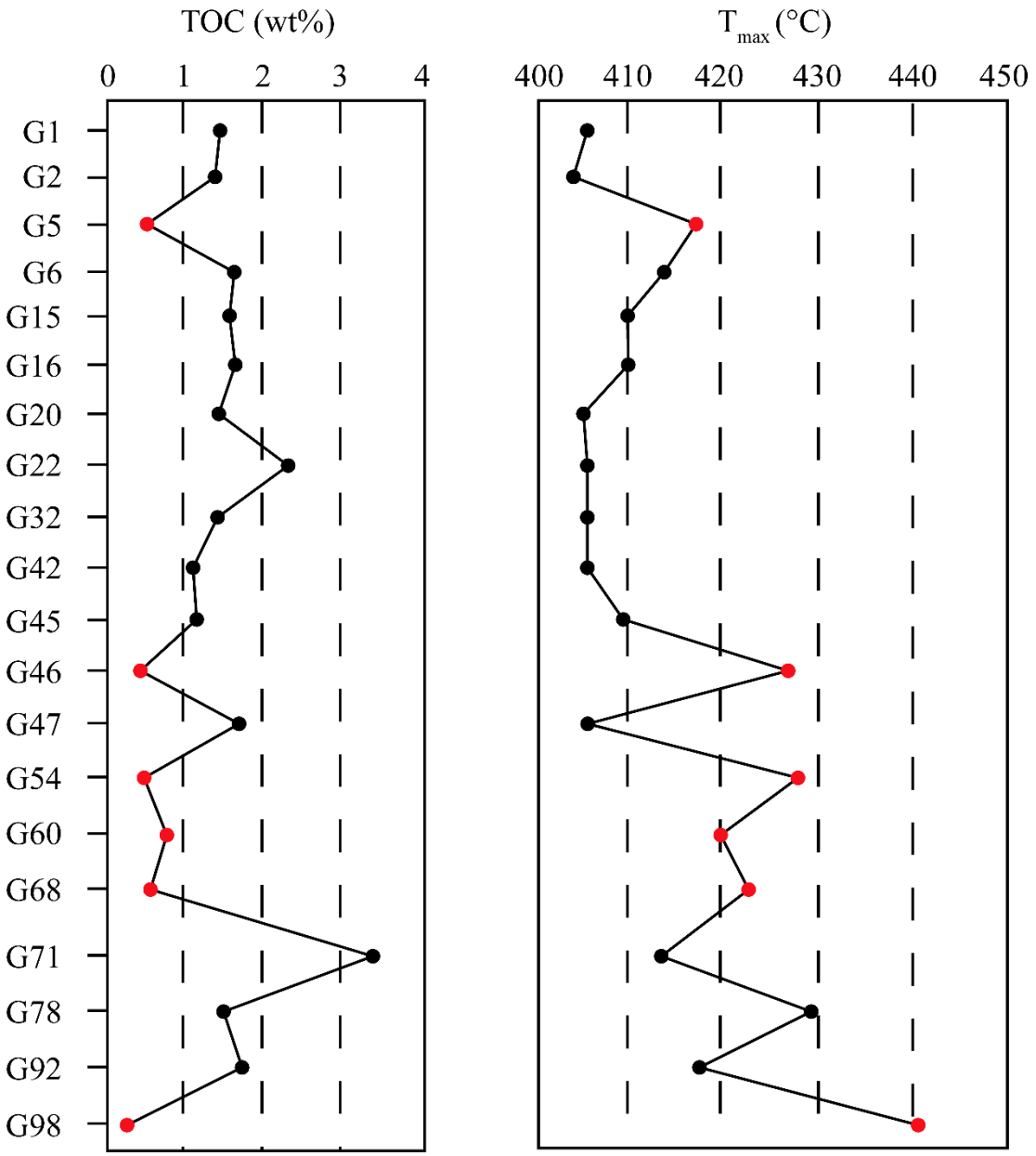

Figure 4.9. Vertical distributions of the TOC and T_{max} in the Iwaya Formation. The red and black points indicate, respectively, the light massive and dark massive samples.

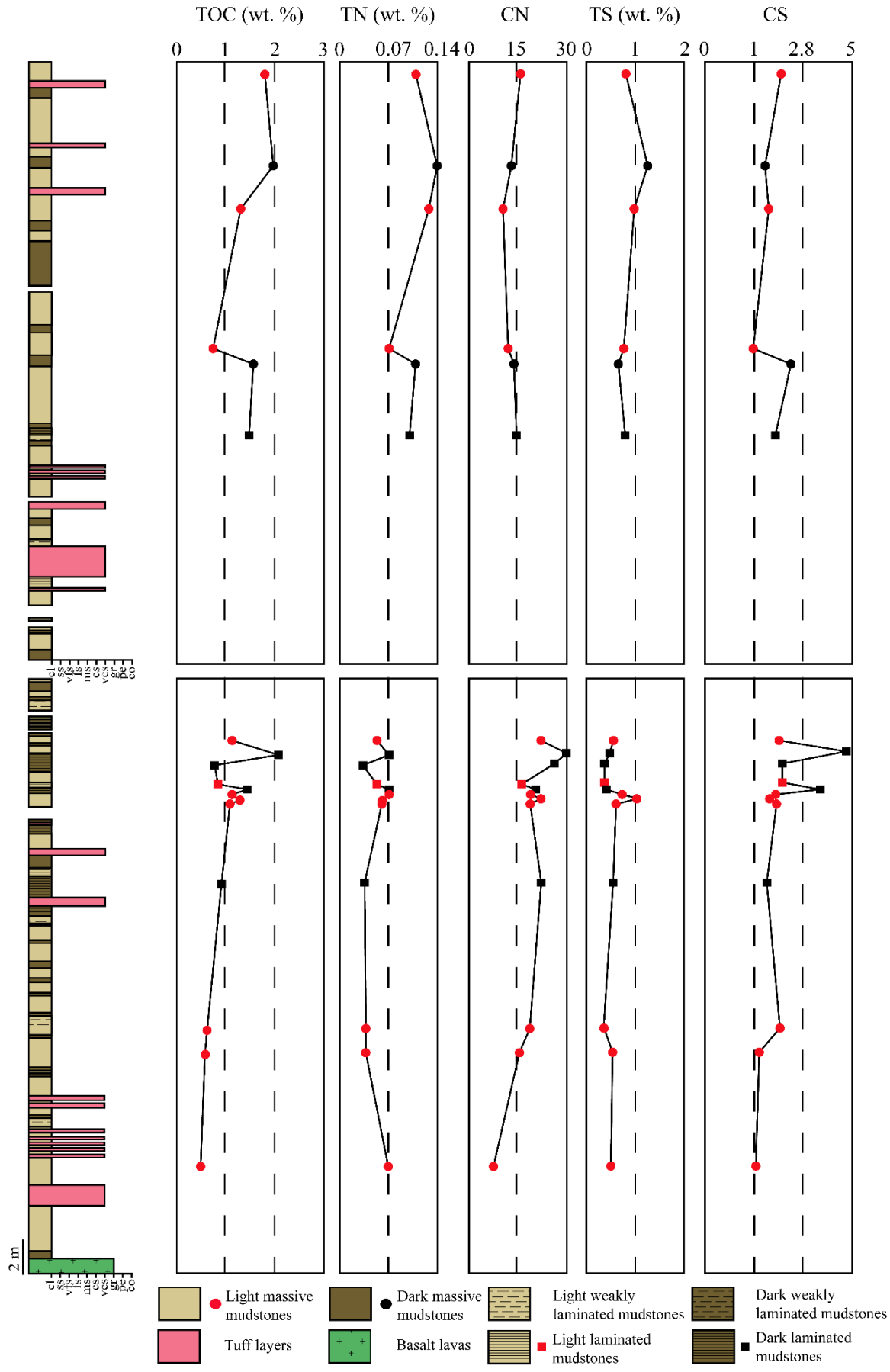

Figure 4.10. Vertical distributions of TOC, TN, and TS contents and C/N and C/S ratios of the Onnagawa Formation in the Sugisawa area.

4.4.3 Inorganic Geochemistry

4.4.3.1 X-Ray Fluorescence

The results of major oxides analysis of the Onnagawa Formation are reported in Table 5. In all the samples, SiO_2 is the most abundant oxide. The detrital SiO_2 was calculated with the equation of Leinen (1977): detrital SiO_2 = 4.33Al + 1.36 Mg^2; the biogenic SiO_2 was calculated subtracting the detrital SiO_2 from the total SiO_2. Other oxides such as Al_2O_3, Fe_2O_3, CaO, MgO, K_2O, and Na_2O are present at variable concentrations in all the samples. The contents of these oxides tend to increase upward along the stratigraphic column. The less abundant oxides in the analyzed samples are the TiO_2, P_2O_5, and MnO.

Based on the ternary plot of SiO2, Al2O3, and CaO of Ross and Bustin (2009), the Onnagawa Formation is dominated by biogenic and detrital quartz. Furthermore, the K_2O/Al_2O_3 ratio is always lower than 0.3, indicating the presence of clay minerals, and their prevalence on Feldspars (Cox and Lowe, 1995). The variable amounts of Fe_2O_3, CaO–MgO, and Na_2O can be associated respectively to the presence of pyrite, calcite and dolomite, and feldspars. On the other hand, the P_2O_5 of the Middle-Late Miocene sediments of the Japan Sea is, generally, associated with the occurrence of apatite minerals.

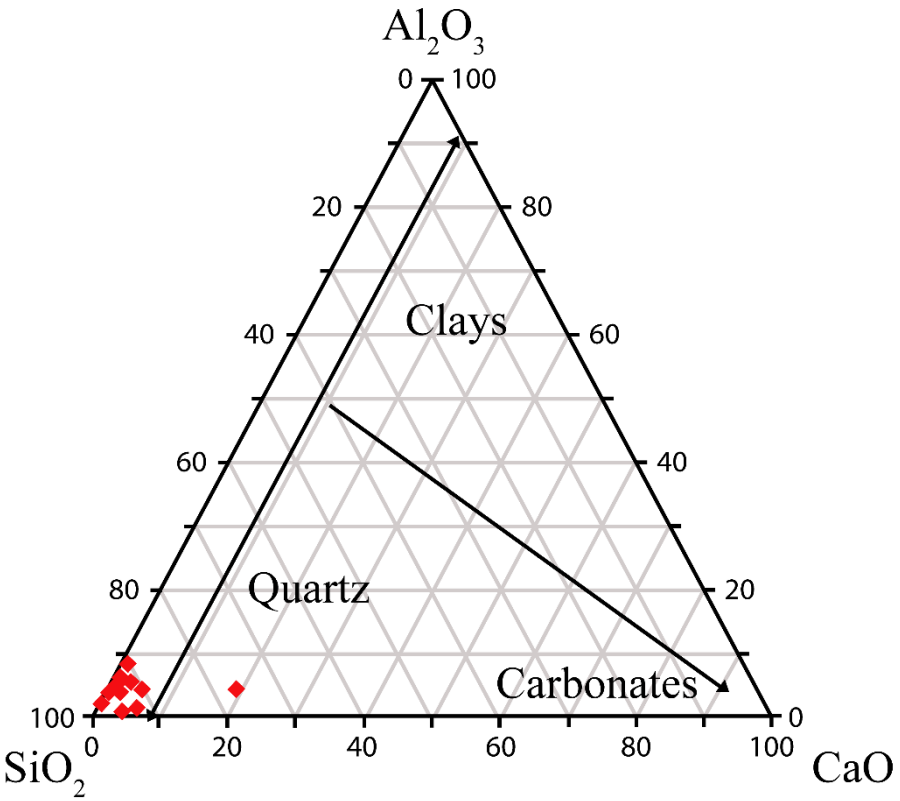

Figure 4.11. Ternary diagram showing the relative proportions of major compositions of SiO_2 (quartz), Al_2O_3 (clays), and CaO (carbonates) in the Onnagawa Formation's samples. (modified from Ross and Bustin, 2009).

Table 5 TOC, TN, TS, and major elements abundances of the Onnagawa Formation from the Sugisawa area.

Sample Elements wt%	SiO_2	$BSiO_2$	$DSiO_2$	TiO_2	Al_2O_3	Fe_2O_3	MgO	CaO	K_2O	Na_2O	P_2O_5	MnO	TOC	TN	TS	C/N	C/S
OG1	91.90	80.74	11.15	0.13	4.62	1.14	0.87	0.21	0.78	0.29	0.03	0.03	0.57	0.07	0.51	8.51	1.13
OG2	93.99	86.16	7.83	0.11	3.33	1.05	0.39	0.14	0.67	0.28	0.02	0.02	0.71	0.04	0.61	16.90	1.16
OG3	95.90	90.70	5.20	0.07	2.24	0.85	0.14	0.06	0.47	0.22	0.02	0.02	0.79	0.04	0.36	19.75	2.17
OG4	67.46	50.79	16.66	0.10	4.12	1.29	9.22	16.48	0.54	0.28	0.06	0.44	0.93	0.04	0.60	23.25	1.55
OG5	92.64	82.63	10.01	0.14	4.24	1.09	0.56	0.19	0.82	0.25	0.06	0.02	1.11	0.06	0.64	18.20	1.73
OG6	90.08	79.81	10.26	0.12	4.12	1.41	1.38	1.78	0.60	0.26	0.20	0.06	1.36	0.06	1.03	22.67	1.32
OG7	93.84	86.07	7.71	0.14	3.36	1.18	0.25	0.09	0.73	0.31	0.07	0.02	1.21	0.07	0.69	17.29	1.75
OG8	94.06	87.77	6.29	0.08	2.53	0.73	0.69	1.09	0.48	0.25	0.06	0.03	0.85	0.05	0.36	17.00	2.34
OG9	93.12	87.90	5.21	0.06	1.77	0.75	1.49	2.20	0.34	0.20	0.04	0.03	1.41	0.07	0.39	20.14	3.58
OG10	92.11	87.91	4.19	0.05	1.07	0.84	2.18	3.37	0.17	0.14	0.05	0.02	0.79	0.03	0.36	26.33	2.17
OG11	88.97	83.29	5.67	0.06	1.43	0.62	3.02	5.33	0.26	0.16	0.07	0.08	2.10	0.07	0.44	30.00	4.83
OG12	85.67	74.56	11.11	0.16	4.34	1.40	1.65	4.57	0.77	0.34	1.04	0.06	1.12	0.05	0.57	22.40	1.97
OG13	87.27	73.36	13.90	0.19	5.65	1.75	1.50	2.11	0.84	0.42	0.22	0.05	1.41	0.09	0.77	16.59	1.84

Table 5 (Continued).

Sample Elements wt%	SiO_2	$BSiO_2$	$DSiO_2$	TiO_2	Al_2O_3	Fe_2O_3	MgO	CaO	K_2O	Na_2O	P_2O_5	MnO	TOC	TN	TS	C/N	C/S
OG14	90.06	77.55	12.51	0.19	5.24	1.50	0.92	0.47	1.09	0.45	0.08	0.00	1.62	0.11	0.66	14.73	2.45
OG15	91.26	80.26	11.00	0.17	4.64	1.51	0.71	0.24	1.00	0.37	0.07	0.02	0.78	0.07	0.79	10.99	0.99
OG16	89.20	76.18	13.02	0.23	5.46	2.02	1.01	0.68	0.90	0.39	0.08	0.03	1.36	0.13	0.96	10.46	1.41
OG17	84.66	65.91	18.74	0.34	7.91	2.59	1.56	0.72	1.52	0.53	0.13	0.03	1.95	0.14	1.32	13.93	1.47
OG18	88.09	72.73	15.36	0.21	6.38	1.84	1.33	0.53	1.08	0.43	0.07	0.02	1.84	0.11	0.86	16.73	2.14

Note: $BSiO_2$ = Biogenic Silica; $DSiO_2$ = Detrital Silica; TOC = Total Organic Carbon; TN = Total Nitrogen; TS = Total Sulfur; C/N = Organic Carbon-Nitrogen ratio; C/S = Organic Carbon-Sulfur ratio; wt% = weight percent.

4.4.4 Pyrite morphology and size

Observation in reflected light showed that the framboidal pyrite is the prevalent phase in the Onnagawa and Iwaya Formation. The framboidal pyrite is variably abundant in the studied samples, but, generally, increases in number in the laminated samples (Table 6). Recognized framboidal pyrite morphologies are shown in Figure 4.10. The framboidal pyrite showed a clear distinction in size between the massive and laminated samples. Generally, massive samples are dominated by overgrown framboids with a diameter larger than 5 μm (Table 6; Figure 4.10a–c). On the other hand, laminated samples are characterized by significantly smaller framboidal pyrite than the massive samples (Table 6; Figure 4.10d–f).

Table 6 Descriptive statistics of framboid pyrite from the Onnagawa Formation.

Sample Name	Lithofacies	Mean Diameter (μm)	Max Diameter (μm)	Min Diameter (μm)	Standard Deviation	Measured Framboids
OG1	Massive	7.77	20	3	3.27	100
OG2	Massive	9.15	40	3	5.69	100
OG4	Laminated	5.06	19	2	2.29	435
OG8	Laminated	4.96	11	2	1.75	102
OG9	Laminated	4.62	15	2	1.92	269
OG11	Laminated	4.60	13	2	2.01	266
OG12	Massive	6.05	20	2	3.01	168
OG15	Massive	8.90	29	3	5.15	174

Table 6 (Continued) Descriptive statistics of framboidal pyrite from the Iwaya Formation.

Sample Name	Lithofacies	Mean Diameter (μm)	Max Diameter (μm)	Min Diameter (μm)	Standard Deviation	Measured Framboids
G1	Massive	7.69	15	5	2.21	120
G2	Massive	9.23	21	5	3.54	115
G5	Massive	7.20	20	5	2.71	39
G20	Massive	7.91	20	4	2.70	104
G22	Massive	7.33	20	3	2.34	110
G47	Massive	7.13	14	5	1.98	115
G54	Massive	6.57	10	3	1.52	26
G60	Massive	7.72	30	4	4.48	36
G68	Massive	8.29	24	4	3.24	75
G92	Massive	7.04	15	4	2.13	133

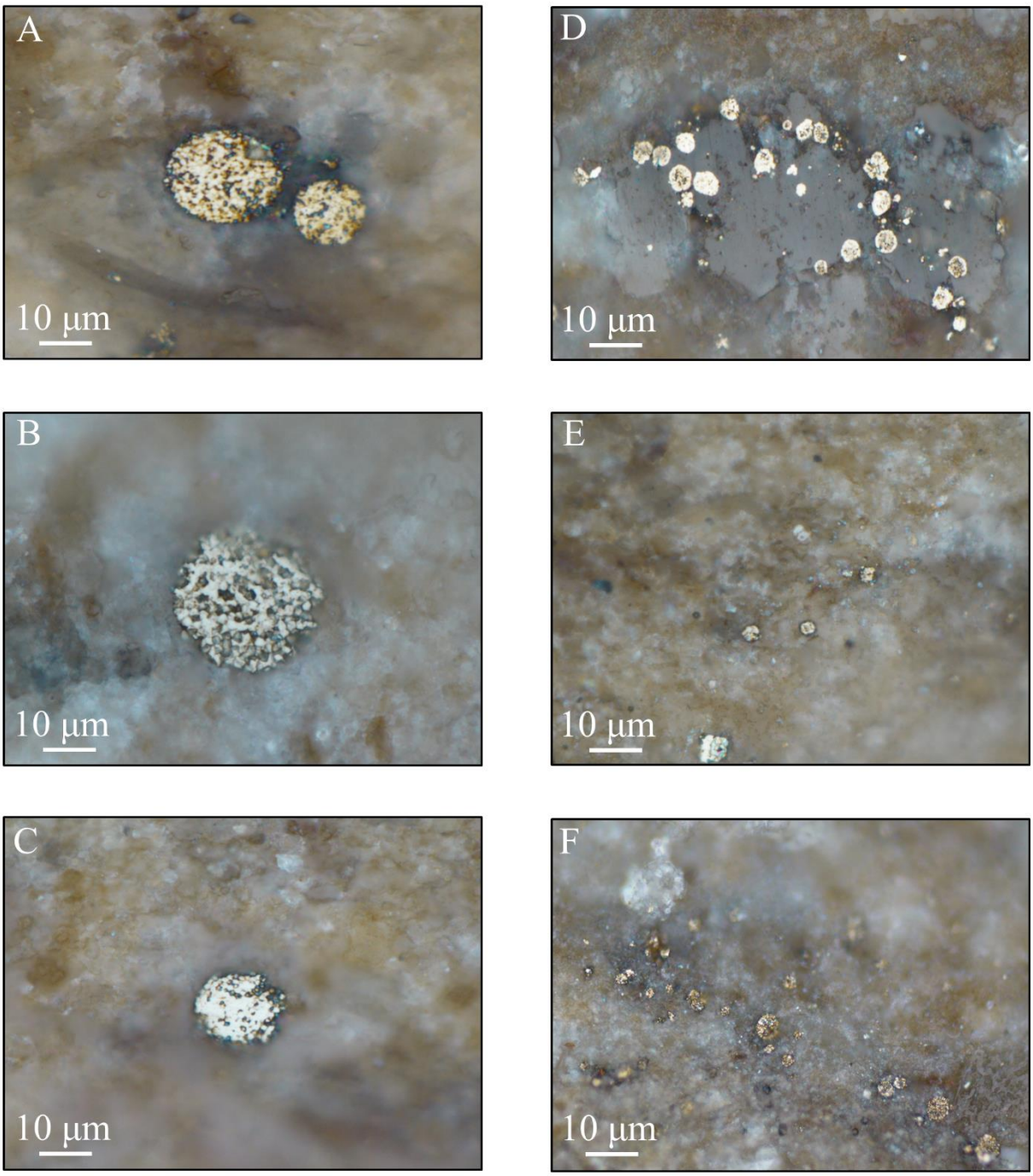

Figure 4.12. Microscopic features of framboidal pyrite from the Onnagawa and Iwaya Formations under reflected-light microscopy. (a–c) Framboidal pyrite from the massive samples; (d–f) Framboidal pyrite from the laminated samples of the Onnagawa Formation.

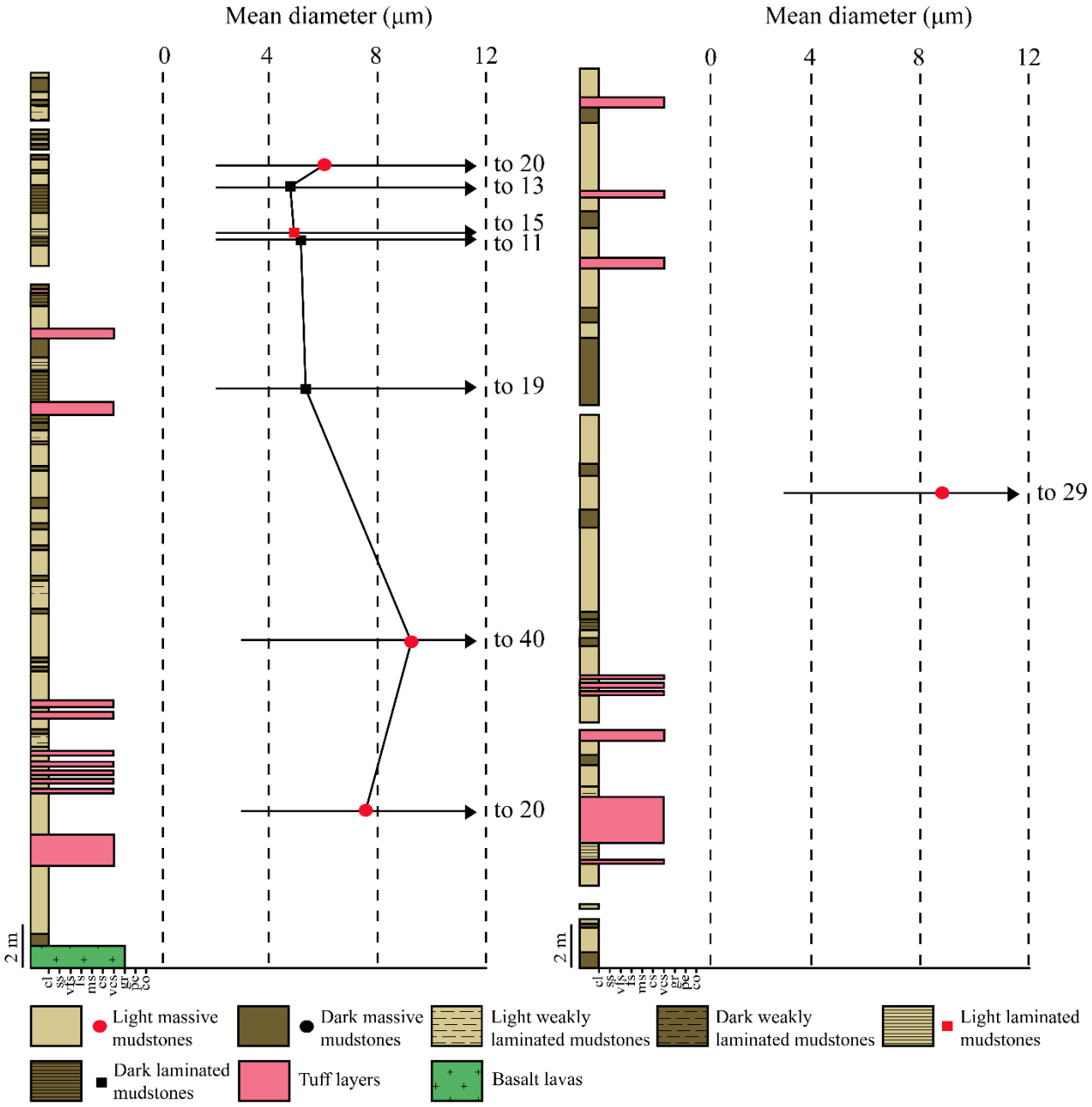

Figure 4.13. Vertical variations of the mean diameter of the framboidal pyrite in the Onnagawa Formation from the Sugisawa area. Arrows crossing the samples indicate the minimum and maximum framboid diameter recognized during microscopic observation.

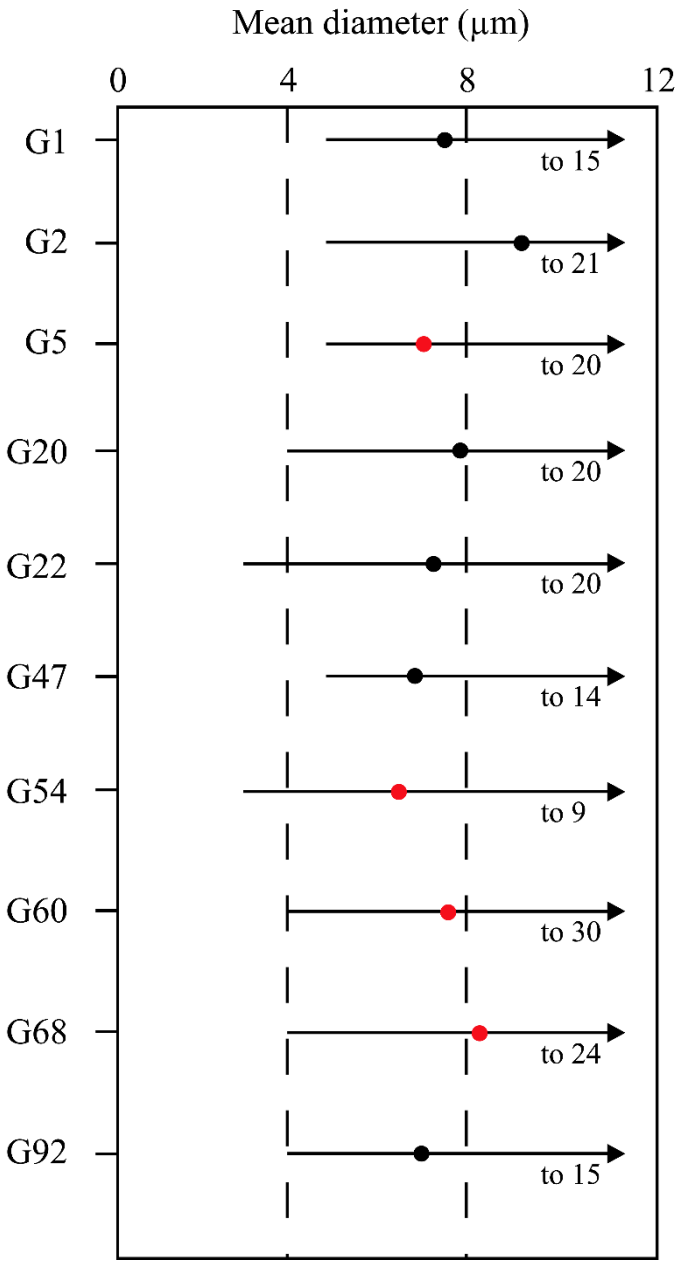

Figure 4.14. Vertical variations of the mean diameter of the framboidal pyrite in the Iwaya Formation from the Gotanzawa area. Arrows crossing the samples indicate the minimum and maximum framboid diameter recognized during microscopic observation. Red and black points indicate, respectively, light and black massive samples.

4.5 Discussion

4.5.1 Kerogen type

A pseudo Van Krevelen diagram (Figure 4.15) was used to interpret the kerogen type in sediments of the Onnagawa and Iwaya Formations (Peters, 1986). The diagram shows that a type II kerogen characterizes the Onnagawa Formation and most of the Iwaya Formation samples. However, some of

the Iwaya Formation samples are characterized by low HI and slightly high OI. Because these samples have a low TOC, the shift from type II to the type III kerogen indicates a process of degradation of the organic matter (Pratt, 1984; Tyson, 1995).

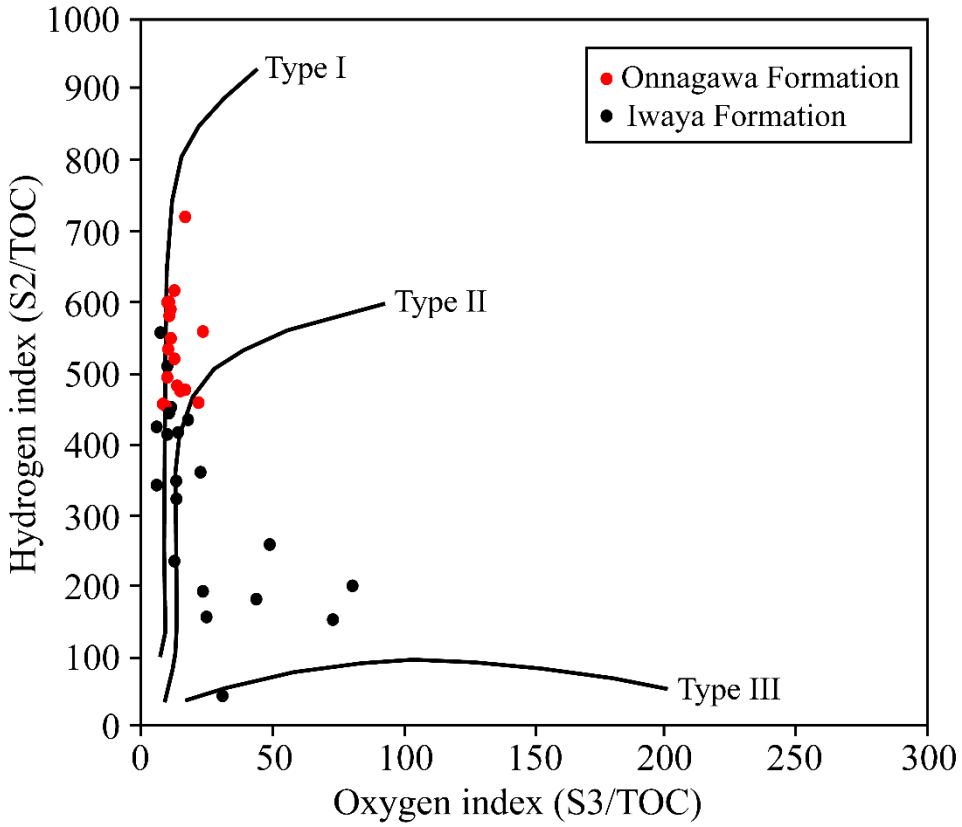

Figure 4.15. Hydrogen index (HI) vs oxygen index (OI) plot of the Onnagawa and Iwaya formations (modified from Peters, 1986).

4.5.2 Source Rock Potential and Thermal Maturity

The hydrocarbon potential and thermal maturity of the Onnagawa and Iwaya Formations were evaluated based on S1 and S2, TOC, and T_{max} values obtained from Rock-Eval pyrolysis (Peters, 1986). Furthermore, the organic richness of these formations was evaluated based on the Tissot and Welte (1984) and Peters's (1986) classification. Based on this study's results, the Onnagawa Formation in the Sugisawa area, as well as the Iwaya Formation, showed a fair to good organic richness (Figures 4.8, 4.9; Table 4). However, some Iwaya Formation samples were poor in organic carbon (Figure 4.9; Table 4).

Through the comparison of the TOC with the source potential (S1+S2), it was possible to consider whether the studied formations could be considered potential source rocks (Figure 4.16). Data show that both the Onnagawa and Iwaya Formations have a variable generative potential from poor to very

good. However, most of the samples of the two formations have a fair/good generative potential (Figure 4.16). These results indicate that the Onnagawa and Iwaya Formations are potential source rocks. However, most of the analyzed samples have a T_{max} lower than 435 °C, thus indicating that these formations are immature for the generation and expulsion of hydrocarbons.

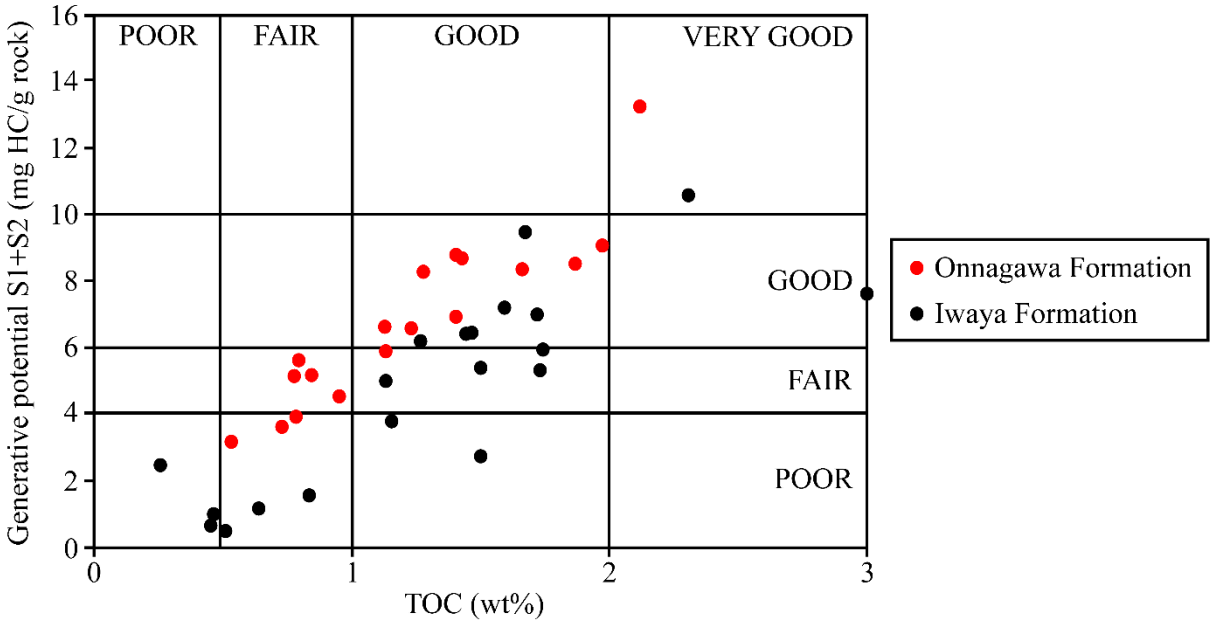

Figure 4.16. Plot of source potential (S1+S2) against TOC *Onnagawa Formation*. Lines separating the different fields are modified from Gottardi et al. (2019).

These data corroborate the previous geochemical studies performed in various outcrops of the Middle-Late Miocene formations of the Akita region (Tsuji et al., 1991; Waseda et al., 1995; Sugii, 1998), that inferred a good potential and the immaturity of these. Although the Onnagawa Formation and its equivalents in outcrop are generally immature source rocks, in various oil fields of the Akita Prefecture, the Onnagawa Formation is mature and was able to expel hydrocarbons (Yokoi et al., 2013; Yokoi and Tsuji, 2015). The higher maturity of the Onnagawa Formation in the oil fields areas probably indicates an increased burial rate or the presence of local thermal anomalies that increased the geothermal gradient

4.5.3 Paleo-environmental controls on the organic richness

4.5.3.1 Source of the detrital fraction

The paleo-weathering intensity at the source of the detrital fraction and the provenance of the detrital fraction of the Onnagawa Formation were quantified through the chemical index of alteration (CIA) (Nesbitt and Young, 1982) and the interpretation of detrital oxides. The CIA was calculated

with the same method used for the Akaishi and Odoji Formations in the Tsugaru Basin area. The CIA of the Onnagawa Formation is in a range of 74–83. This range of values indicates that a moderate/high chemical weathering and a warm-humid climate were active at the source of the detrital fraction. As in the case of the Tsugaru Basin samples, the CIA interpretation in the Onnagawa Formation agrees with the plot SiO_2–(Al_2O_3+K_2O+Na_2O) (Figure 4.17).

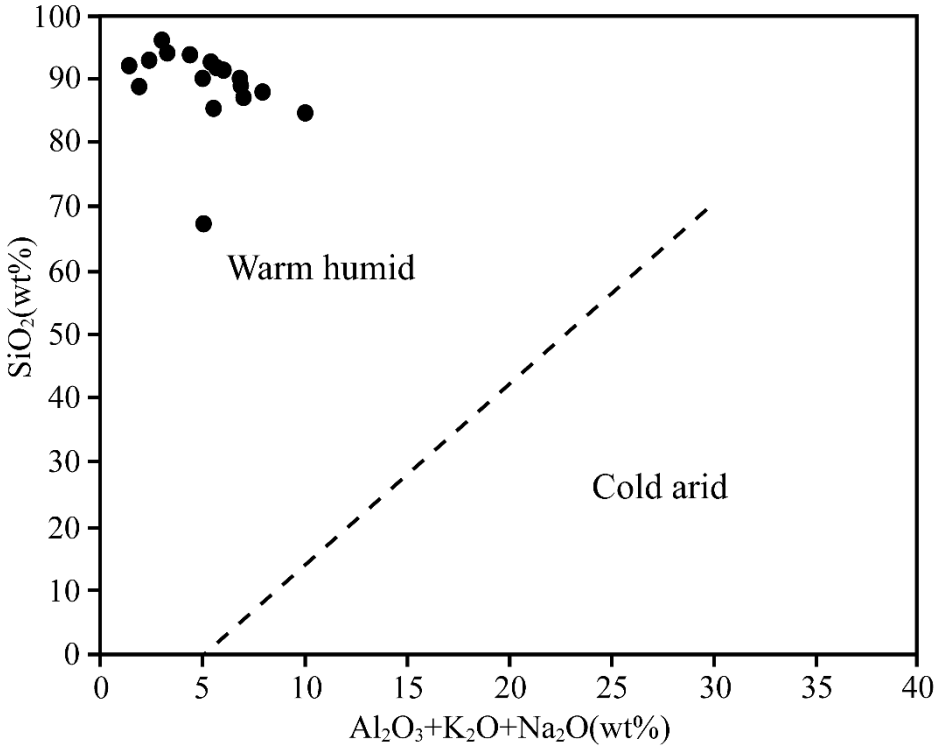

Figure 4.17. Plot of SiO_2 versus Al_2O_3+K_2O+Na_2O for the discrimination of paleoclimate conditions (modified from Chen et al., 2020).

The provenance of the detrital fraction was, firstly, inferred from the Al_2O_3/TiO_2 ratio. The Onnagawa Formation's Al_2O_3/TiO_2 ranges from 21 to 40, indicating that the detrital fraction of these sediments likely originated from a felsic source rock. The diagram of provenance by Roser and Korsch (1988) confirms that the detrital fraction derived from a source of felsic composition and, more specifically, from a passive continental margin or a recycled orogenic province.

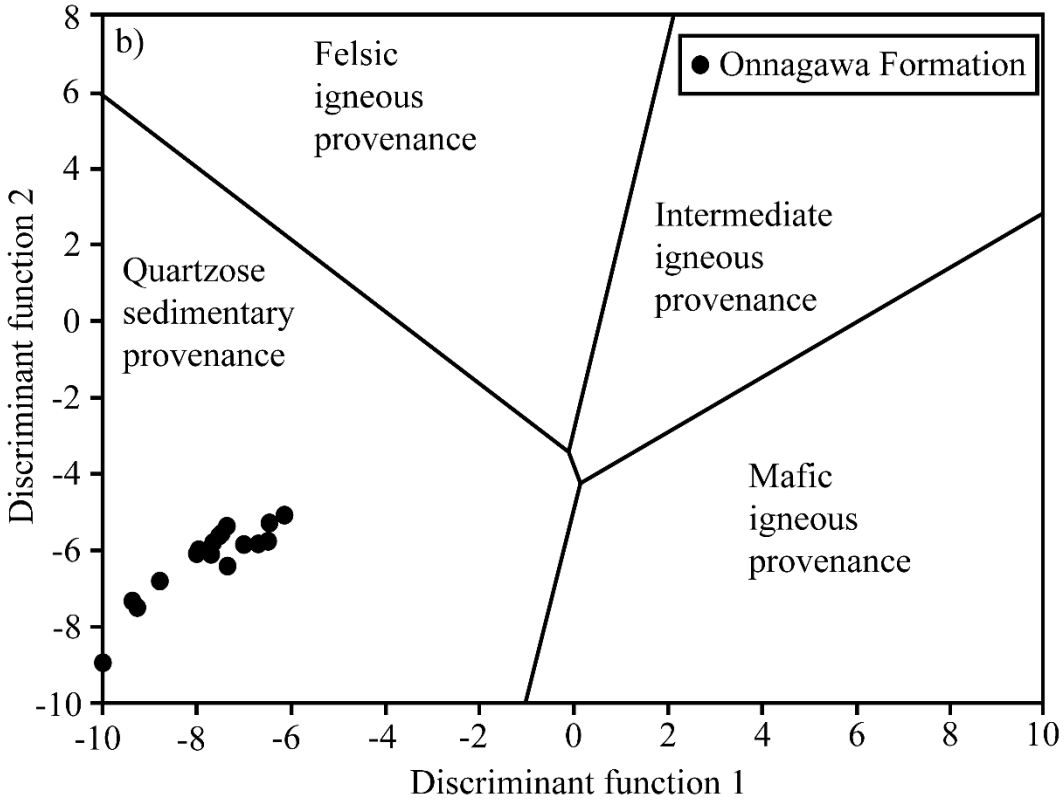

Figure 4.18. Provenance discrimination diagrams for the Akaishi, Odoji, and Onnagawa Formations. F1 = (−1.773×TiO_2%) + (0.607×Al_2O_3%) + (0.76×Fe_2O_{3T}%) + (−1.5×MgO%) + (0.616×CaO%) + (0.509×Na_2O%) + (−1.22 × K_2O%) + (−9.09). F2 = (0.445×TiO_2%) + (0.07×Al_2O_3%) + (−0.25×Fe_2O_{3T}%) + (−1.142×MgO%) + (0.438×CaO%) + (0.432×Na2O%) + (1.426×K_2O%) + (−6.861). After Roser & Korsch (1988).

Similarly, to the Tsugaru Basin formations, the detrital fraction of the Onnagawa Formation originated from the continental rocks from the Asian continent or northeastern Honshu. Therefore, the detrital fraction variation in the Onnagawa Formation is related to the monsoon intensity and the river supply (Tada, 1991, 1994; Kimura et al., 2004). Based on the two hypotheses, the low detrital fraction content of the Onnagawa Formation is motivated by a low-intensity of the Asian monsoon and with a low river supply from the northeastern Honshu area. Some studies (Zachos et al., 2001; Wan et al., 2007; Clift et al., 2014; Tada et al., 2016) documented that the Asian monsoon activity before 8 Ma was still not intense. These interpretations have a good correlation with the detrital fraction variation measured in this study.

On the other hand, no studies found evidence of a large riverine source in northeastern Honshu. Therefore, the low amount of detritus in the Onnagawa Formation can be explained with a smaller riverine supply than in the late Miocene.

The detrital oxides range of the Onnagawa Formation is comparable with the Odoji Formation`s one (Figure 3.26); since the Onnagawa and Odoji Formations have similar stratigraphic age, their

detrital contents may have been influenced by the low-intensity Asian monsoon and low supply from a riverine source.

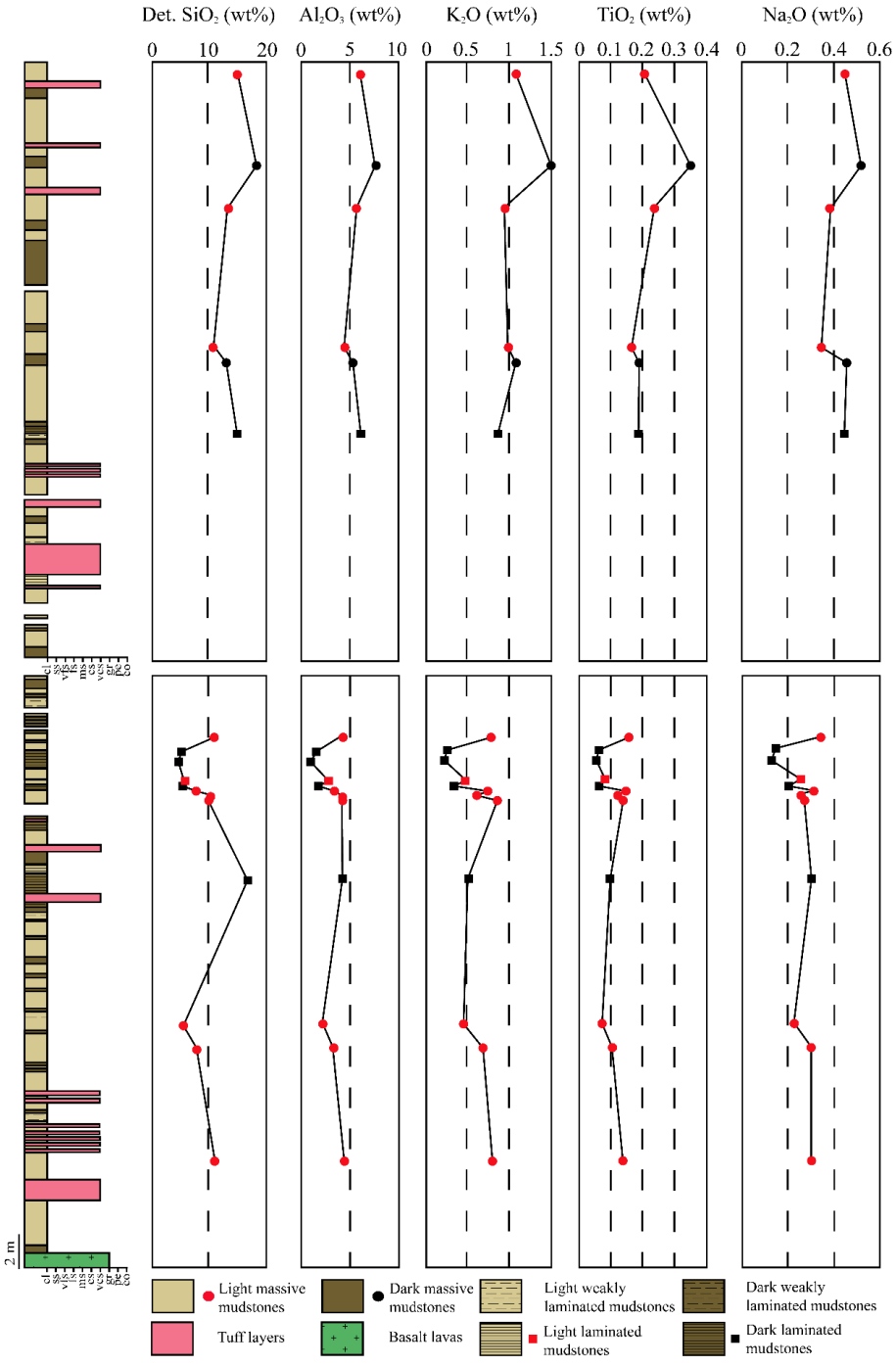

Figure 4.19. Vertical distribution of detrital SiO_2, Al_2O_3, K_2O, TiO_2, and Na_2O contents of the Onnagawa Formation from the Sugisawa area. The grain size fraction abbreviations are as follows: cl, clay; sl, silt; vfs, very fine sand; fs, fine sand; ms, medium sand; cs, coarse sand; vcs, very coarse sand; gr, granule; pe, pebble; co, cobble.

The detrital SiO2, Al2O3, and K2O contents show a generally positive correlation with the TOC (Figure 4.20). These detrital oxides are associated with the clay minerals, which generally contribute positively to the preservation of the TOC in sediments (Piper and Isaacs, 1984; Waseda et al., 1995; Ross and Bustin, 2009; Zeng et al., 2015). Therefore, the positive correlation of the detrital oxides with the TOC possibly indicates a positive influence of the clay minerals content in the Onnagawa Formation.

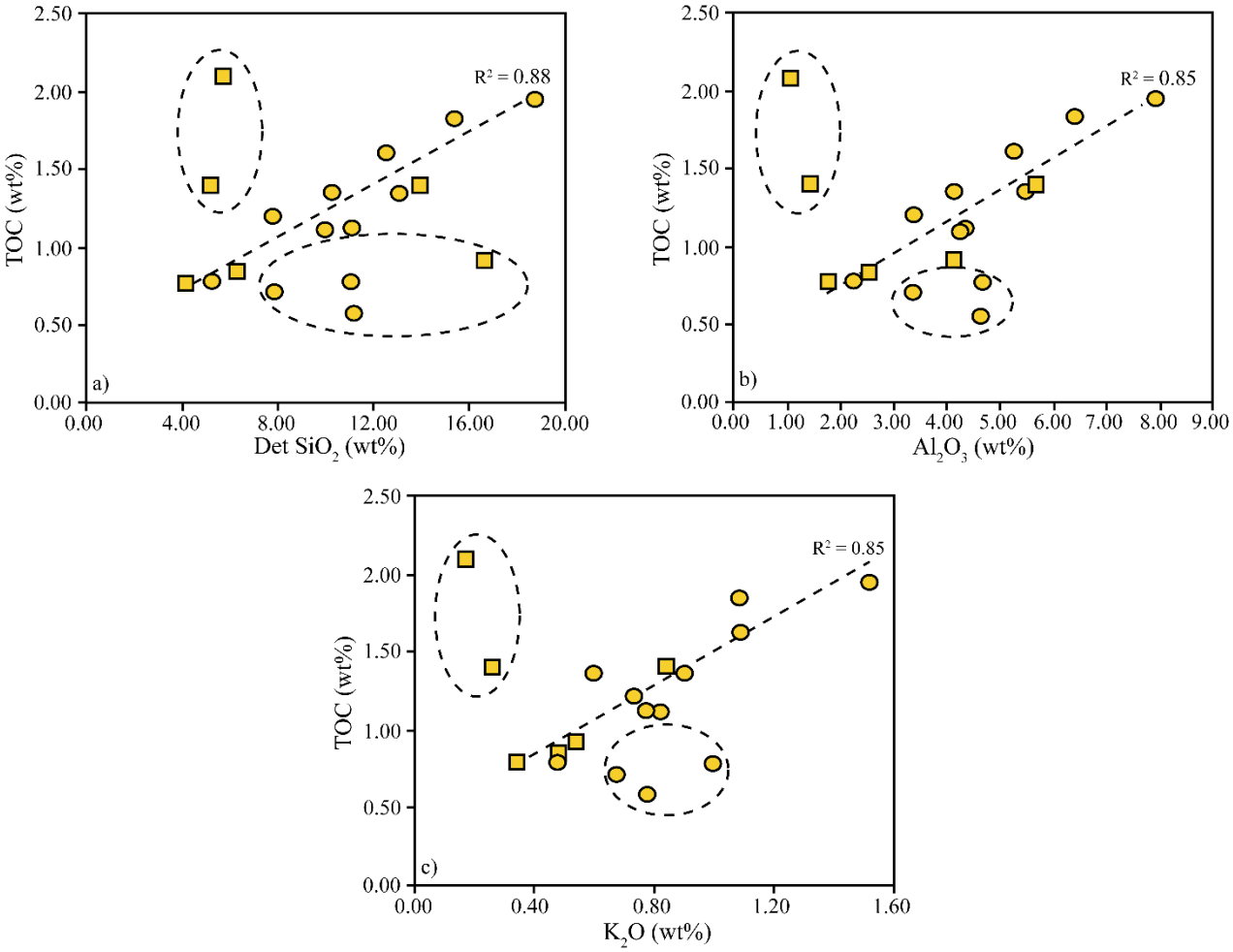

Figure 4.20. Cross plots of detrital SiO_2 (wt%), Al_2O_3 (wt%), and K_2O (wt%) versus total organic carbon (TOC) (wt%) of the samples from the Onnagawa Formation. Yellow squares and circles are respectively the laminated and massive samples of the Onnagawa Formation.

4.5.3.2 Paleoproductivity

The Onnagawa Formation deposited in a period of intense surface water productivity, associated with the large diffusion of diatom organisms (Aoyagi and Omokawa, 1992; Koizumi and Yamamoto, 1992). The high contents of the biogenic SiO_2 and the C/N ratios generally lower than 20 indicate that the Onnagawa Formation's sediments were mostly composed of marine diatomaceous organic

matter (Figure 4.10; Table 5). Furthermore, various studies (Tada, 1991, 1994; Yamamoto and Watanabe, 1995; Yamamoto et al., 1999) associated the biogenic silica with the diatoms abundancy, and consequently with the bio-productivity. The biogenic SiO_2 content of the Onnagawa Formation is generally higher than 70%, indicating that a condition of high paleo-productivity was established throughout the deposition period.

The plot of biogenic SiO_2 against TOC revealed a moderate negative correlation between these two elements in the Onnagawa Formation (Figure 4.21). The studies from Tada (1994), Waseda et al. (1995), and Bohacs et al. (2005) recognized a similar negative correlation in the Japan Sea siliceous sediments and some sections of the Monterey Formation, in California. Bohacs et al. (2005) interpreted this negative correlation as an effect of the biogenic dilution. Because of the intense upwelling, large volumes of biogenic silica were deposited in the Onnagawa Formation sediments. Therefore, the biogenic SiO2 probably diluted the organic matter, leading to smaller amounts of TOC in some horizons than others.

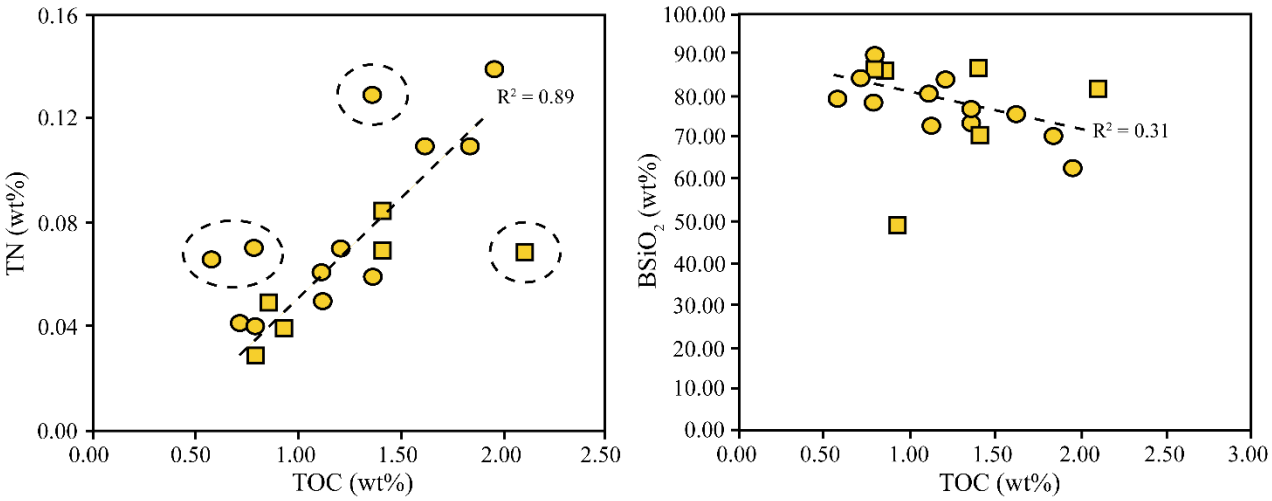

Figure 4.21. Cross plots of TN (wt%), and biogenic SiO_2 (wt%) versus total organic carbon (TOC) (wt%) of the samples from the Onnagawa Formation in the Sugisawa area.

4.5.3.3 Redox condition in the bottom waters

Based on the Onnagawa and Iwaya Formations lithological features, a preliminary interpretation of the paleo-redox condition was performed. The Onnagawa Formation samples are characterized by the occurrence of both massive and laminated facies, while the Iwaya Formation is characterized exclusively by massive facies. This feature suggests that the bottom waters oscillated from oxygenated (massive facies) to low-oxygenated (laminated facies) in the Sugisawa area. On the other hand, they remained oxygenated during the interval of deposition of the Iwaya Formation. The

framboidal pyrite diameter and the C-S relationship were used as additional methods to confirm the lithofacies interpretation.

The data from Table 6 and Figures 4.13, 4.14, and 4.22 indicate that the framboidal pyrite in the massive samples is generally larger than in the laminated samples. Additionally, in agreement with several studies (Wilkin et al., 1996; Lyons and Severmann, 2006; Wei et al., 2016; Liu et al., 2019), the massive samples are characterized by framboidal pyrite larger than 5 μm. Therefore, the framboidal pyrite size corroborates the lithofacies interpretation.

The C-S relationships gave additional insights about the paleoredox conditions in the Onnagawa Formation (Berner and Raiswell, 1983). The plot in Figure 4.22 indicates that all the massive samples and the laminated samples of the Onnagawa Formation are in the area of normal marine oxygenated conditions. This apparent disagreement between laminated lithofacies and the C-S ratio was explained by Tada and Iijima (1992) as an effect of silica dilution. In environments with high silica, the iron's biogenic dilution can limit the formation of pyrite.

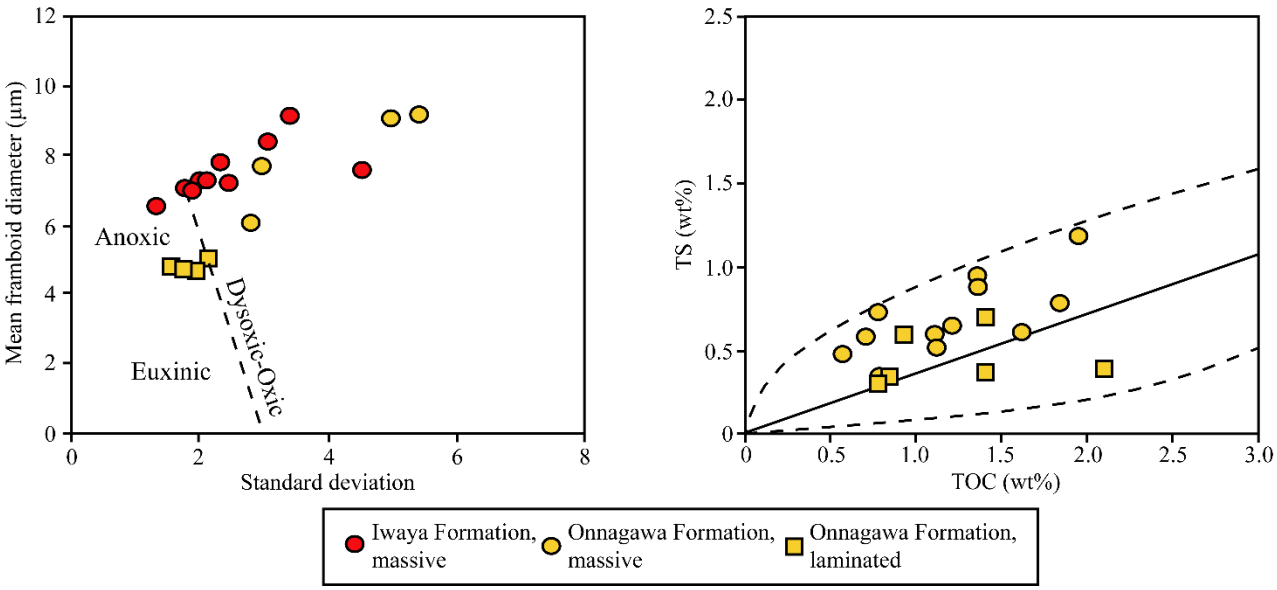

Figure 4.22. Left: mean diameter versus standard deviation plot of framboidal pyrite data of the Iwaya and Onnagawa Formations; Right: cross plot of sulfur and organic carbon in the sediments of the Onnagawa Formation. The outlined area denotes the region of normal marine sediments (after Berner and Raiswell, 1983).

Lithofacies features and geochemical proxies in the Iwaya and Onnagawa Formations indicated two distinct conditions in the Sugisawa and Gotanzawa areas. According to the previous studies of Tada (1991), Tsuji et al. (1991), and Tada (1994), massive horizons deposited in the Akita Basin in periods of limited inflow of low-oxygen water from the Pacific Ocean (sea-level lowstand intervals). On the other hand, laminated horizons deposited in periods of high inflow of low-oxygen water from

the Pacific Ocean (sea-level highstand intervals). Based on the data interpretations, the Sugisawa area was intermittently influenced by the oxygen minimum zone (OMZ) waters from the North Pacific, while these waters did not influence the Gotanzawa area.

It is commonly believed that anoxic conditions in the bottom water favors the preservation of organic matter and consequently determine high values of the TOC (Demaison and Moore, 1980; Allen and Allen, 2013). However, a marked difference in the TOC content between the massive and the laminated samples of the Onnagawa Formation was not detected (Figure 4.10). Similarly, the Iwaya Formation showed good values of TOC (Figure 4.9). These results suggest that the paleo-redox conditions of bottom water probably did not significantly influence the TOC content.

4.6 Conclusions

Sedimentological and geochemical characterization of the Onnagawa Formation in the Sugisawa area and the Iwaya Formation in the Gotanzawa area allowed us to evaluate the source rock potential and the thermal maturity of these formations and to reconstruct the paleoenvironmental conditions in the Akita Basin during the Middle-Late Miocene.

Rock-Eval pyrolysis data revealed that both the formations generally have good TOC content and generative potential. However, the T_{max} ranges indicated that these formations are mostly immature for the generation of hydrocarbons.

Analysis of detrital oxides contents revealed a provenance of detrital fraction in the Onnagawa Formation from a felsic source located in Asia or northeastern Honshu. This fraction was probably eroded and transported to the Japan Sea margin through the Monsoon and riverine input; these observations point out a relationship between Monsoon cycles, riverine cycles, and detrital fraction content. Variations of the detrital fraction showed a good correlation with TOC in most of the Onnagawa Formation samples, suggesting that dilution of organic matter by detritus favored the TOC preservation.

The high concentrations of the biogenic SiO_2 in the Onnagawa Formation indicate high primary productivity. In some cases, the high primary productivity favored organic matter production and the burial of TOC buried in sediments. In other cases, the large amounts of the biogenic SiO_2 determined an auto-dilution process that reduced the organic carbon even during low-oxygen intervals.

Lithofacies variations from massive to laminated revealed that the bottom waters paleo-redox condition varied from dysoxic to anoxic in the Sugisawa area. On the other hand, the presence of exclusively massive samples in the Gotanzawa area indicated oxygenated bottom waters. The observation of the framboidal pyrite confirmed this hypothesis. These data indicate that the Akita Basin was characterized by a different paleo-redox condition in the bottom waters. Lastly, a

difference in TOC was not detected between massive and laminated samples, possibly indicating that the paleo-redox conditions did not affect the preservation of organic matter and organic carbon.

CHAPTER 5

Discussion

In this chapter, data from the sedimentological and geochemical characterization of formations in Akita and Aomori regions will be compared. Firstly, the source rock potential of sedimentary formations will be discussed. Secondly, we will present a possible model of the evolution of the Sea of Japan in the two areas through the interpretation of the various sedimentological and geochemical proxies.

5.1 Source rock evaluation in Akita and Aomori regions

Rock-Eval pyrolysis analysis of samples from formations of Akita and Aomori regions elucidated the source rock potential through the organic richness, kerogen type, and thermal maturity. In both areas, the Middle-Late Miocene siliceous mudstones (Onnagawa and Iwaya Formations in Akita, Odoji Formation in Aomori) showed a generally fair/good organic richness and a possible potential for generating hydrocarbons (Figures 3.20 and 4.16). These formations are mostly composed of type II kerogen (Figure 3.19 and 4.15), typical of oil-prone organic matter. However, the T_{max} indicated that these formations are mostly thermally immature source rocks, and they were unable to expel hydrocarbons. This study's results agreed with several studies performed on outcrop sequences in Akita (Tsuji et al., 1991; Waseda et al., 1995; Sugii, 1998) and Aomori (Aoyagi and Omokawa, 1992; Ujiié, 1995). Even if the results from this and previous studies indicated a comparable trend, the interpretation of these results is generally local and cannot be extended to all the northern Tohoku region. Therefore, to have a clear definition of the hydrocarbons potential in the Akita and Aomori regions, subsurface data from the Japanese Association for Petroleum Technology (JAPT) and the Japanese National Gas Association will be presented.

According to the data published by the Japanese National Gas Association (1992) and the Japanese Association for Petroleum Technology (1993), many locations of the Akita Prefecture were drilled for oil & gas exploration (Figure 5.1). Some oil and gas fields such as the Yabase and Yurihara-Ayukawa are currently producing oil and gas. On the other hand, at the current state, only the data from the Nishitsugaru-Oki well are available in the Aomori Prefecture (Figure 5.1).

Data from the Akita Prefecture wells indicate that the Onnagawa Formation is an important target for hydrocarbons exploration in all the locations. According to the data of the Japanese National Gas Association (1992), in the Mogamigawa-Oki and Nikaho wells, the Onnagawa Formation is characterized generally by fair/good TOC contents. Additionally, Yokoi et al. (2013) reported TOC values in the range of 2–5 wt% in the Onnagawa Formation of the Yurihara-Ayukawa oil and gas

field. On the other hand, the thermal maturity of the Onnagawa Formation is variable throughout all the regions and determined by different factors. Two of the main factors are the degree of burial/subsidence and local thermal anomalies (igneous intrusions). According to Allen and Allen (2013), when the sediments are progressively buried at higher depths, they are generally affected by higher temperatures. Therefore, a higher burial determines an increase in thermal maturity. On the other hand, in areas with intense volcanic activity, the basin fill may be intruded by igneous bodies (dikes or sills) with high temperature. The contact between the sediments and the igneous bodies determines a local increase in temperature and, consequently, a higher thermal maturity (Allen and Allen, 2013).

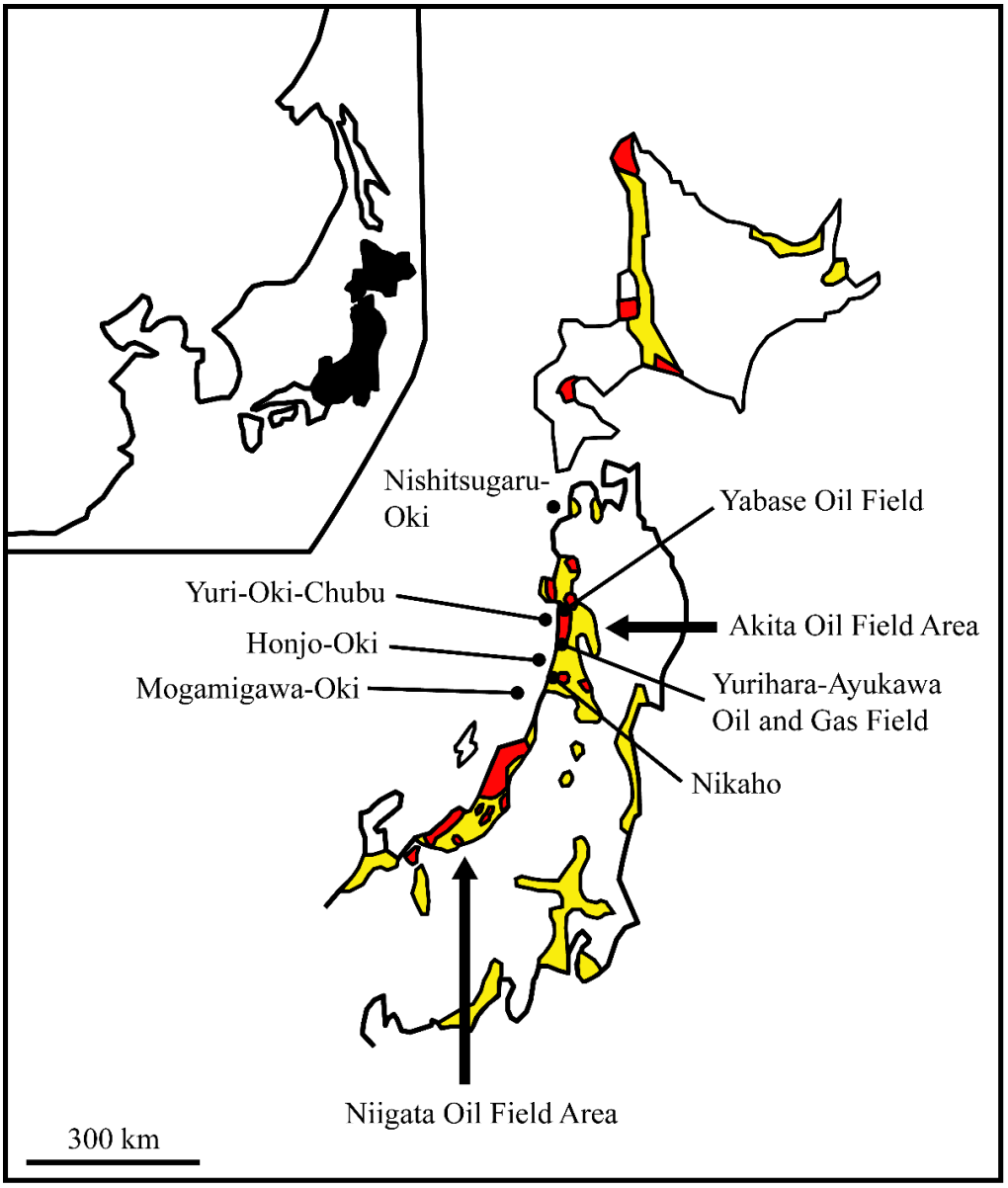

Figure 5.1. Index map of northern Japan showing the oil and gas fields (red) and the prospective areas for petroleum exploration (yellow). Black points indicate some of the exploration and production wells, and oil and gas fields in the Akita and Aomori Prefectures (Compiled with the data of the Japanese National Gas Association (1992), the Japanese Association for Petroleum Technology (1993), and Ujiié et al. (2004)).

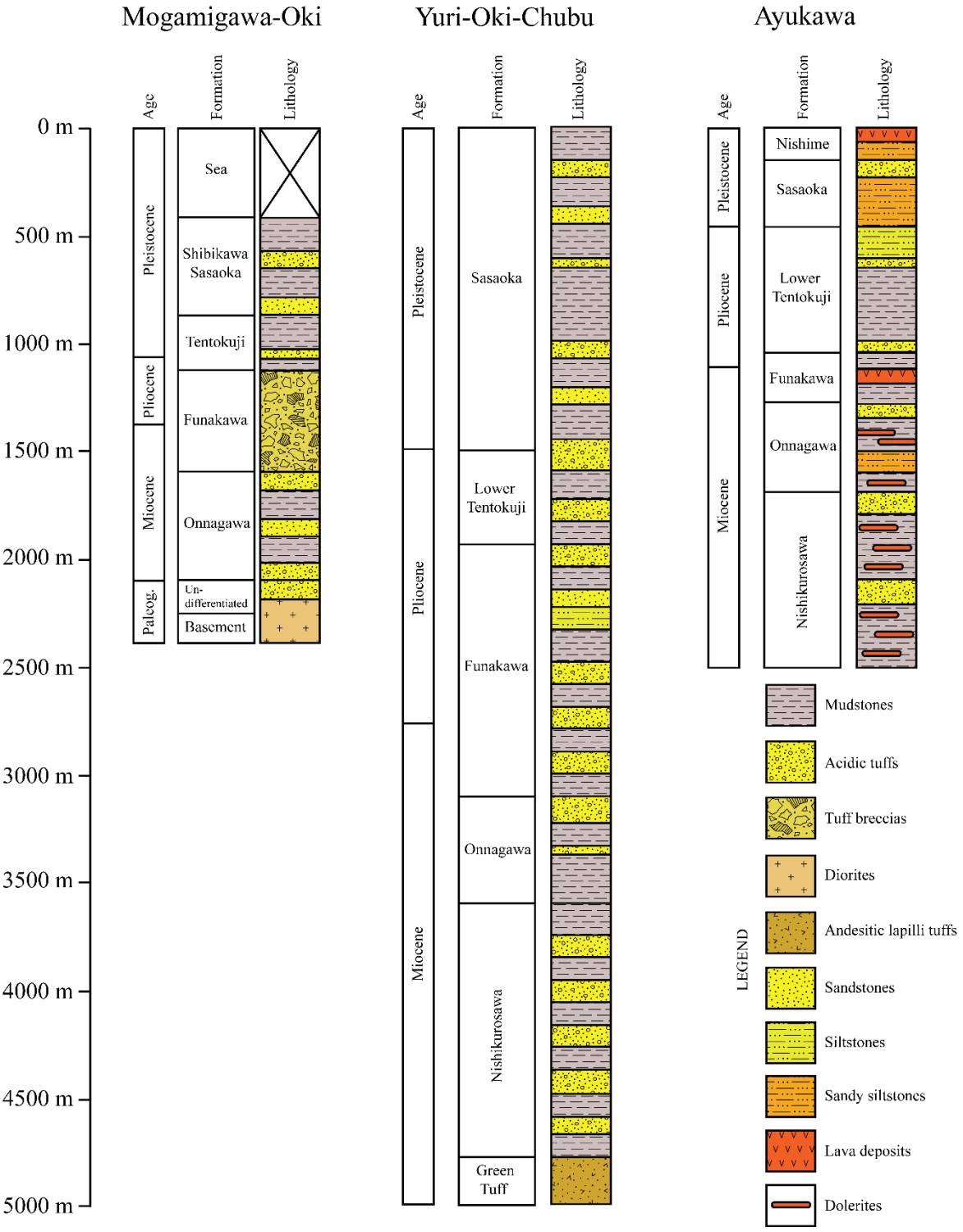

Figure 5.2. Stratigraphic columns of three example wells drilled in the Akita Prefecture. The stratigraphic columns were compiled using the data of the Japanese National Gas Association (1992), the Japanese Association for Petroleum Technology (1993), and Ujiié et al. (2004)).

The wells data reported in Figure 5.2 show that the Onnagawa Formation had a variable burial depth in various locations of the Akita Prefecture. In the Mogamigawa-Oki well, the highest values of the Vitrinite Reflectance (VRo%) is 0.55% at 2100 m (Japanese National Gas Association, 1992). This value indicates that the Onnagawa Formation reached an early oil maturity stage at this depth. On the other hand, in the Yuri-Oki-Chubu well, the Onnagawa Formation was buried between 3000 m and 3500 m (Ujiié et al., 2004). According to Ujiiè et al. (2004), VRo% of the Onnagawa Formation in this well is 0.70%, indicating an oil maturity stage. These data suggest that the burial depth determined a different thermal maturity in the two areas. However, Yokoi et al. (2013) reported high thermal maturity and productive source rock horizons in the Onnagawa Formation at depths shallower than 2000 m (Figure 5.2). In the Ayukawa oil and gas field, several dolerite bodies intruded into the Onnagawa Formation. The presence of hot bodies intruded in the Onnagawa Formation determined an increase in the Onnagawa Formation's thermal maturity. Based on the above data, both the burial and the thermal anomaly factors should be considered for evaluating the thermal maturity of the Onnagawa Formation for future oil and gas exploration in the Akita Prefecture.

In the Aomori Prefecture, limited subsurface data are available. However, the Nishitsugaru-Oki and the DTH27-1 wells are characterized by a Miocene succession with different thicknesses (Figure 5.3). Based on the results of this study, the Middle-Late Miocene formations (Akaishi and Odoji Formations) VRo% was in a range of 0.30–0.35% between 900 m and 1100 m (Figure 3.22); the VRo% increased until 0.43% at 1500 m, in the Odose Formation. On the other hand, in the Nishitsugaru-Oki well, VRo% increase linearly until 1900 m, and reach the highest value (0.49%; T_{max} = 440 °C) (Japanese Association for Petroleum Technology, 1993). However, the interpreters of the Nishitsugaru-Oki well did not find an increase in the thermal maturity below 1900 m (Akaishi and Odoji Formations). The data from these two wells indicate that the burial depth somewhat increased thermal maturity, but not enough to determine values typical of the oil generation stage.

Ujiié (1995) hypothesized the presence of another possible prospective area east of the Tsugaru Basin. In this area, the Neogene succession reaches a thickness of more than 2000 m, and several oil seepages were found along an N-S oriented anticlinal fold. The presence of oil seeps possibly indicates the presence of an active petroleum system. However, at the current state, the thermal maturity of the Middle Miocene formations in the subsurface of this area is unknown. Future geological investigations in this area could be useful to identify the presence of a petroleum system in southeastern Aomori Prefecture.

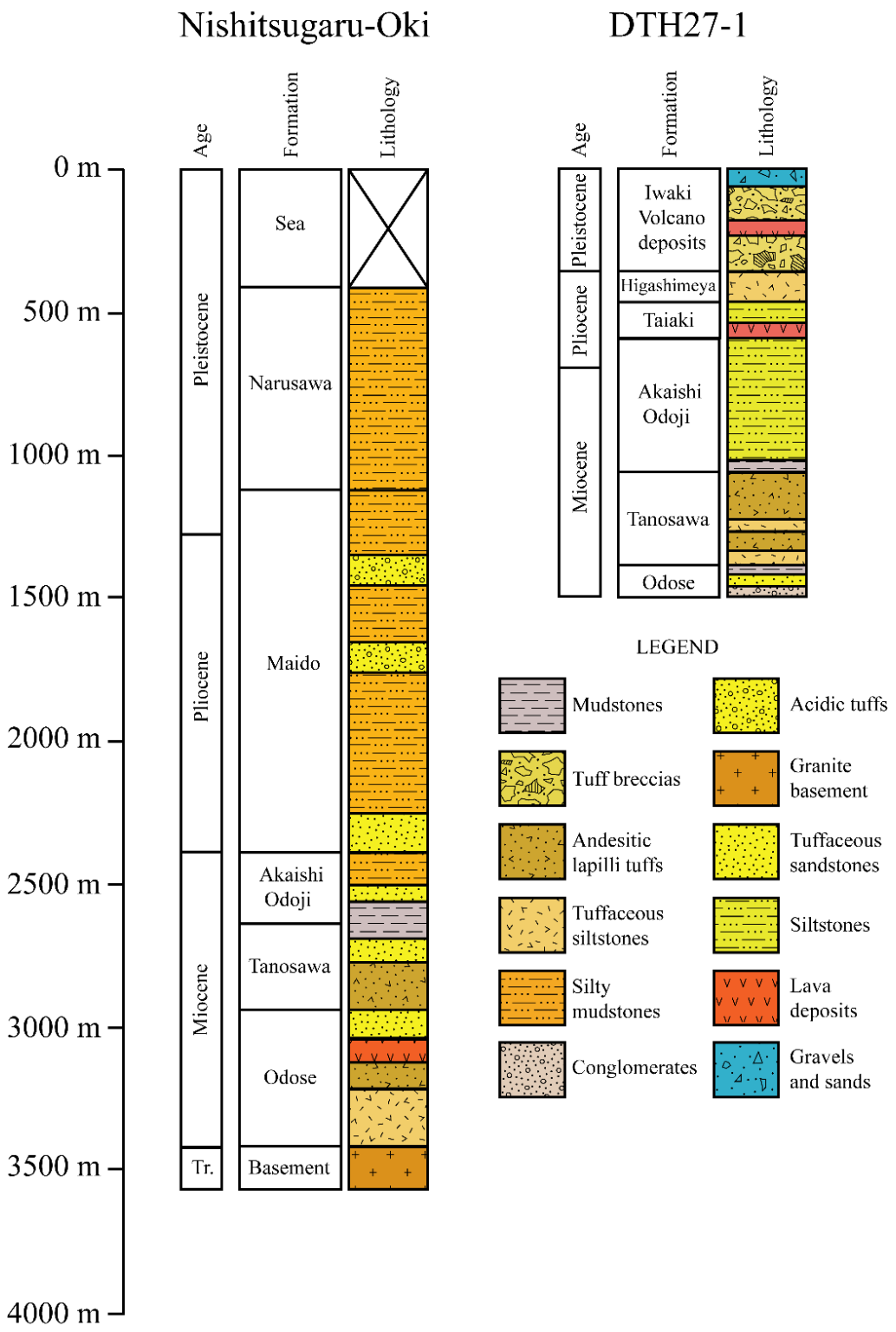

Figure 5.3. Stratigraphic columns of the MITI Nishitsugaru-Oki and DTH27-1 wells in the Aomori Prefecture. The stratigraphic columns were compiled using the data from this study, the Japanese National Gas Association (1992), and the Japanese Association for Petroleum Technology (1993).

5.2 Paleoenvironment of the Japan Sea

Based on the sedimentological and geochemical data discussed in this study, it was possible to interpret the variations in detrital influx, paleo-productivity in the surface water, and paleo-redox conditions in the bottom waters in the Akita and Aomori regions.

5.2.1 Detrital Fraction

The interpretation of the detrital oxides indicated that the detrital fraction of the Onnagawa, Odoji, and Akaishi Formations originated from a felsic composition source rock associated with granitic or continental rocks (Figure 3.25 and 4.18). Kimura et al. (2004) hypothesized a provenance from Asia for the Onnagawa Formation at the Oga Peninsula. Because the Onnagawa Formation in Sugisawa and the Odoji and Akaishi Formations in Tsugaru have a similar geochemical composition with the Onnagawa Formation of Kimura et al. (2004) and are stratigraphically correlated, the detrital fraction in both the study areas probably originated from the same source area in the Asian continent. One of the main paleoenvironmental changes in the Middle-Late Miocene period is the increase of the East Asian Winter Monsoon (EAWM) at 15–10 Ma and 8 Ma (Wan et al., 2007; Clift et al., 2014; Tada et al., 2016) (Figure 5.4). On the other hand, in this study, we detected an increase of detrital fraction at the top of the Onnagawa and Odoji Formations and in the Akaishi Formation (Figures 3.26 and 4.19). According to Koizumi and Matoba (1989) and Nemoto and Wakabayashi (1995), the top of the Onnagawa and Odoji Formations is at ~8–9 Ma. The age agreement between the EAWM activity and the formations indicates a relationship between the detrital input and the monsoon intensity increase.

Previous studies from Tada (1991, 1994) hypothesized a potential riverine input of detrital material from the land areas located on the east margin of the northwestern Honshu basin. These land areas are rich in felsic granites formed when the Japanese Islands were still part of the Eurasian continent; therefore, their composition matches with provenance from a felsic source. This hypothesis suggests a relationship between the river sediment supply and the detrital oxides' contents. Specifically, the increase of the detrital fraction in the Akaishi Formation suggests that the river supply in the Late Miocene was higher than in the Middle Miocene.

As evidenced in (Figures 3.27 and 4.20), variations of detrital oxides (detrital SiO_2, Al_2O_3, K_2O) generally showed a positive correlation with the TOC in the Odoji and Onnagawa Formations. This correlation indicates that, in these formations, the detrital fraction preserved the organic matter from bacterial degradation. On the other hand, the lack of correlation in the Akaishi Formation indicates that the detrital fraction did not favor the preservation of the TOC.

5.2.2 Paleoproductivity

Siliceous formations from both the Tsugaru Basin and Akita Basin deposited in a period of intense biological activity of diatoms in the surface water (Tada, 1994). The presence of cold surface water and the upwelling of nutrients (N, P, and Si) favored the blooming of diatoms (Koizumi and Yamamoto, 2018). The decrease of the temperature in the surface water was probably the result of the combination between the Middle-Late Miocene global cooling and the inflow of cold water from the north Pacific Sea (Tada, 1994). On the other hand, the intensification of the EAWM in the Middle-Late Miocene influenced the mobility of deep-water upwelling currents and the upwelling of nutrients.

Figures 3.28 and 4.21 indicated a moderate negative correlation between the biogenic SiO_2 and the TOC. This result suggested that periods of high biogenic SiO_2 deposition (high biogenic production) in the two study areas determined a supersaturation of biogenic SiO_2 in the bottom waters, which resulted in the biogenic dilution of the organic matter.

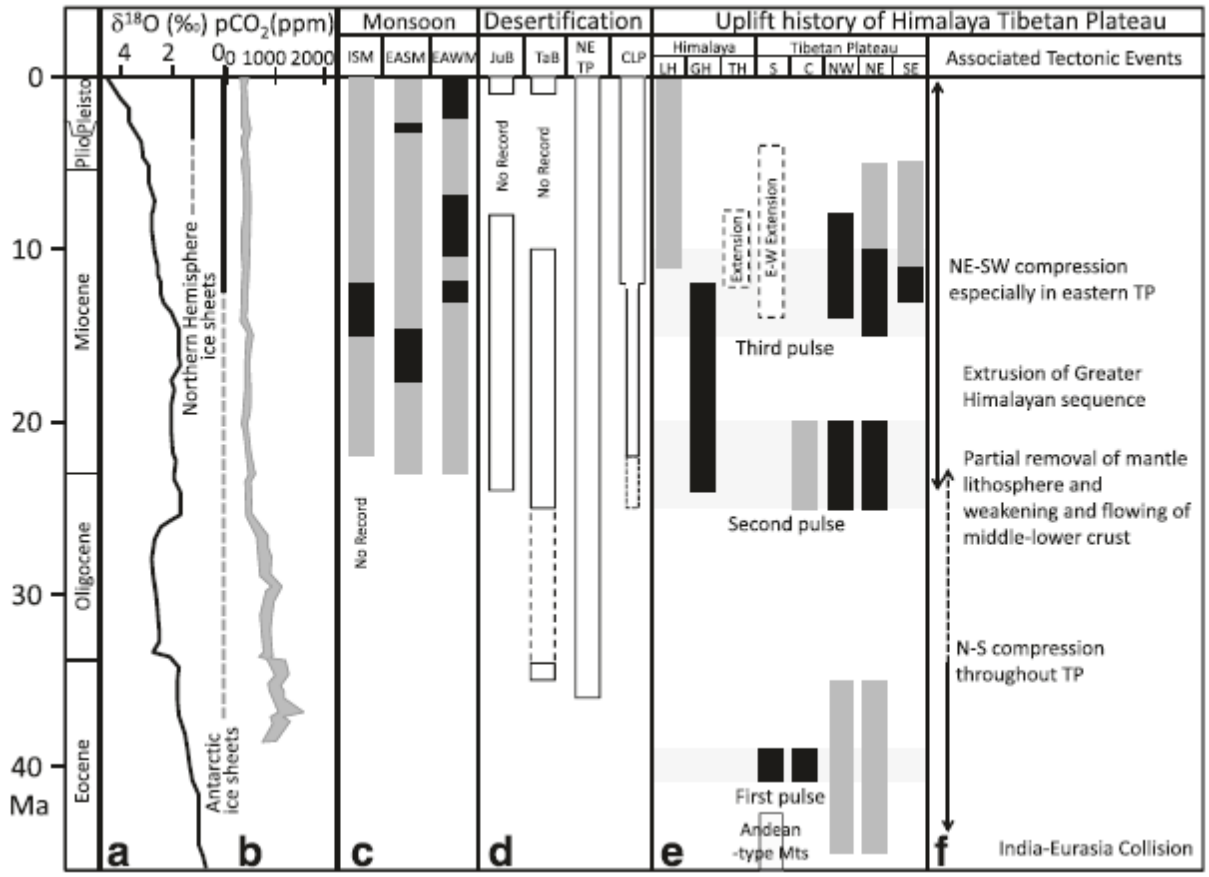

Figure 5.4. Evolution of Asian monsoons, desertification, HTP uplift, and their relationship with global changes during the Cenozoic (from Tada et al., 2016). The monsoon shows an increase in the intensity at 15–10 Ma and 8 Ma (black bars).

5.2.3 Paleo-redox conditions

According to Tada (1991, 1994), low-oxygen conditions in the bottom waters of the northern Japan basins were likely determined by the inflow of the Oxygen Minimum Zone (OMZ) waters from the Pacific Sea, during periods of high sea-level; in these periods the OMZ water was able to inflow and determined a different oxygenation condition in the basins. However, this study revealed different paleo-oxygenation conditions in the Tsugaru Basin and the Akita Basin.

The presence of massive/bioturbated sediments and the occurrence of framboidal pyrite typical of an oxygenated condition in the Odoji Formation indicate that the OMZ water did not influence the bottom water of the Tsugaru Basin area. Differently, Tada et al. (1986) described a lithofacies alternation between massive and laminated in the sediments of the Odoji Formation of the Ajigasawa area (west of Tsugaru area), suggesting and intermittent influence of OMZ waters in that basin, during periods of high and low sea-level periods. On the other hand, this and Tada et al. (1986) studies found similar features of the Akaishi Formation, which suggest the establishment of oxic bottom water in both the Tsugaru and Ajigasawa areas. The establishment of oxic conditions may be related to a stable low stand of the sea-level, which did not allow the inflow of OMZ water. Another hypothesis reported in Tada (1994) links the lack of inflow of the OMZ waters to the shoaling of the sill that connected the northern Japan basins to the Pacific Sea.

Based on lithofacies description of the sediments in the Sugisawa and Gotanzawa areas, and the framboidal pyrite size distribution, different locations of the Akita Basin were characterized by a different interaction with the Pacific Sea's OMZ waters. The presence of alternations of massive and laminated sediments and the occurrence of framboidal pyrite of different diameters in the Onnagawa Formation possibly indicate an intermittent influence of the OMZ water from the Pacific Sea in the Sugisawa area. On the other hand, the occurrence of exclusively massive samples with large-sized framboidal pyrite indicates that OMZ waters did not influence the Gotanzawa area.

Low-oxygen conditions in the bottom waters are generally regarded as a factor that influences the preservation of the organic matter and TOC in sediments. The comparison between the TOC content in the different formations analyzed in this study is shown in Figure 5.5. In the Onnagawa Formation, there is not a marked difference between the massive and the laminated samples, suggesting that the bottom water conditions did not influence the TOC content. Additionally, the massive sediments of the Iwaya in Gotanzawa and the Odoji Formation in the Tsugaru Basin showed generally good values of the TOC, indicating that also in these locations, the bottom water conditions did not affect the TOC. However, the Akaishi Formation is characterized by low TOC contents and degraded organic matter (Figure 3.19). This feature indicates that the establishment of the oxic condition in the bottom water probably affected the TOC.

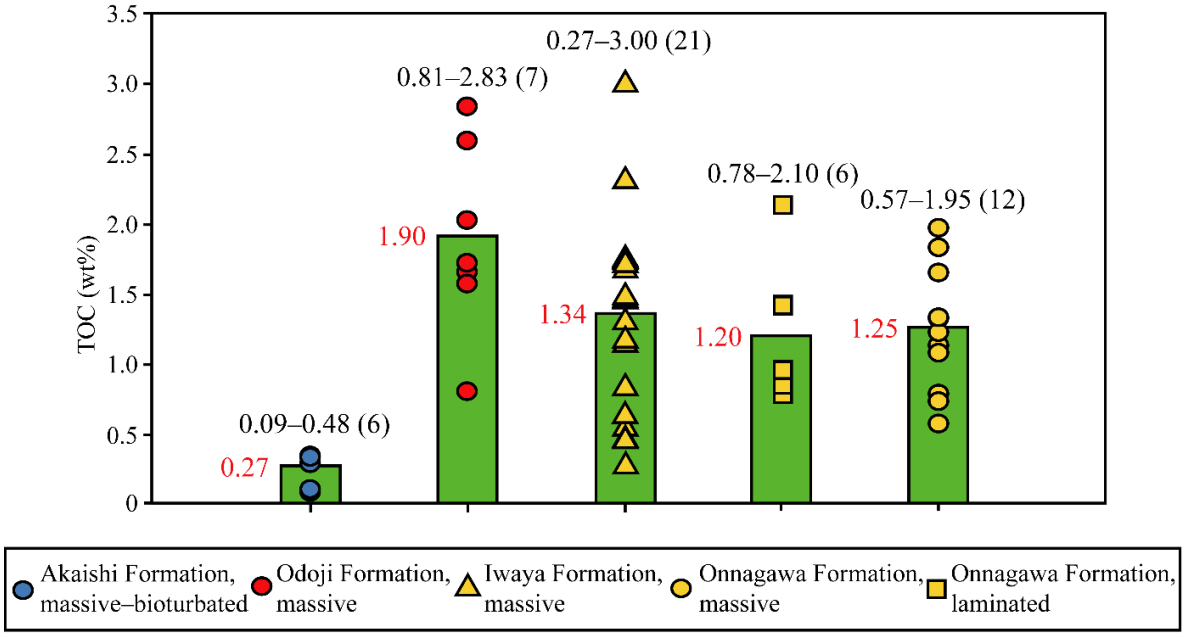

Figure 5.5. Comparison of TOC contents in the different lithofacies of the Akaishi, Odoji, Iwaya, and Onnagawa Formations. The green bars, red values indicate the average TOC, while the black values indicate the TOC ranges and the number of samples.

5.2.4 Paleoenvironment of the Japan Sea

Based on the lithological and geochemical data discussed in this study, we propose some paleoenvironmental models that describe the setting of the Sea of Japan in the Akita and Aomori regions during the Middle-Late Miocene period (Figure 5.6).

Both regions were characterized by variable input of detrital material transported from the Asian continent to the Japan Sea by the increasing Asian monsoon. Alternatively, the detrital fraction was possibly transported from the land areas of northeastern Japan by the riverine input. The surface waters of the Aomori and Akita Basins were characterized by the biological activity of the phytoplankton (diatoms), and deep upwelling currents were bringing large amounts of nutrients to the sea surface. The upwelling process was probably facilitated by the strength of monsoon wind, the cold surface water, and the paleo-topography of the seafloor. The OMZ water from the Pacific Sea was inflowing in the northern Japan region from the Pacific Sea during periods of high sea-level; in these periods, the OMZ water was able to inflow and determine a low-oxygenation condition. As discussed above, the Tsugaru Basin area was not influenced by the OMZ water suggesting that the

paleo-depth of the Tsugaru basin was shallower than the OMZ. According to Tada (1994), the OMZ layer was distributed between -500 m and -1500 m. Therefore, the paleo-depth of the Tsugaru Basin was probably shallower than 500 m (upper bathyal) (Figure 5.6d–e).

On the other hand, based on the data of Tada et al. (1986), the Ajigasawa area paleo-depth was likely higher than 1000 m. Therefore, this area was likely influenced by the intermittent influence of OMZ waters during high and low sea-level cycles. The paleoenvironmental reconstruction in Aomori during the deposition of the Akaishi Formation is uncertain. This and Tada et al. (1986) studies found similar features of the Akaishi Formation, which suggest that oxic bottom waters were present in both the Tsugaru and Ajigasawa areas. The establishment of oxic conditions was possibly related to a stable low stand of the sea level or to the shoaling of the sill that connected northern Japan to the Pacific Sea.

The presence of alternations of massive and laminated sediments in the Sugisawa area and exclusively massive sediments in the Gotanzawa area suggest that basins with different paleo-depth characterized the Akita region (Figure 5.6b–c). The paleo-depth in the Sugisawa area was probably more profound than 1000 m. Therefore, this area was influenced by the inflow of OMZ water. On the other hand, the presence of massive samples in the Gotanzawa area probably indicates the lack of the inflow of the OMZ water. Therefore, the Gotanzawa area’s paleo-depth was shallower than 500 m.

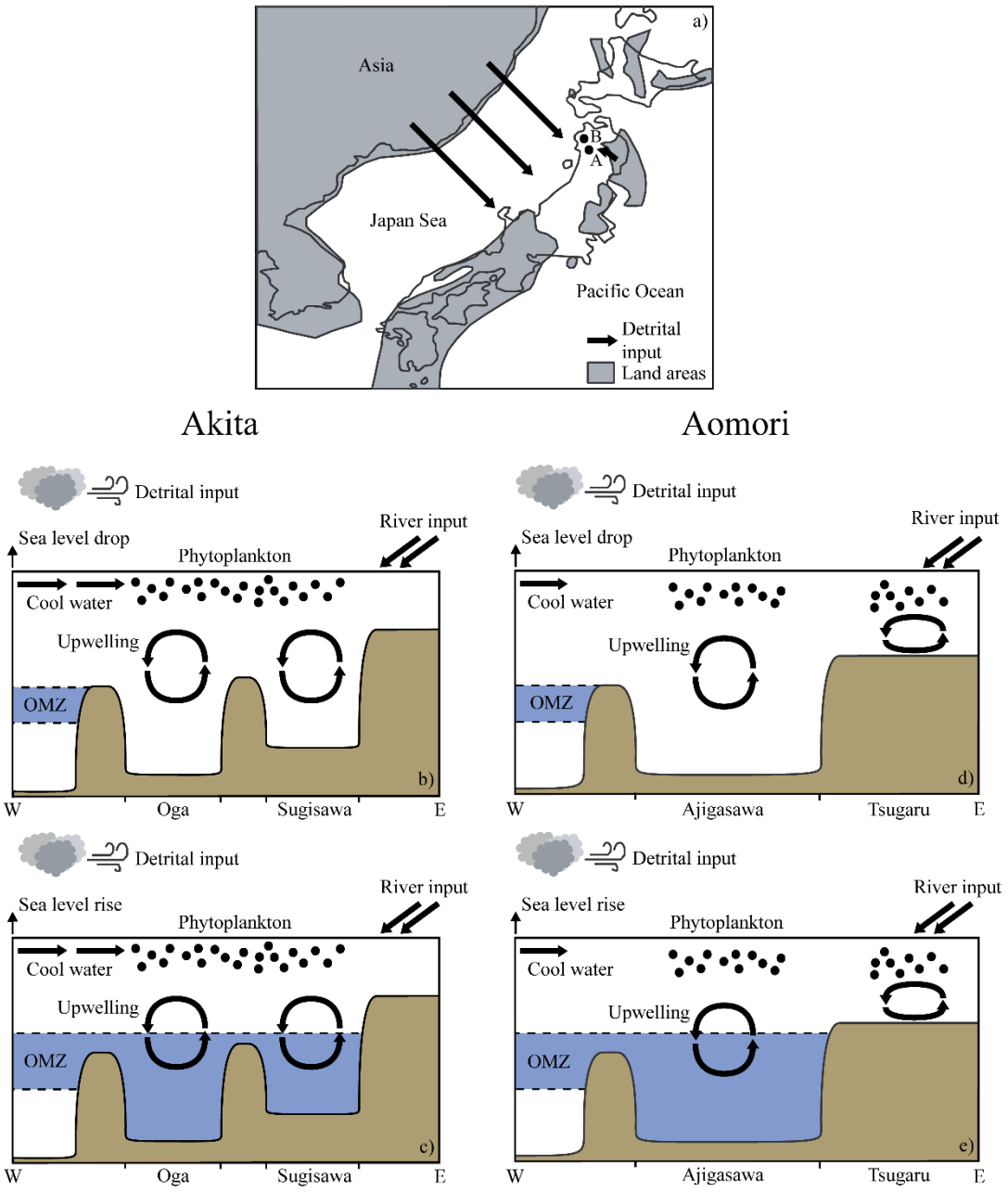

Figure 5.6. (a) Paleogeographic map of the Japanese Islands during the Middle Miocene (modified from Iijima and Tada, 1990 and Ozawa et al., 2008); (b–c) During the deposition of the lower and middle parts of the Onnagawa Formation, the relative sea-level variations determined an oscillation between oxygenated and low oxygenated bottom waters. The surface waters were characterized by intense paleo-productivity, but the input of the detrital fraction from the Asian monsoon was still low. Differently, during the deposition of the upper part of the Onnagawa Formation, the sea level was low, and an oxygenated marine environment developed. In this phase, the surface water productivity was still high, and the higher intensity of the Asian monsoon determined an increase of the detrital fraction; (d–e) Differently from the Akita Basin, the relative sea-level variations did not influence the oxygenation of the bottom waters in the Tsugaru Basin. The deposition of the Odoji Formation in this area always occurred in an oxygenated marine environment. Similarly to the Akita Basin, the paleo-productivity in the surface waters was high, and the detrital input increased along the Odoji and the Akaishi Formations.

CHAPTER 6

Conclusions

The sedimentological and geochemical characterization of siliceous formations from Akita and Aomori regions allowed to evaluate their source rock potential and to interpret the paleoenvironmental in the Japan Sea in the Middle-Late Miocene period.

Data from the Rock-Eval pyrolysis revealed that the Onnagawa and Iwaya Formations in Akita, and the Odoji Formation in Aomori have a fair/good organic richness and generative potential. However, based on the T_{max} values, these formations are immature for the hydrocarbons generation.

Compiled information from previous wells in the Akita Prefecture indicated that the Onnagawa Formation and its equivalents are mature for oil generation in various locations of the region. The two main factors that determined the maturation of potential source rocks were the burial depth or geothermal gradient anomalies determined by the intrusion of igneous bodies inside the Onnagawa Formation. These geothermal anomalies allowed the maturation of the Onnagawa Formation even at relatively shallow depths. On the other hand, in the Aomori Prefecture, previous investigations did not locate geothermal anomalies driven by igneous intrusions. Therefore, in this region, the main factor affecting the thermal maturity was probably the burial depth. However, the higher burial depth of the Middle-Late Miocene formations in the south-western than in the south-eastern sectors of the Aomori Prefecture did not determine a significative increase of the thermal maturity. At the current state, the mature horizons for the oil generation are still not located. Future research in the Aomori Prefecture should focus on the area east of the Tsugaru Basin, where in the past several oil seepages were located, and the Miocene succession is the thickest.

Analysis of organic and inorganic fractions of the sediments allowed to assess the variations in the primary productivity, the redox conditions in the bottom water, and the detrital fraction input in the two regions. Conclusions are as follows:

(1) Paleoweathering proxy revealed a medium to high chemical weathering and a warm-humid climate at the source of the detrital fraction. Based on the geochemical data, the detrital fraction had a felsic composition, and its provenance area was possibly located on the Asian continent. The variation in the amount of the detrital fraction delivered in the Sea of Japan was possibly related to the variation of the monsoon activity in the Middle-Late Miocene period.

(2) The high concentrations of the biogenic silica in the Middle-Late Miocene sediments indicate high primary productivity. The intense upwelling and the presence of cold surface waters favored the presence of nutrients that stimulated the bio-productivity of the diatoms. From this productivity, considerable amounts of organic matter were input in the water column.

(3) Different paleo-oxygenation conditions characterized the Tsugaru Basin, the Sugisawa, and the Gotanzawa areas. As suggested by the lithofacies variations and size of framboidal pyrite, the Tsugaru Basin and the Gotanzawa areas developed similar oxidizing conditions in the bottom water. On the other hand, the Sugisawa area was characterized by oxygenated and low-oxygenated intervals.
(4) The primary productivity primarily influenced the organic carbon contents of the Middle-Late Miocene formations in the two study areas. In some cases, the surface water productivity compensated for the degradation process of the oxidizing water column. In other cases, the large amounts of deposited biogenic silica created an auto-dilution process that reduced the organic carbon contents even during the low-oxygen intervals.

The detrital fraction input during the deposition of the Middle-Late Miocene siliceous possibly diluted the organic matter and positively influenced the organic carbon content.

The presence of oxidizing conditions in the Tsugaru basin area and some periods in the Sugisawa area did not always result in the degradation of the organic matter. The more evident case of oxic degradation is represented by the Akaishi Formation in which the TOC is markedly low.

This study showed that the paleoenvironmental conditions of the Japan Sea’s margin were determined by the interaction of several factors, including the paleo-climate, the dynamic of sea currents, and the Asian monsoon activity. These factors influenced the preservation of the TOC in different ways. Therefore, future studies in the Aomori and Akita Basins should be extended to several locations to compare the different data and have a clear image of the evolution of the Japan Sea’s margin. Further studies will clarify the relationship between the sedimentation of siliceous formations and the Japan Sea`s evolution.

References

Allen, P.A., Allen, J.R. (2013). Basin Analysis: Principles and Application to Petroleum Play Assessment (3rd edition). John Wiley & Sons, Ltd.

Aoyagi, K., Omokawa, M. (1992). Neogene diatoms as the important source of petroleum in Japan. Journal of Petroleum Science and Engineering, 7, 247-262.

Asquith, G., Krygowski, D. (2004). Basic Well Log Analysis (2nd edition). AAPG Methods in Exploration Series, 16. American Association of Petroleum Geologists, Tulsa, Oklahoma.

Behar, F., Beaumont, V., De, B., Penteado, H.L. (2001). Rock-Eval 6 technology: performances and developments. Oil & Gas. Science and. Technology. Revue de l'Institut Francais du Petrole, 56, 111-134.

Berner, R.A., Raiswell, R. (1983). Burial of organic carbon and pyrite Sulphur in sediments over Phanerozoic times: a new theory. Geochimica et Cosmochimica Acta, 47, 855-862.

Berner, R.A., Raiswell, R. (1984). A new method for distinguishing fresh water from marine sedimentary rocks. Geology, 12, 365-368.

Bohacs, K.M., Grabowski, G.J. Jr., Carroll, A.R., Mankiewicz, P.J., Miskell-Gerhardt, K.J., Schwalbach, J.R., Wegner, M.B., Simo, J.A.T., 2005. Production, Destruction and Dilution–the many paths to source-rock development. SEPM Special Publication 82, 61–101.

Chen, G., Gang, W., Chang, X., Wang, N., Zhang, P., Cao, Q., Xu, J., 2020. Paleoproductivity of the Chang 7 unit in the Ordos Basin (North China) and its controlling factors. Palaeogeography, Palaeoclimatology, Palaeoecology 551, 109741.

Clift, P.D., Wan, S., Blusztajn, J., 2014. Reconstructing chemical weathering, physical erosion and monsoon intensity since 25 Ma in the northern South China Sea: A review of competing proxies. Earth-Science Reviews 130, 86–102.

Cox, R., Lowe, D.R., Cullers, R.L. (1995). The influence of sediment recycling and basement composition on evolution of mudrock chemistry in the southwestern United States. Geochimica et Cosmochimica Acta, 59, 2919-2940.

Demaison, G.J., Moore, G.T. (1980). Anoxic environments and oil source bed genesis. American Association of Petroleum Geologists Bulletin, 64, 1178-1209.

Espitalié, J., Laporte, J.L., Madec, M., Marquis, F., Leplat, P., Paulet, J., Boutefeu, A. (1977). Méthode rapide de characterisation des roches mères, de leur potentiel pétrolier et de leur degré d'évolution. Revue de l'Institut Francais du Petrole et Annales des Combustibles Liquides, 32, 23-42.

Fedo, C.M., Nesbitt, H.W., Young, G.M. (1995). Unravelling the effects of potassium metasomatism in sedimentary rocks and paleosols, with implications for paleoweathering conditions and provenance. Geology, 23, 921-924.

Glenn, C.R., Arthur, M.E. (1985). Sedimentary and geochemical indicators of productivity and oxygen contents in modern and ancient basins: the Holocene Black Sea as the “type” anoxic basin. Chemical Geology, 48, 325-354.

Gottardi, R., Adams, L.M., Borrok, D., Teixeira, B. (2019). Hydrocarbon source rock characterization, burial history, and thermal maturity of the Steele, Niobrara and Mowry Formations at Teapot Dome, Wyoming. Marine and Petroleum Geology, 100, 326-340.

Hanagata, S., Miwa, M., (2002). Miocene-Pliocene microfossil biostratigraphy and paleoenvironment in the Fukaura district, Aomori Prefecture, northern Japan (in Japanese with English abstract). Journal of the Geological Society of Japan, 108, 767-776.

Hayashi, K.I., Fujisawa, H., Holland, H.D., Ohmoto, H. (1997). Geochemistry of ca. 1.9 Ga sedimentary rocks from northeastern Labrador, Canada. Geochimica et Cosmochimica Acta, 61, 4115-4137.

Hibi, Y. (2020). Lithofacies and stratigraphic distribution of the Miocene hard mudstone in Akita Prefecture, northern Japan (unpublished master’s thesis). Akita University, Japan.

Iijima, A., Tada, R., Watanabe, Y. (1988). Developments of Neogene sedimentary basins in the northeastern Honshu Arc with emphasis on Miocene siliceous deposits. Journal of the Faculty of Science, University of Tokyo, Section II, 21, 417-446.

Ishiwatari, R., Uzaki, M. (1987). Diagenetic changes of lignin compounds in a more than 0.6 million-year-old lacustrine sediments (Lake Biwa, Japan). Geochimica et Cosmochimica Acta, 51, 321-328.

Iwasa, S. (1962). Studies on the oil-bearing Tertiary, and the geotectonic history of the Tsugaru district in Aomori prefecture, Japan (in Japanese with English abstract). Journal of Japanese Association for Petroleum Technology, 27, 407-441.

Japan National Gas Association (1992). Petroleum and natural gas resources in Japan (in Japanese): Tokyo, Japan National Gas Association, 520 p.

Japan Association for Petroleum Technology (1993). Recent petroleum developments in Japan (in Japanese): Tokyo, Japan Association for Petroleum Technology, 60 p.

Jasper, J.P., Gagosian, R.B. (1990). The sources and deposition of organic matter in the Late Quaternary Pygmy Basin, Gulf of Mexico. Geochimica et Cosmochimica Acta, 54, 117-132.

Jingu, H., Ujiié, Y. (1990). Diagenesis of the Neogene sediments in the southwestern part of the Tsugaru Basin, northern Honshu, Japan (in Japanese with English abstract). Journal of Japanese Association for Petroleum Technology, 96, 421-435.

Jolivet, L., Tamaki, K. (1992). Neogene kinematics in the Japan Sea region and volcanic activity of the Northeast Japan Arc. In: Tamaki, K., Suyehiro, K., Allan, J., McWilliams, M., et al. (Editors). Proceedings of the Oceanic Drilling Program Scientific Results, 127/128 (2), 1311-1331.

Kano, K., Ohguchi, T., Ishikawa, Y., Yanai, K., Fujimoto, Y., Uemura, K., Ogasawara, K., Komazawa, M. (2011). Geology of the Aniai District 2nd Edition (in Japanese with English abstract), Quadrangle Series 1:50000 Akita, 4.

Kato, S. (1992). District of the Oshima Peninsula and Aomori. In *Japan Natural Gas Association and Japan Offshore Petroleum Development Association, eds., Petroleum and natural gas resources in Japan* (revised edition) (in Japanese) (pp. 41-53). Tokyo, Japan Natural Gas Association and Japan Offshore Petroleum Development Association.

Katz, B.J. (2005). Controlling factors on source rock development-a review of productivity, preservation, and sedimentation rate. In: Harris, N.B. (Ed.), *The Deposition of Organic-carbon-rich Sediments: Models, Mechanisms and Consequences*, SEPM Special Publication, 82, 7-16

Keil, R.G., Tsamakis, E., Fuh, C.B., Giddings, J.C., Hedges, J.I. (1994). Mineralogical and textural controls on the organic composition of coastal marine sediments. Hydrodynamic separation using SPLITT fractionation. Geochimica et Cosmochimica Acta, 58, 879-893.

Kimura, S., Shikazono, N., Kashiwagi, H., Nohara, M. (2004). Middle Miocene-early Pliocene paleo-oceanic environment of Japan Sea deduced from geochemical features of sedimentary rocks. Sedimentary Geology, 164 (1), 105-129.

Koizumi, I., Yamamoto, H. (2018). Diatom ooze and diatomite–diatomaceous sediments in and around the North Pacific Ocean., JAMSTEC Rep. Res. Dec. 27, 26–46.

Koizumi, I., Sato, M., Matoba, Y. (2009). Age and significance of Miocene diatoms and diatomaceous sediments from northeast Japan. Palaeogeography, Palaeoclimatology, Palaeoecology, 272, 85–98.

Kondla, D., Sanei, H., Clarkson, C.R., Goodarzi, F. (2017). High resolution characterization of a core from the Lower Jurassic Gorgondale Member, Western Canada Sedimentary Basin. Marine and Petroleum Geology, 83, 50-59.

Larionov, V.V. (1969). Borehole Radiometry. Moscow, U.S.S.R., Nedra.

Lafargue, E., Espitalié, J., Marquis, F., Pillot, D. (1998). Rock-Eval 6 applications in hydrocarbon exploration, production and in soil contamination studies. Revue de l'Institut Francais du Petrole, 53, 421-437.

Leventhal, J.S. (1983b). Organic carbon, sulfur, and iron relationship in ancient shales as indicators of environment of deposition. Eos, Wash., 64, 739.

Li, D., Li, R., Tan, C., Zhao, D., Xue, T., Zhao, B., Khaled, A., Liu, F., Xu, F., 2019. Origin of silica, paleoenvironment, and organic matter enrichment in the Lower Paleozoic Niutitang and Longmaxi formations of the northwester Upper Yangtze Plate: Significance for hydrocarbon exploration 103, 404–421.

Liu, Z., Chen, D., Zhang, J., Lu, X., Wang, Z., Liao, W., Shi, X., Tang, J., Xie, G. (2019). Pyrite Morphology as an Indicator of Paleoredox Conditions and Shale Gas Content of the Longmaxi and Wufeng Shales in the Middle Yangtze Area, South China. Minerals, 9, 1-18.

Matsuzaki, K.M., Itaki, T., Tada, R., Kamikuri, S. (2018). Paleoceanographic history of the Japan Sea over the last 9.5 million years inferred from radiolarian assemblages (IODP Expedition 346 Sites U1425 and U1430. Progress in Earth and Planetary Science, 5, 54.

Meyers, P.A. (1997). Organic Geochemical proxies of paleoceanographic, paleolimnologic and paleoclimatic processes. Organic Geochemistry, 27, 213-250.

Nakajima, T. (2017). Granites of Japan: A review at 2017. Jour. Geol. Soc. Japan 124, 603–625 (in 756 Japanese with English abstract).

Nemoto, N., Wakabayashi, H. (1995). Foraminifera of the Kitakanegasawa Formation (newly named) in the northeastern part of Fukaura Town, Aomori Prefecture, Northeast Japan (in Japanese with English abstract). Earth Science (Chikyu Cagaku), 49, 203-220.

Nesbitt, H.W., Young, G.M. (1982). Early Proterozoic climates and plate motions inferred from major element chemistry of lutites. Nature, 299, 715-717.

Oyedotun, T.D.T. (2018). X-Ray fluorescence (XRF) in the investigation of the composition of earth materials: a review and an overview. Geology, Ecology, and Landscapes, 2, 148-154.

Peters, K.E. (1986). Guidelines for evaluating petroleum source rock using programmed pyrolysis. American Association of Petroleum Geologists Bulletin, 79, 318-329.

Peters, K.E., Cassa, M.R. (1994). Applied source rock geochemistry. In: Magoon, L.B., Dow, W.G. (Eds.), *The Petroleum System from Source to Trap*. American Association of Petroleum Geologists Memoir, 60, 93-117.

Piper, D.Z., Isaacs, C.M. (1984). Geochemistry of Minor Elements in the Monterey Formation, California: Seawater Chemistry of Deposition. U.S. Geological Survey Professional Paper 1566.

Prahl, F.G., Bennett, J.T., Carpenter, R. (1980). The early diagenesis of aliphatic hydrocarbons and organic matter in sedimentary particulates from Dabob Bay, Washington. Geochimica and Cosmochimica Acta, 44, 1967-1976.

Prahl, F.G., Ertel, J.R., Gonaji, M.A., Sparrow, M.A., Eversmever, B. (1994). Terrestrial organic carbon contributions to sediments on the Washington margin. Geochimica et Cosmochimica Acta, 58, 3048-3055.

Pratt, L.M. (1984). Influence of paleoenvironmental factors on preservation of organic matter in Middle Cretaceous Greenhord Formation, Pueblo, Colorado. American Association of Petroleum Geologists Bulletin, 68, 1146–1159.

Prell, W.L., Kurtzbuck, J.E. (1992). Sensitivity of the Indian monsoon to forcing parameters and implications for its evolution. Nature, 360, 647-652.

Premuzic, E.T., Benkovitz, C.M., Gafney, J.S., Walsh, J.J. (1982). The nature and distribution of organic matter in the surface sediments of world oceans and seas. Organic Geochemistry, 4, 63-77.

Raiswell, R. (1982). Pyrite texture, isotopic composition, and the availability of Iron. American Journal of Science, 282, 1244-1263.

Roser, B.P., Korsch, R.J. (1988). Provenance signatures of sandstone-mudstone suites determined using discriminant function analysis of major-element data. Chemical Geology, 68, 119-138.

Ross, D.J.K., Bustin, R.M. (2009). Investigating the use of sedimentary geochemical proxies for paleoenvironment interpretation of thermally mature organic-rich strata: examples from the Devonian/Mississippian shales, Western Canadian Sedimentary. Basin Chem. Geol., 260, 1-19.

Sato, H. (1994). The relationship between late Cenozoic tectonic events and stress field and basin development in Northeast Japan. Journal of Geophysical Research: Solid Earth, 99 (B11), 22261-22274.

Savrda, C.E., Bottjer, D.J., Gorsline, D.S. (1984). Development of a comprehensive oxygen-deficient marine biofacies model: Evidence from Santa Monica, San Pedro, and Santa Barbara Basins, California continental borderland. American Association of Petroleum Geologists Bulletin, 68, 1179-1192.

Savrda, C.E., Bottjer D.J., (1986). Trace-fossil model for reconstruction of paleo-oxygenation in bottom waters. Geology, 14, 3-6.

Sawlowicz, Z. (2000). Framboids: from their origin to application. Prace Mineralogiczne, 88, 1-88.

Scotti, P., 2003, Thermal constraints from the organic matter: Atti Ticinensi di Scienze della Terra, v. 9, Serie Speciale, p. 23-32.

Silliman, J.E., Meyers, P.A., Bourbonniere, R.A. (1996). Record of postglacial organic matter delivery and burial in sediments of Lake Ontario. Organic Geochemistry, 24, 463-472.

Sugii, D. (1998). Depositional environment of the Miocene Onnagawa Formation distributed in Akita Prefecture-based on lithofacies, trace fossils and geochemical analysis (in Japanese with English abstract).

Sumi, K., Moritani, T. (1972). Geology of the Yonaizawa District (in Japanese with English abstract), Quadrangle Series 1:50000 Aomori, 5.

Sweeney, J.J., Burnham, A.K. (1990). Evaluation of a Simple Model of Vitrinite Reflectance Based on Chemical Kinetics (1). AAPG Bulletin, 74, 1559-1570.

Tada, R., Watanabe, Y., Ijima, A. (1986). Accumulation of laminated and bioturbated Neogene siliceous deposits in Ajigasawa and Goshogawara areas, Aomori Prefecture, northeast Japan. Journal of the Faculty of Science, University of Tokyo, Section II, 21, 139-167.

Tada, R. (1991). Origin of rhythmical bedding in middle Miocene siliceous rocks of the Onnagawa Formation, northern Japan. Journal of Sedimentary Petrology, 61, 1123-1145.

Tada, R. (1994). Paleoceanographic evolution of the Japan Sea. Palaeogeography, Palaeoclimatology, Palaeoecology, 108, 487-508.

Tada, R., Zheng, H., Clift, P.D. (2016). Evolution and variability of the Asian monsoon and its potential linkage with uplift of the Himalaya and Tibetan Plateau. Progress in Earth and Planetary Science, 3, 1-26.

Takahashi, S., Yamasaki, S., Ogama, K., Kaiho, K., Tsuchiya, N. (2015) Redox conditions in the end early Triassic Panthalassa. Paleogeography, Paleoclimatology, Paleoecology, 432, 15-28.

Telford, W.M., Geldart, R.P., Sheriff, R.E. (1990). Applied Geophysics. Cambridge University Press.

Thompson, M. (2008). CHNS Elemental Analysers. Technical Reports of the Royal Society of Chemistry.

Tissot, B.P., Welte, D.H. (1984). Petroleum Formation and Occurrence (2nd ed.). Berlin, Springer-Verlag.

Tribovillard, N.P., Algeo, T.W., Lyons, T., Riboulleau, A. (2006). Trace metals as paleoredox and paleoproductivity proxies: an update. Chemical Geology, 232, 12-32.

Tsuji, T., Masui, Y., Waseda, A., Inoue, Y., Kurita, H., Kai, K. (1991). The Onnagawa Formation in the vicinity of Yashima Town, Akita Prefecture, Northern Japan-with special reference to the lithological units, the depositional environments and their relation to source rock characteristics (in Japanese with English Abstract).

Tyrrell, T. (1999). The relative influences of nitrogen and phosphorus on oceanic primary production. Nature, 400, 525-531.

Tyson, R.V. (1995). Sedimentary Organic Matter: Organic Facies and Palynofacies (1st ed.). Chapman and Hall

Ujiié, Y. (1995). Petroleum Source Rocks from the Neogene Tsugaru Basin, Northern Honshu, Japan. AAPG Bulletin, 79, 880-894.

Ujiié, Y., Sherwood, N., Faiz, M., Wilkins, R.W.T. (2004). Thermal maturity and suppressed vitrinite reflectance for Neogene petroleum source rocks of Japan. AAPG Bulletin, 88, 1335–1356.

Wan, S., Li, A., Clift, P.D., Stuut, J.W. (2007). Development of the East Asian monsoon: Mineralogical and sedimentological records in the northern South China Sea since 20 Ma. Palaeogeography, Palaeoclimatology, Palaeoecology 254, 561–582.

Wang, L., Shi, X., Jiang, G. (2012). Pyrite morphology and redox fluctuations recorded in the Ediacaran Doushantuo formation. Paleogeography, Paleoclimatology, Paleoecology, 333, 218-227.

Wang, Z., Wang, J., Fu, X., Zhan, W., Yu, F., Feng, X., Song, C., Chen, W., Zeng, S. (2017). Organic material accumulation of Carnian mudstones in the North Qiangtang Depression, eastern Tethys: Controlled by the paleoclimate, paleoenvironment, and provenance. Marine and Petroleum Geology, 88, 440-457.

Waseda, A. (1996). Correlation between vitrinite reflectance and Rock-Eval T_{max} for argillaceous rocks from national petroleum exploration wells in Japan (in Japanese with English abstract). Res. Org. Geochem., 11, 39–43.

Waseda, A., Tsuji, T., Kajiwara, Y., Nishita, H. (1995). Organic facies and depositional environment of the Onnagawa Formation, comparison with the Monterey Formation (in Japanese with English abstract). Journal of the Japanese Association for Petroleum Technology, 60, 50-60.

Wei, H., Wei, X., Qiu, Z., Song, H., Shi, G. (2016). Redox conditions across the G-L boundary in South China: Evidence from pyrite morphology and sulfur isotopic compositions. Chemical Geology, 440, 1-14.

Weltje, G.J., Tjallingii, R. (2008). Calibration of XRF core scanners for quantitative geochemical logging of sediment cores: Theory and application. Earth Planet Science Letters, 274, 423-438.

Wignall, P.B., Newton, R. (1998). Pyrite framboid diameter as a measure of oxygen deficiency in ancient mudrocks. American Journal of Science, 298, 537-552.

Wignall, P.B., Bond, D.P.G., Sun, Y., Grasby, S.E., Beauchamp, B., Joachimiski, M.M., Blomeier, D.P.G. (2015). Ultra-shallow-marine anoxia in an early Triassic shallow marine clastic ramp (Spitsbergen) and the suppression of benthic radiation. Geol. Mag., 153, 316-331

Wilkin, R.T., Barnes, H.L., Brantley, S.L. (1996). The size distribution of framboidal pyrite in modern sediments: An indicator of redox conditions. Geochimica et Cosmochimica Acta, 60, 3897-3912.

Wilkin, R.T., Arthur, M.A., Dean, W.E. (1997). History of water column anoxia in the Black Sea indicated by pyrite framboid size distributions. Earth and Planetary Science Letters, 148, 517-525.

Yamamoto, M., Watanabe, Y., 1995. Molecular geochemical approach to the Paleoceanographic assessment of Neogene sediments of Yashima area, Akita Basin, Japan. Journal of the Japanese Association for Petroleum Technology 60, 27–38.

Yamamoto, M., Watanabe, Y., Watanabe, M., 1999. Paleooceanographic controls on the deposition of Neogene petroleum source rocks, NE Japan Bull. (in Japanese with English abstract) Geol. Surv. Japan 50, 361–376.

Yokoi, S., Waseda, A., Tsuji, T. (2013). Tight oil potential in Japan. Journal of the Japanese Association for Petroleum Technology, 78, 68-78.

Yokoi, S., Tsuji, T. (2015). Tight Oil Potential in Neogene Monterey-Like Biosiliceous Shale of Japan. Search and Discover Article #51119 (2015), posted August 3, 2015.

Zachos, J., Pagani, M., Sloan, L., Thomas, E., Billups, K., 2001. Trends, Rhythms, and Aberrations in Global Climate 65 Ma to Present. Science 292, 686–693.

Zeng, S., Wang, J., Fu, X., Chen, W., Feng, X., Wang, D., Song, C., Wang, Z. (2015). Geochemical characteristics, redox conditions, and organic matter accumulation of marine oil shale from the Changliang Mountain area, northern Tibet, China